**Universidade de Aveiro** Departamento de Química
**Ano 2020**

**Bruna Filipa Brito Neves**

# Novas ferramentas baseadas em abordagens de espetrometria de massa para a identificação de lípidos complexos nitrados

# New tools based on mass spectrometry approaches for the identification of nitrated complex lipids

**Universidade de Aveiro** Departamento de Química
**Ano 2020**

**Bruna Filipa Brito Neves**

# Novas ferramentas baseadas em abordagens de espetrometria de massa para a identificação de lípidos complexos nitrados

# New tools based on mass spectrometry approaches for the identification of nitrated complex lipids

Tese apresentada à Universidade de Aveiro para o cumprimento dos requisitos necessários à obtenção do grau de Mestre em Bioquímica com especialização em Métodos Biomoleculares, realizada sob a orientação científica da Doutora Tânia Melo, Investigadora Doutorada (Nível I) do Departamento de Química da Universidade de Aveiro, e da Doutora Maria do Rosário Domingues, Professora Associada com Agregação do Departamento de Química da Universidade de Aveiro

Apoio financeiro de fundos de Investimento Europeus FEDER/COMPETE/POCI – Operational Competitiveness and Internationalisation Programme, à Unidade de Investigação de Química Orgânica da Universidade de Aveiro (FCT UID/QUI/00062/2019), ao Laboratório Associado LAQV-REQUIMTE da Universidade de Aveiro (UIDB/50006/2020), ao Laboratório Associado Centro de Estudos do Ambiente e do Mar (CESAM) da Universidade de Aveiro (UIDB/50017/2020+UIDP/50017/2020) e à Rede Nacional de Espectrometria de Massa (LISBOA-01-0145-FEDER-402-022125)

Dedico este trabalho aos meus pais

*"Sê tudo em cada coisa.*
*Põe quanto és no mínimo que fazes"*

Fernando Pessoa

**o júri**

presidente

Prof. Doutor Mário Manuel Quialheiro Simões
Professor Auxiliar do Departamento de Química da Universidade de Aveiro

vogais

Prof. Doutora Maria Manuel Silva Oliveira
Professora Auxiliar do Departamento de Química da Universidade de Trás-os-Montes e Alto Douro

Doutora Tânia Sofia Rodrigues de Melo
Investigadora Doutorada (Nível I) do Departamento de Química da Universidade de Aveiro

**agradecimentos**

Agradeço à Doutora Tânia Melo e à Professora Rosário Domingues pela orientação deste trabalho, pelos conhecimentos transmitidos, pela disponibilidade, rigor e incentivo constantes. Sinto-me muito grata por todas as oportunidades que me concederam, ao longo dos últimos três anos, para poder crescer como profissional e ser cada vez melhor.

Agradeço também aos restantes coautores dos trabalhos apresentados nesta tese pelo seu contributo.

De uma forma geral, agradeço aos colegas e amigos do grupo de Espectrometria de Massa pelo carinho como me receberem desde o início desta jornada, pela ajuda sempre que necessário e pelo agradável ambiente de trabalho. Agradeço à Doutora Cristina Barros pela amabilidade desde a minha chegada ao grupo e pelo apoio nos espectrómetros e no laboratório.

Aos meus pais, de uma forma muito especial, agradeço a oportunidade de me deixarem seguir os meus sonhos e a confiança que depositam em mim todos os dias. Agradeço a liberdade de escolha, a presença constante e força para seguir sempre em frente.

Ao João, à Ana, à minha madrinha, ao Rui e à Lili agradeço o amor e apoio incondicionais, o alento nos momentos bons e menos bons, e a compreensão pelo caminho que escolhi, que tantas vezes nos fez estar mais longe (fisicamente) do que perto.

Agradeço à Unidade de Investigação de Química Orgânica, da Universidade de Aveiro (FCT UID/QUI/00062/2019), ao Laboratório Associado para a Química Verde da Rede de Química e Tecnologia (LAQV-REQUIMTE) da Universidade de Aveiro (UIDB/50006/2020), ao Laboratório Associado do Ambiente e do Mar (CESAM) da Universidade de Aveiro (UIDB/50017/2020+UIDP/50017/2020) e à Rede Nacional de Espectrometria de Massa (LISBOA-01-0145-FEDER-402-022125).

O meu profundo agradecimento a todos os que, direta ou indiretamente, tornaram possível a realização desta tese.

**palavras-chave**

Fosfolípidos, glicerolípidos, *stress* nitrativo, *stress* nitroxidativo, lipoxidação, espetrometria de massa *tandem*

**resumo**

Nos últimos anos, o interesse em produtos que resultam de reações de nitração a nível endógeno tem crescido, nomeadamente os ácidos gordos nitrados ($NO_2$-FA), os quais têm sido considerados importantes moléculas de sinalização. Os $NO_2$-FA têm sido reportados *in vivo*, quer na sua forma livre quer na forma de aductos com proteínas, e mais recentemente foram detetados em fosfolípidos ($NO_2$-PLs) e triglicerídeos nitrados ($NO_2$-FA-TAG). Também já foram reportados aductos de $NO_2$-PLs com proteínas. Os $NO_2$-FA livres, esterificados ou na forma de aductos com proteínas têm sido detetados *in vitro* e *in vivo* usando abordagens baseadas em espetrometria de massa (MS), com ou sem separação por cromatografia líquida. Estas identificações têm sido possíveis através da deteção do seu padrão de fragmentação típico e pela presença de iões diagnóstico característicos em condições de espetrometria de massa *tandem* (MS/MS). No entanto, estudos recentes sobre a caracterização estrutural de $NO_2$-PLs sugeriram que estas informações podem variar dependendo do tipo de espectrómetro de massa e da técnica de dissociação utilizada para induzir a sua fragmentação em MS/MS. Esta é uma questão importante, podendo dificultar a identificação destes derivados nitrados e nitroxidados em amostras biológicas. Assim, o conhecimento dos melhores parâmetros para obter a informação mais útil em MS é crucial para a sua identificação. Deste modo, os objetivos deste trabalho são (a) identificar os padrões de fragmentação típicos em MS usando diferentes plataformas instrumentais, de modo a contribuir para uma melhor identificação dos derivados nitrados e nitroxidados de lípidos complexos obtidos a partir de modelos biomiméticos *in vitro*, e (b) desenvolver estratégias lipidómicas para melhorar a sua identificação em amostras biológicas complexas utilizando as metodologias baseadas em MS/MS.

Para alcançarmos os objetivos propostos, avaliamos o efeito da energia de colisão (NCE) em condições de MS/MS, utilizando dissociação induzida por colisão de alta energia (HCD) numa Q-Exactive Orbitrap, no padrão de fragmentação para identificar as condições de aquisição e os iões diagnóstico que melhor permitem detetar os PLs nitrados e, assim, permitir a sua identificação e quantificação em amostras biológicas.

Os fosfolípidos nitratos e nitroxidados foram sintetizados através de um sistema mimético de nitração *in vitro* com tetrafluoroborato de nitrónio ($NO_2BF_4$), que foi usado para nitrar moléculas padrão de fosfatidilcolina (PC) e fosfatidiletanolamine (PE). Os resultados obtidos mostraram que a intensidade da perda neutra (NL) característica de ácido nitroso ($HNO_2$, 47 Da) diminui com o aumento da NCE, tornando-se indetetável com uma NCE mais elevada. Contudo, os iões fragmento correspondentes aos aniões carboxilato dos ácidos gordos modificados, observados em espectros de MS/MS adquiridos na Q-Exactive Orbitrap, foram identificados como potenciais iões diagnóstico que permitem identificar fosfolípidos nitrados através de uma análise lipidómica por HCD-MS/MS. Esta metodologia foi aplicada na análise de extratos lipídicos de células co-cultivadas com PC nitrada, para a validação dos resultados obtidos

na caracterização de $NO_2$-PL em modelos biomiméticos. Os resultados obtidos neste capítulo demonstraram que a NCE usada influência significativamente a abundância relativa de iões diagnóstico dos PLs nitrados e nitroxidados determinando, assim, quais os iões fragmento observados sendo por isso um fator chave para o sucesso da identificação destes PLs nitrados em amostras biológicas.

Uma vez que o perfil de fragmentação dos PLs nitrados obtido em HCD-MS/MS demonstrou ser diferente do anteriormente reportado para a dissociação induzida por colisão (CID) em espectrómetros de massa do tipo Trapa Linear (LXQ-LIT), avaliamos as potencias diferenças na abundância relativa dos iões diagnóstico característicos e no padrão de fragmentação dos derivados nitroso e nitro de diferentes classes de PLs. Estas espécies foram obtidas após nitração *in vitro* e a sua caracterização foi realizada por MS/MS utilizando dois métodos diferentes de ativação de iões em MS/MS: CID em LXQ-LIT e HCD em Q-Exactive Orbitrap. Os resultados deste capítulo revelaram que as principais diferenças entre os espectros de MS/MS adquiridos em CID-LXQ-LIT e HCD-Orbitrap estão relacionadas com uma abundância relativa diferente e, consequentemente, uma intensidade distinta dos iões diagnóstico característicos dos PLs nitrados.

Os triglicerídeos nitrados e nitroxidados foram também caracterizados por HCD-MS/MS em Q-Exactive Orbitrap. O seu padrão de fragmentação incluí a presença de iões produto formados pela NL de $HNO_2$ com uma elevada abundância relativa, demonstrando ser semelhante ao padrão de fragmentação dos $NO_2$-PLs obtido em CID-LXQ-LIT.

No geral, os resultados obtidos nesta tese fornecem novos conhecimentos sobre a identificação do padrão de fragmentação característico de derivados nitrados e nitroxidados dos $NO_2$-FA esterificados com PLs e TAG utilizando abordagens baseadas em HCD-MS e MS/MS. Esta informação pode ser utilizada com sucesso na análise direcionada de lípidos nitrados e nitroxidados em amostras biológicas, em diferentes contextos, nomeadamente na saúde ou associado a doenças, e assim contribuir para determinar as propriedades biológicas e função sinalizadora *in vivo* destas moléculas nitradas.

**keywords**

Phospholipids, glycerolipids, nitrative stress, nitroxidative stress, lipoxidation, tandem mass spectrometry

**abstract**

Over the last years, the interest in products resulting from endogenous nitration reactions has increased, namely in nitro-fatty acids ($NO_2$-FAs) that are considered as important signaling molecules. Although $NO_2$-FA were detected *in vivo* as free species or adducted to proteins, esterified forms were only recently reported as nitrated phospholipid ($NO_2$-PLs) and nitrated triacylglycerides ($NO_2$-FA-TAG), together with the occurrence of lipoxidation adducts of $NO_2$-PLs. The free, esterified and nucleophilic-adducted $NO_2$-FA, generated in *in vitro* mimetic systems and *in vivo*, were detected using mass spectrometry (MS)-based approaches, coupled or not to liquid chromatography, with the identification of their typical fragmentation pattern and characteristic reporter ions under tandem MS (MS/MS) conditions. However, recent studies on the structural characterization of $NO_2$-PLs allowed to suggest that both the information can vary depending on the type of mass spectrometer and the dissociation technique used to induce the fragmentation. This is a key issue since it can hinder the identification of these nitrated and nitroxidized derivatives in biological samples. Thus, an understanding of what analytical parameters are best to obtain the most useful information is a key issue for the identification of these modified PLs species. In this way, the aims of this work are (a) the identification of typical fragmentation patterns using different MS instrumental platforms to improve the accurate detection of the nitrated and nitroxidized derivatives of complex lipids obtained from *in vitro* biomimetic models systems, and (b) the development of lipidomic strategies to improve their identification in complex biological samples using the optimized high-throughput MS-based methodologies.

To accomplish our goal, we first evaluate the influence of the normalized collision energy (NCE), under higher-energy collisional dissociation (HCD)-MS/MS conditions in Q-Exactive Orbitrap, in the fragmentation pattern to identify the most suitable acquisition conditions and reporter ions to detect nitrated PLs. This will contribute to identify and quantify these species in biological samples. Nitrated and nitroxidized PLs species were synthesized through an *in vitro* mimetic system of nitration with nitronium tetrafluoroborate ($NO_2BF_4$), which was used to nitrate phosphatidylcholine (PC) and phosphatidylethanolamine (PE) standards. The results showed that the intensity of the typical NL of nitrous acid ($HNO_2$, 47 Da) diminishes with increasing NCE, becoming non-detectable for a higher NCE. However, fragment ions corresponding to the carboxylate anions of the modified fatty acyl chain were identified as potential reporter ions to detect nitrated PLs when using the HCD-MS/MS in lipidomics analysis. This methodology was applied in the analysis of cell lipid extracts treated with nitrated PC, which allowed the detection of $NO_2$-PC and the validation of the developed methodology. The results obtained in this chapter revealed that the relative abundance of reporter ions of nitrated and nitroxidized PLs is significantly affected by the NCE applied. which in fact determines what fragment ions are

observed, being a key factor for the successful of the detection of these nitrated PLs in biological samples.

As the fragmentation fingerprinting of nitrated PLs obtained under HCD-MS/MS conditions revealed to be dissimilar to the one previously reported under collision-induced dissociation (CID)-MS/MS, we evaluated the potential differences on the relative abundance of the typical reporter ions and fragmentation pattern of nitroso and nitro derivatives of different classes of PLs. These species were generated *in vitro* and their characterization was performed using MS/MS approaches based on two different ion activation methods: CID in a LXQ-Linear Trap (LIT) and HCD in a Q-Exactive Orbitrap. The results presented in this chapter revealed that the major differences between MS/MS spectra from CID-LXQ-LIT and HCD-Orbitrap are related with different relative abundance, and consequently distinct intensity, of specific reporter ions of nitrated PLs.

Nitrated and nitroxidized triacylglycerides generated *in vitro* were also characterized by HCD-MS/MS in a Q-Exactive Orbitrap. Its fragmentation pattern included the typical NL of $HNO_2$ with a high relative abundance, revealing to be more similar with the fragmentation pattern of nitrated PLs obtained in CID-LXQ-LIT.

Overall, the results gathered in this thesis provide new insights into the nitrated and nitroxidized derivatives of esterified $NO_2$-FA in PLs and TAG, and the identification of their fragmentation fingerprinting based on advanced HCD-MS and MS/MS approaches. This information can be successfully used for targeted analysis of nitrated and nitroxidized lipids in biological samples, in different circumstances, namely in health and/or in disease conditions contributing to determine the biological properties and *in vivo* signaling actions of these nitrated molecules.

**Publications and communications**

The results presented in this thesis already originated one publication in an international scientific journal and one poster communication (as first author) in a national meeting.

**Poster communication**

Neves, B., Duarte, S., Domingues, P., Pérez-Sala, D., Oliveira, M.M., Domingues, R. and Melo, T. New tools for target identification of bioactive nitrated phospholipids in biological samples using lipidomics. Workshop CESAM “One Health Day – Emerging Diseases”, 11 November, University of Aveiro, Portugal, 2020.

**Publications in international scientific journals**

Neves, B., Duarte, S., Domingues, P., Pérez-Sala, D., Oliveira, M.M., Domingues, R. and Melo, T. Advancing target identification of nitrated phospholipids in biological systems by HCD specific fragmentation fingerprinting in Orbitrap platforms. *Molecules*. 25, 1-19 (2020).

## Contents

## List of Figures

**CHAPTER I**



**CHAPTER III**

## APPENDIX A. SUPPLEMENTARY MATERIAL OF SECTION III.1.

## CHAPTER I



## CHAPTER III



## APPENDIX A. SUPPLEMENTARY MATERIAL OF SECTION III.1.

| | |
|---|---|
| **2-cLA-TAG** | 1,3-dipalmitoyl-2-conjugated-linoleoyl-glycerol |
| **3-cLA-TAG** | 1,2-dipalmitoyl-3-conjugated linoleoyl-glycerol |
| **ABTS$^{\bullet+}$** | 2,20-azino-bis-3-ethylbenzthiazoline-6-sulphonic acid |
| **APCI** | Atmospheric pressure chemical ionization |
| **CID** | Collision-induced dissociation |
| **CL** | Cardiolipins |
| **DDA** | Data dependent acquisition |
| **DPPH$^{\bullet}$** | 2,2-diphenyl-1-picrylhydrazyl |
| **DTT** | Dithiothreitol |
| **dMPC** | 1,2-dimyristoyl-*sn*-glycero-3-phosphocholine |
| **dMPE** | 1,2-dimyristoyl-*sn*-glycero-3-phosphoethanolamine |
| **ESI** | Electrospray ionization |
| **Iac-B** | Biotinilated ioadoacetamide |
| **iNOS** | Inducible nitric oxide synthase |
| **GFP** | Green fluorescent protein |
| **GSNO** | S-nitrosoglutathione |
| **PC** | Phosphatidylcholine |
| **PE** | Phosphatidylethanolamine |
| **PIPES** | Piperazine-N,N′-bis(2-ethanesulfonic acid) |
| **PLs** | Phospholipids |
| **PS** | Phosphatidylserine |
| **HCD** | Higher energy collision-induced dissociation |
| **HESI-II** | Heated electrospray ionization |
| **HILIC** | Hydrophilic interaction liquid chromatography |
| **$HNO_2$** | Nitrous acid |
| **HPLC** | High performance liquid chromatography |
| **LC** | Liquid chromatography |
| **LIT** | Linear Ion Trap |
| **LPA** | Lysophosphatidic acid |
| **MAG+DAG** | Monoacyl- and diacylglycerides |
| **$[M+H]^+$** | Protonated ion |
| **$[M-H]^-$** | Deprotonated ion |
| **$[M+OAc]^-$** | Acetate adducts |
| **MS** | Mass spectrometry |
| **MS/MS** | Tandem mass spectrometry |
| **$MS^n$** | Multistage tandem mass spectrometry |
| **NL** | Neutral loss |
| **NMR** | Nuclear magnetic resonance |
| **$NO_2BF_4$** | Nitronium tetrafluoroborate |
| **$NO_2$-FA** | Nitro-fatty acids or Nitroalkene derivatives of fatty acids |
| **$NO_2$-OA** | Nitro-oleate or Nitro-oleic acid |
| **$NO_2$-LA** | Nitro-linoleic acid |
| **$NO_2$-cLA** | Nitro-conjugated linoleic acid |

| | |
|---|---|
| **$NO_2$-SA** | Nitro-stearic acid |
| **OA** | Oleic acid |
| **ORAC** | Oxygen radical absorbance capacity |
| **PA** | Phosphatidic acid |
| **PAPC** | 1-palmitoyl-2-arachidonoyl-*sn*-glycero-3-phosphocholine |
| **PAPE** | 1-palmitoyl-2-arachidonoyl-*sn*-glycero-3-phosphoethanolamine |
| **PLPC** | 1-palmitoyl-2-linoleoyl-*sn*-glycero-3-phosphocholine |
| **PLPE** | 1-palmitoyl-2-linoleoyl-*sn*-glycero-3-phosphoethanolamine |
| **POPC** | 1-palmitoyl-2-oleoyl-*sn*-glycero-3-phosphocholine |
| **POPE** | 1-palmitoyl-2 oleoyl-*sn*-glycero-3-phosphoethanolamine |
| **POPS** | 1-palmitoyl-2-oleoyl-*sn*-glycero-3 phosphoserine |
| **Q** | Quadrupole |
| **RNS** | Reactive nitrogen species |
| **ROS** | Reactive oxygen species |
| **TLCL** | Tetralinoleoyl cardiolipin |
| **TOF** | Time-of-flight |

# Chapter I. INTRODUCTION

## I.1. Reactive nitrogen species (RNS) and Free nitro-fatty acids

Reactive nitrogen species (RNS) has different reactivity towards biomolecules and include species as nitric oxide ($^{\bullet}NO$), nitrogen dioxide ($^{\bullet}NO_2$), nitronium cation ($NO_2^+$) or peroxynitrite ($ONOO^-$)/peroxynitrous acid (ONOOH), which decompose to yield $^{\bullet}NO_2$ and hydroxyl radical ($^{\bullet}OH$)[1,2]. Generation and action of RNS are usually associated with reactive oxygen species (ROS)[2–4] and both have key regulatory functions playing roles as signaling molecules in health and disease[1,3]. RNS can easily diffuse and accumulate in the hydrophobic environment of the biological membranes[2], where they can act as potent oxidizing and/or nitrating agents, responsible for mediate nitration, nitrosation, nitroxidation and/or oxidation of biomolecules, such as membrane lipids[4,5]. However, the choice for one process over the others and the yield of these reactions is dependent on several factors including the site of production of the reactive species, the amount of RNS versus ROS; pH; the oxygen levels; the partition between hydrophobic and hydrophilic cellular compartments; and the presence of secondary target molecules (transition metals, thiols and scavengers)[6].

Nitration reactions occur under nitrative stress conditions and correspond to the covalent addition of a nitro group ($NO_2$) to biomolecules. In the case of lipids, RNS can modify unsaturated fatty acids (FA) via non-enzymatic reactions with formation of nitro derivatives of FA, also called nitroalkene derivatives or nitro-fatty acids ($NO_2$-FA)[6,7]. The exact mechanism of FA nitration *in vivo* remains far from being completed undisclosed; however, some proposals have been considered to explain the generation of $NO_2$-FA, namely electrophilic substitution, and free radical-induced nitration. The free radical-induced nitration of FA mediated by nitrogen dioxide ($^{\bullet}NO_2$) is the most prominent nitration process *in vivo*[8], which can occur during digestion[9], metabolic stress and inflammation[10]. This mechanism of nitration, which is mediated by $^{\bullet}NO_2$ and occurs at low oxygen tension, involves a homolytic attack to the double bond of the unsaturated FA yielding a β-nitroalkyl radical capable to react with a second $^{\bullet}NO_2$ to generate a nitronitrite or dinitro intermediate. Nitroalkenes derivatives are further generated from these intermediates due the loss of nitrous acid ($HNO_2$). The nitro-hydroxy derivatives of FA can also be formed from the hydrolysis of these intermediates. Electrophilic substitution at the double bond mediated by $NO_2^+$ also yields $NO_2$-FA[11], as summarized in Figure I.1.

The generation of $NO_2$-FA can be considered as the first step of nitration reactions. During both electrophilic and free-radical-mediated nitration of FA, the $NO_2$-FA do not represent the final products; $NO_2$-FA are prone to be further nitrated or oxidized, which make them precursors of other modified derivatives. $NO_2$-FA can undergo additional reactions with RNS to be further nitrated to yield nitronitroso or dinitro derivatives. Under oxidative stress conditions, nitroxidation reactions can also occur leading to the generation

of modified derivatives that combine both nitro and oxidized modifications, also referred as nitroxidized derivatives (i.e. nitro-hydroxy, nitro-hydroperoxy, nitro-epoxy and nitro-keto). Different positional isomers have also been identified for all of these nitrated and nitroxidized derivatives[12,13].

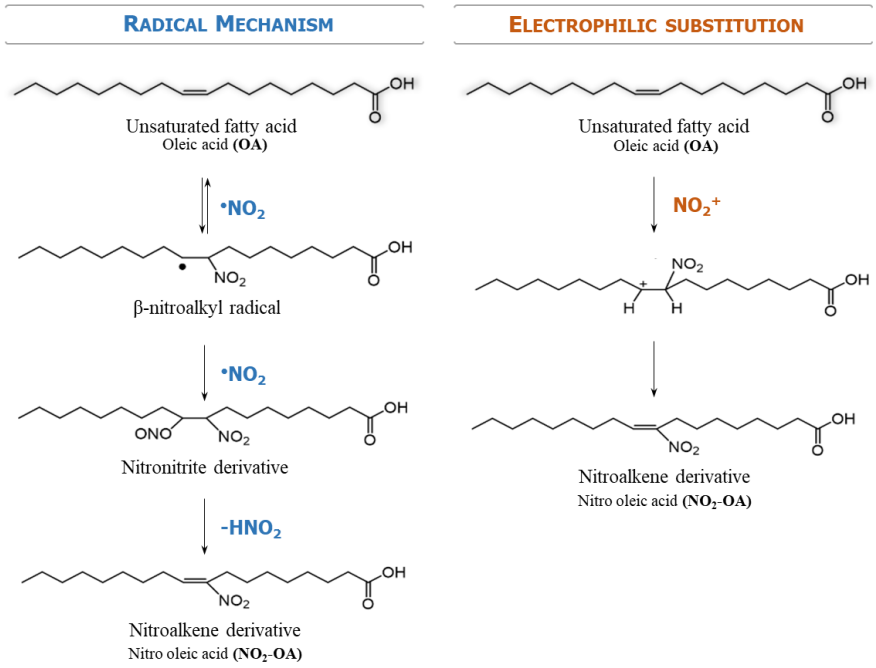


**Figure I.1.** Representative mechanisms of nitration of free $NO_2$-FA exemplified for oleic acid (OA).

Nitro-oleate or nitro-oleic acid ($NO_2$-OA), which is the nitro derivative of oleic acid (OA, 18:1n-9), is the $NO_2$-FA that is mostly studied[13]. On the other hand, conjugated linoleic acid ($NO_2$-cLA) has been reported as the most suitable FA to undergo nitration *in vivo* and *in vitro*[14]. However, other $NO_2$-FA and nitroxidized derivatives have also been identified and characterized in different biological samples as red blood cells, urine, plasma and tissues under (patho)physiological conditions within a dynamic range from pico to micromolar, as recently reviewed[13]. Two studies using experimental models as myocardial ischemia and reperfusion[15,16] demonstrated that the amounts of $NO_2$-FA significantly increase under oxidative stress and inflammatory conditions. Nevertheless, half-life, steady-state levels and signaling activities of $NO_2$-FA can be regulated by their different metabolic pathways. $NO_2$-FA are irreversibly inactivated by prostaglandin reductase-1 (PGR-1)[17]. Packing into complex lipids in lipoproteins (mainly chylomicrons and VLDL) and conjugation with albumin's hydrophobic pockets allows $NO_2$-FA to reach the systemic circulation for transport and distribution among biological compartments to exert biological actions, to be metabolized or inactivated[18–20]. Also, esterification in complex lipids and adduction to

peptides/proteins contribute to $NO_2$-FA stabilization. These are considered the most abundant reservoirs of $NO_2$-FA until further mobilization to display their biological actions[21,22]. Nucleophilic adduction with glutathione (GSH) has been associated with $NO_2$-FA inactivation, subsequent mitochondrial β-oxidation and excretion through urine[23].

Research work on nitration of FA has been mainly related to animal systems being scarcely studied in plants, even nowadays. $NO_2$-FA were only recently identified in plants. Nitro-linoleic acid ($NO_2$-LA, 18:2n-6) was identified in both cell-suspension cultures and seedlings of the model plant *Arabidopsis thaliana*, in the roots, leaves and subcellular (mitochondrial and peroxisomal) fractions from pea (*Pisum sativum*) and in leaves from rice (*Oryza sativa*) plants, while $NO_2$-cLA and $NO_2$-OA were found in extra-virgin olive oil and fresh olives, respectively[24–26].The modulation of $NO_2$-FA levels occurs not only during plant's development but also in response to increased levels of ROS and RNS. As in animal systems, increased levels of $NO_2$-FA were detected in *Arabidopsis* plants under abiotic stress conditions such as mechanical wounding, low temperature, and cadmium stress, as well as in cell-suspension cultures under salinity-induced stress[24]. These external sources, rising mainly from the ingestion of plants, extra-virgin olive oil and fresh olives, contribute to rise and modulate the endogenous levels of $NO_2$-FA. Therefore, $NO_2$-FA can be obtained from dietary consumption or generated endogenously either by $^{\bullet}NO_2$-mediated reactions during digestion, inflammation, and stressful conditions or after acidic-catalyzed nitrite ($NO_2^-$) reactions in gastric compartment (Figure I.2). The combination of the acidic conditions of the stomach, the presence of free or esterified FA and RNS (as $NO_2^-$ and $^{\bullet}NO_2$ generated from acid-induced decomposition of dietary $NO_2^-$ in stomach) leads to the gastric generation of $NO_2$-FA. Upon absorption at intestinal level and endogenous distribution via plasma to target tissues, $NO_2$-FA can exert their protective effects.

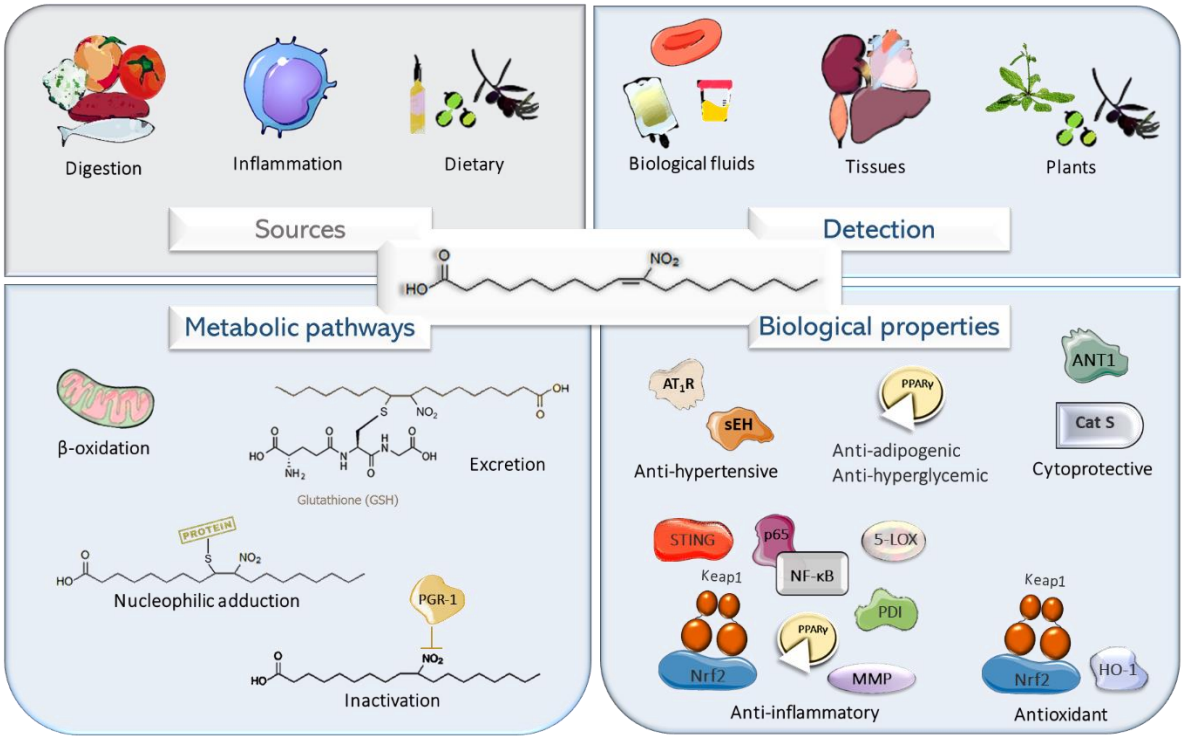


**Figure I.2.** Overview of generation, identification, metabolic pathways and biological activities of free nitro-fatty acids.

Despite nitration of FA leads to an array of nitrated and nitroxidized derivatives, the $NO_2$-FA are the most studied products of nitration reactions. In fact, the formation of $NO_2$-FA both in animals and plants has been associated with several biological activities as it will be described in the following section.

### I.1.1. Formation and biological activities of Free nitro-fatty acids

The interest of the scientific community in $NO_2$-FA has been raised in last years. This is mainly due to the knowledge on their biological roles and the recognition of their pluripotent signaling actions in animal systems[13] (Figure I.2.). $NO_2$-FA were reported to be one of the main players in the health benefits associated with the Mediterranean diet, namely the decrease in the risk of cardiovascular disease[27]. Nitroalkenes indeed demonstrated to afford beneficial effects in a variety of preclinical animal models of disease, namely cardiovascular disease[28,29], nephropathy and renal ischemia/reperfusion[30], myocardial ischemia/reperfusion and ischemia preconditioning[15,30,31], diabetes and metabolic syndrome[32], pulmonary inflammation[33,34] and chronic inflammatory disease[35]. The obviously considerable therapeutic potential of $NO_2$-FA prompted the research to move forward to human trials. Phase II clinical trials using 10-nitro-oleic acid, CXA-10 (10-nitro-9(E)-octadec-9-enoic acid), are underway for the treatment of patients with focal segmental glomerulosclerosis and pulmonary arterial hypertension. $NO_2$-FA appear to be well tolerated

when administered via intravenous injections or orally, and demonstrated favorable pharmacokinetics, tolerability and safety[36–38]. More recently, the role of $NO_2$-FA in the modulation of antioxidant responses and plant-defense mechanism against oxidative stress due to abiotic stress conditions was demonstrated by the research works of Mata-Pérez and co-authors[24,39].

The $NO_2$-FA's signaling roles are mediate through different processes including (a) aqueous decay reactions and transduction of •NO signaling[32,40]; (b) receptor-dependent signaling actions namely by triggering and regulating peroxisome proliferator-activated receptor gamma (PPARγ)-dependent expression of target genes in the immune system or relevant to inflammatory diseases[41–44]; and (c) electrophilic adduction to proteins[13,24,26,33].

The release of •NO by $NO_2$-FA in animal systems has been associated with vasorelaxation properties[8,21,45,46]. Inhibition of lipid peroxidation process and antioxidant properties[47], and anti-inflammatory actions[48] have also been associated with the capacity of $NO_2$-FA to release and act as •NO donors. Also in plant, $NO_2$-LA (18:2 n-6) revealed to be able to release •NO *in vitro* by using different experimental approaches including in *Arabidopsis* cell cultures[39] and *in vivo* from *Arabidopsis thaliana* roots[49] and leaves[50]. In this case, release of •NO from $NO_2$-FA was suggested to potentially play a key role in plant development, in several biotic and abiotic processes, in the modulation of antioxidant responses against abiotic stress conditions, and in post-translational modifications (PTMs) of proteins mediated by •NO[49]. The exact mechanism by which $NO_2$-FA can generate •NO in aqueous environments remains to be completely elucidated. A modified Nef reaction with formation of a nitroso-hydroxy intermediate able to generate •NO[21] or alternatively a rearrangement in the $NO_2$-FA structure with isomerization of the nitroalkene moiety to a $NO_2^-$ ester followed by N–O bond hemolysis[45] are the two mechanisms proposed and accounting for the generation of •NO from $NO_2$-FA. Nevertheless, the release of •NO from $NO_2$-FA in animal systems is considered to be of minor biological significance as the incorporation and stabilization of $NO_2$-FA in lipoproteins and lipid membranes inhibits the release of •NO[21] in hydrophobic compartments. Also, low yields of •NO decay from $NO_2$-FA accounted for less than 1% *in vitro*[46]. Otherwise, •NO release from $NO_2$-FA in plants was 4.7-40-fold higher than in animal systems, which may be high enough for potential and relevant biological effects in plants[25].

The electrophilic capacity of $NO_2$-FA, due to the presence of a nitroalkene moiety, is seen as the main mechanism underlying its biological and modulatory signaling actions[13,51]. The high electronegativity and electron-withdrawing power of the $NO_2$ group makes the methylenic β-carbon adjacent to the $NO_2$ group electron poor and with potential susceptibility to nucleophilic attack. This enables the occurrence of reversible covalent

reaction between the $NO_2$-FA and target nucleophiles in peptides and proteins, namely the deprotonated thiolate group of cysteine through S-nitroalkylation, and the nucleophilic amino group of the imidazole moiety of histidine or the amino groups of lysine and arginine via Michael addition[13,51,52]. Thereby, protein's PTMs and the formation of nitro-lipoxidation adducts occurs, whose reversible nature is associated with apparent lack of toxicity and the possibility of redox regulation[13,22].

The PTMs induced by the presence of the $NO_2$-FA moiety lead to alteration/modulation of the structure and localization/distribution of target proteins and, consequently, culminates in the regulation of their function. This will trigger a series of downstream redox signaling events, which will impact the patterns of gene expression programs, enzyme function and activity, metabolic and inflammatory responses, and cell signaling networks[53,54].This way, through the generation of $NO_2$-FA-protein adducts, $NO_2$-FA display their biological roles as anti-inflammatory, anti-hypertensive, anti-thrombotic agents and anti-tumorigenic agents and cytoprotective effects (as reviewed by Melo and co-authors[13]). Largely characterized protein targets to undergo S-nitroalkylation and Michael addition with $NO_2$-FA in animal systems include: p65 subunit of nuclear factor kappa B (NF-κB); heme oxygenase-1 (HO-1); mitogen-activated protein kinase (MAPK) phosphatase 1 (MPK-1); Kelch-like ECH associated protein 1 (Keap 1); metalloproteinases (MMP-7 and MMP-9); glyceraldehyde-3-phosphate dehydrogenase (GAPDH); protein disulfide isomerase (PDI); and transient receptor potential (TRP) channels; PPARγ; 5-lipoxygenase (5-LOX); and soluble epoxide hydrolase (as reviewed by Melo and co-authors[13]). Ascorbate peroxidase, a primary antioxidant systems in plants, was recently identified as a target to undergo Michael addition reaction with $NO_2$-LA[55], suggested to block protein's enzymatic activity thus modulating its function (Figure I.2.).

$NO_2$-FA properties are closely related with their metabolism, structural features, levels and place of generation, which may influence the type of targets where they can act[44,56]. Reduction of $NO_2$-FA by PGR-1 is considered the main mechanism of the inactivation of electrophilic character of $NO_2$-FA yielding non-electrophilic nitroalkanes derivatives[17]. Mitochondrial β-oxidation leads to generation of $NO_2$-FA with shorter chains, which have high hydrophilicity. This has an impact not only on the distribution profile and partitioning of $NO_2$-FA between hydrophobic and hydrophilic compartments but also in the chemical reactivity and pharmacological profiles by altering accessibility to their targets [22]. Chain length and the position of the $NO_2$ group makes some $NO_2$-FA structural isomers more reactive towards protein targets, and thus more biologically active, than others[57]. In the next section it will be described the mass spectrometry (MS) and tandem mass spectrometry

(MS/MS)-based approaches that have been used for the analysis of nitrated and nitroxidized FA and the $NO_2$-FA-protein adducts from *in vitro* models and *in vivo* samples.

### I.1.2. Identification and characterization of Free nitro-fatty acids by MS

The detection and accurate quantification of $NO_2$-FA in biological samples (animals or plants) is a remarkable challenge hampered by several factors. The low relative amounts, artefactual generation during sample work-up and chromatographic analysis under acidic pH conditions, requirement of extensive control experiments, sensitivity to light, and thermally instability are major analytical issues in the analysis of $NO_2$-FA[13,58]. Moreover, metabolic pathways such as mitochondrial β-oxidation[22]; electrophilic capacity and reversible protein adduction reactions[13,24,26,54,59]; esterification and incorporation into complex lipids[20,60–62]; irreversible inactivation by PGR-1 with formation of non-electrophilic nitroalkanes[17] or inactivation through conjugation with reduced GSH for further excretion in urine[23], and different distribution among tissues and biofluids[21,43] also hinder the detection and quantitative measurements of $NO_2$-FA.

The advances in mass spectrometry (MS) methodologies and instruments have achieved a higher sensitivity level suitable for the identification of these key signaling molecules. High-throughput MS and tandem MS-based lipidomics approaches has contributed to the detection, quantification and structural characterization of free $NO_2$-FA, along with their positional and functional isomers, and lipoxidation adducts[12,13,63].

Detection and quantitation of several $NO_2$-FA, but also nitroxidized derivatives and isomeric species, in biomimetic models, plants, tissues, cells and biofluids has been performed by MS and MS/MS-based lipidomics approaches using either untargeted or targeted approaches, and coupled or not to reversed phase (RP) liquid chromatography (LC), in different MS-platforms (Linear Ion Trap, Q-Trap, Triple quadrupole, Orbitrap) (as recently reviewed by Melo and co-authors[13]). Biomimetic systems include the incubation of pure FA standards (oleic, linoleic, conjugated linoleic, cholesteryl linoleic, or arachidonic acids) with chemically synthetized RNS such $NO_2^-$ in acidic conditions[26,64], $ONOO^-$, $NO_2^+$ and $^{\bullet}NO_2$[12,43] or mimicking gastric conditions of digestion with artificial gastric juice and $NO_2^-$[26]. With these simple approaches it is possible to generate an array of nitrated and nitroxidized derivatives of FA in relatively high yields for an in-depth characterization of the type of modifications that can occurs in biological systems. Among the biological samples where nitro or nitroxidized derivatives of palmitoleic, oleic, linoleic, conjugated linoleic, cholesteryl linoleic, linolenic, arachidonic, eicosapentaenoic, docosahexaenoic, or docosapentaenoic acids were detected, it is possible to highlight plasma, red blood cells and urine from (un)healthy humans, or different cellular and murine models of inflammation

and myocardial ischemia-reperfusion (as reviewed by Melo and co-authors[13]). Plant-derived models, extra-virgin olive oil and fresh olives were used to screen the presence of $NO_2$-FA from plant origin[24–26].

$NO_2$-FA are preferentially analyzed by MS in negative-ion mode as $[M-H]^-$ ions[64] but they can also be analyzed in positive-ion mode as $[M+H]^{+}$[12], $[M+Li]^{+}$[65] , $[M+Na]^{+}$[66] and $[M+NH_4]^{+}$[62] ions. Identification at MS level is based on specific mass shifts depending on the type of modification and the switch of FA *m/z* value's from odd (unmodified FA) to even ($NO_2$-FA) due to addition of a nitrogen-containing moiety. Under MS/MS conditions, product ions of $NO_2^-$ (*m/z* 46) can be observed in negative-ion mode. The typical neutral loss (NL) of 47 Da ($HNO_2$) and product ions due to cleavage of the hydrocarbon chain in the vicinity of the $NO_2$ group can be found both in positive- and negative-ion mode. Thus, positional isomers of $NO_2$-FA can be discriminated through the presence of fragment ions formed by cyclization followed by heterolytic carbon chain fragmentation, which generates almost exclusively moieties containing an aldehyde and a nitrosamine. For the polyunsaturated $NO_2$-FA, products ions derived from cyclization reactions yielding 5- or 6-atom heterocycles were also found[12,67].

Identification of reversible PTMs of peptides/proteins by $NO_2$-FA has been performed in biomimetic studies comprising the incubation of $NO_2$-FA and peptides/protein standards in controlled reactions systems with further MALDI or ESI-MS and MS/MS analysis, with or without RP-LC and tryptic digestion. Detection under MS conditions is usually performed in positive-ion mode as singly, $[M+H]^+$ ions, or multiple charged ions, $[M+nH]^{n+}$, based on the mass increment against the unmodified peptide due to the $NO_2$-FA covalently attached. MS/MS data provide information on the typical fragmentation pathways of $NO_2$-FA-peptide/protein adducts, which allows to confirm the nature of the modification, pinpoint the location and the target residues for adduction, and establish the characteristic reporter ions based on the identification of specific mass shifts of the typical b, y and immonium ions of peptide[59]. The $NO_2$-FA moiety will induce alterations in the fragmentation fingerprint and will increase the retention time of the modified peptides[59], thus different chromatographic behavior under RP-LC-MS.

The knowledge gathered aid the detection of these nitro-lipoxidation adducts in complex biological samples from animal origin (cells, tissues, biological fluids) and in plants using RP-LC-MS-based bottom-up proteomics approaches. Modified peptides obtained after tryptic digestion of $NO_2$-FA-protein adducts are possible to be unequivocally identified by (un)targeted analysis using different MS platforms (as MALDI TOF/TOF, Linear Ion Trap, Orbitrap, Q-Trap, or triple quadrupole)[13]. Confirmation of $NO_2$-FA-proteins adducts is

usually performed by β-mercaptoethanol (BME) trans-nitroalkylation, through the exchange of $NO_2$-FA from proteins to BME.

These methodological approaches were used to detect several $NO_2$-FA-peptides/protein lipoxidation adducts as reviewed by Melo and co-authors[13] including (a) $NO_2$-OA or $NO_2$-LA with GAPDH and GSH *in vivo* in healthy human red cells; (b) $NO_2$-OA and thiols of proteins and GSH in liver and plasma of $NO_2$-OA-treated mice; (c) $NO_2$-OA-protein adducts via cysteine residue in fresh olives; (d) $NO_2$-OA with Keap1 in Keap 1-transfected HEK-293T cells treated with $NO_2$-OA; (e) $NO_2$-OA and angiotensin II type 1 receptor (AT1-R) in HEK-293T cells overexpressing AT1R treated with $NO_2$-OA; (f) $NO_2$-OA or $NO_2$-LA with albumin in the plasma from $NO_2$-FA-treated mice; (g) $NO_2$-OA with PPAR-γ in PPARγ-transfected HEK-293T cells treated with $NO_2$-OA; (h) $NO_2$-OA with stimulator of IFN genes (STING) in STING-transfected HEK-293T cells treated with 10-$NO_2$-OA; (i) $NO_2$-OA with p65 subunit of Nk-KB from heart tissue of $NO_2$-OA-treated mice; (j) $NO_2$-OA with metalloproteinase, Fp subunit of mitochondrial complex II and Catephsin S; (k) $NO_2$-LA-GSH adducts *in vitro* and in $NO_2$-LA-treated MCF7 cells; (l) $NO_2$-LA with adenine nucleotide translocase 1 (ATN 1) after $NO_2$-FA infusion into intact perfused heats; (m) $NO_2$-AA with PDI.

With these research works was possible to unveil the reactivity of $NO_2$-FA to be dependent on the position of the $NO_2$ and chain length, and cysteine and histidine residues to be the main targets to undergo lipoxidation reactions[13].

More recently, ascorbate peroxidase recombinant protein from *Arabidopsis thaliana* was also unveiled as a target form Michael addition reaction. Its incubation with increasing concentration of $NO_2$-LA and C18-LC-MS/MS analysis in Q-Exactive hybrid quadrupole Orbitrap® after tryptic digestion showed two histidine residues (His 43 and His 163) to be the preferential targets for PTMs[55]. In fact, the dynamic metabolism of $NO_2$-FA due its ability to react with proteins or to be esterified in complex lipids makes their identification and characterization a challenge. In the next chapter it will be described the identification and biological potential of nitro-fatty acids esterified in complex lipids, including phospholipids (PLs) and glycerolipids.

### I.2. Esterified nitro-fatty acids

Recent research in the field of lipid nitration has demonstrated that $NO_2$-FA can occur *in vivo* as esterified forms in complex lipids as nitrated and nitroxidized derivatives of phospholipids (PLs)[19,20,60,61,68] and glycerolipids (*e.g*. triacylglycerides, TAG) [19,33,62].

Free fatty acids are present in low abundance in cells, tissue compartments and foodstuffs; FA are more commonly found as part of more complex lipids. RNS in its turn are able to accumulate within the hydrophobic environment of biological membranes [29,63,69] where FA esterified in PLs are predominant. In this way it is expected that FA incorporated in PLs to be targets of nitration and nitroxidation reactions to generate nitrated and nitroxidized derivatives of PLs, via free-radical mechanisms or electrophilic substitutions as reported for $NO_2$-FA (Figure I.3.).

Moreover, FA are also present as part of the energy-storage glycerolipids. The acidic gastric conditions during digestion promotes a nitroxidative environment propitious to the generation of $NO_2$-FA. Dietary $NO_2$-FA esterified into TAG can be targets to undergo acid-catalyzed nitration by dietary $NO_2^-$ in stomach, where the acidic conditions of digestion also favors the generation of $^{\bullet}NO_2$ from $NO_2^-$, thus free radical-mediated nitration reactions. In this regard, esterified forms of $NO_2$-FA can be generated either by direct nitration of the esterified fatty acyl moiety or by the incorporation of free $NO_2$-FA into complex lipids[19,20,62]. Specific patterns of incorporation in complex lipids were reported for $NO_2$-FA where the higher the unsaturation degree the lower the net extents of esterification[20].

Regardless being generated from direct nitrated or upon esterification, nitrated and nitroxidized derivatives of complex lipids may serve as a pool of electrophilic $NO_2$-FA to be further mobilized by (phospho and lipoprotein)lipases or can be seen as a mechanism for their bio-distribution. Moreover, it can also provide new opportunities for better understanding the metabolism, pharmacokinetics, and the potential biological and pharmacological actions of $NO_2$-FA[20,62].

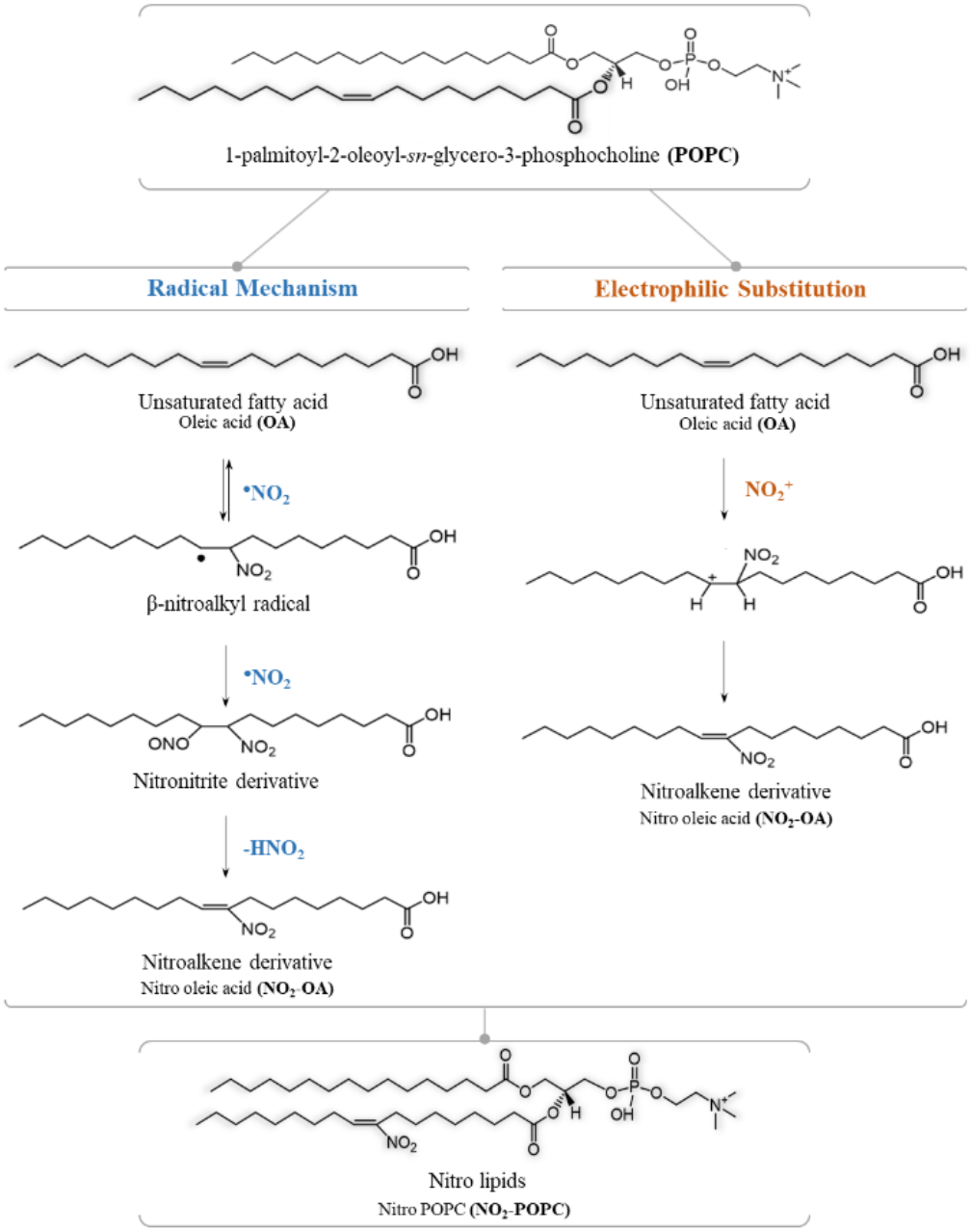


**Figure I.3.** Representative mechanisms of nitration of esterified $NO_2$-FA exemplified for phosphatidylcholine (PC) containing the oleic acid (OA). Nitrogen dioxide ($^{\bullet}NO_2$) reacts with esterified OA moiety to form the β-nitroalkyl radical that reacts with other $^{\bullet}NO_2$ leading to the generation of a nitronitrite derivative. Subsequently occurs the loss of $HNO_2$ with formation of esterified $NO_2$-OA. On the other hand, electrophilic substitution at the double bond mediated by nitronium cation ($NO_2^+$) also yields $NO_2$-OA-PC.

Similarly to reported for $NO_2$-FA, detailed identification, structural characterization and quantification of nitrated complex lipids has been performed using ESI-MS and MS/MS-based lipidomics approaches, coupled or not to LC[19,20,60–62]. Nevertheless, this is a topic of research that it is still in its infancy. A quick search on Scopus by "nitrated phospholipids" display a total of 6 publications (excluding review articles) between 2016-2020, while "nitroalkenes in triacylglycerides" return only 3 publications (excluding review articles) between 2015-2020. This shows the novelty and the need of further research in the field of complex lipid nitration/nitroxidation.

In the next section it will be described the MS-based lipidomics approaches that have been used for the detection of nitrated and nitroxidized derivatives of PLs and TAG, and the biological properties already reported for esterified $NO_2$-FA.

### I.2.1. Nitrated phospholipids detected by MS

Single and multiple nitrated and nitroxidized PLs derivatives, including different positional and functional isomers, were reported for phosphatidylcholine (PC), phosphatidylethanolamine (PE), phosphatidylserine (PS) and cardiolipin (CL) using *in vitro* biomimetic models. In these studies, direct nitration of esterified FA moiety has occurred after incubation of synthetic PLs standards with nitronium tetrafluoroborate ($NO_2BF_4$) in hydrophobic environments[60,61,68,70], as summarized in Table I.1. In these studies, detection of nitrated complex lipids was based on the identification of specific mass shifts under MS conditions depending on the type of modification. These mass shifts include ions with +29 Da in the case of nitroso derivatives, +45 Da in the case of nitro or nitroso-hydroxy derivatives (29 Da + 16 Da from hydroxy group), + 74 Da in the case of nitro-nitroso derivatives or +90 Da in the case of dinitro derivatives (Table I.2). Therefore, multiple nitrated derivatives can be detected by the mass increments corresponding to the insertion of successive modifications, while nitroxidized species correspond to the simultaneous presence of nitrated derivatives and oxidative modifications, with mass increments of +16 Da (hydroxy group) and +32 Da (hydroperoxy group). In Figure I.4. it is exemplified the presence of these ions for nitrated 1-palmitoyl-2-oleoyl-*sn*-3-phosphocholine (POPC). Detailed structural characterization of these modified species was performed by MS/MS-based approaches in positive- ($[M+H]^+$ for PC, PE and PS) and negative-ion mode ($[M-H]^-$ for PE, PS and CL; $[M+OAc]^-$ for PC) using LXQ-Linear Ion Trap (LIT) or Q-Exactive Orbitrap instrument, with or without C5 or C30-RP-LC-ESI-MS[60,61,68,70], which allowed to identify the typical fragmentation profile of each modified derivative.

**Table I.1.** Nitrated complex lipids identified using *in vitro* biomimetic model systems.

| ***In vitro* biomimetic model systems** | | | |
|---|---|---|---|
| **Nitrated species** | **Experimental model** | **Method** | **Ref.** |
| Nitro derivative of POPC, PLPC, PAPC, POPE, PLPE, PAPE, POPS, PLPS, and PAPS with identification of positional isomers: 9- and 10-$NO_2$-OA-PL; 9-, 10- and 13-$NO_2$-LA-PL; and 11-, 12-, 14-, and 15-$NO_2$-AA-PL | Incubation of each PL standard (1 mg) with $NO_2BF_4$ (1 mg) in $CHCl_3$ (1 mL) for 1h, r.t. at 750 rpm | Direct infusion ESI-MS and CID-MS/MS using LXQ-LIT, both in positive- and negative-ion mode<br>Direct infusion ESI-MS using Q-TOF 2 hybrid quadrupole time-of-flight, in positive-ion mode | 60 |
| (Di)Nitroso, (di)nitro, nitronitroso, and nitroxidized derivatives ((NO)O-PL, $(NO_2)$O-PL, $(NO_2)$(2O)-PL, $(NO_2)_2$O-PL, $(NO_2)_2$(2O)-PL) of POPC, PLPC, PAPC, POPE, PLPE, and PAPE | Incubation of each PL standard (1 mg) with $NO_2BF_4$ (1 mg) in $CHCl_3$ (1 mL) for 1h, r.t. at 750 rpm | Direct infusion ESI-MS and CID-MS/MS using LXQ-LIT, both in positive- and negative-ion mode<br>C5-RP-LC-ESI-MS and CID-MS/MS using Waters Alliance 2690 HPLC system coupled online to LXQ-LIT mass spectrometer, both in positive- and negative-ion mode | 61 |
| NO-POPS<br>$NO_2$-POPS<br>$(NO_2)$O-POPS<br>$(NO_2)$(NO)-POPS<br>$(NO_2)$(2O)-POPS<br>$(NO_2)_2$-POPS | Incubation of POPS (1 mg) with $NO_2BF_4$ (1 mg) in $CHCl_3$ (1 mL) for 1h, r.t. at 750 rpm | Direct infusion ESI-MS and CID-MS/MS using LXQ-LIT mass spectrometer, in negative-ion mode. Direct infusion ESI-MS and HCD-MS/MS using Q-Exactive hybrid quadrupole Orbitrap® mass spectrometer, in negative-ion mode<br>C5-RP-LC-ESI-MS and CID-MS/MS using Waters Alliance 2690 HPLC system coupled online to LXQ-LIT mass spectrometer, in negative-ion mode | 68 |
| NO-TLCL<br>$(NO)_2$-TLCL<br>$(NO)_3$-TLCL<br>$(NO)_4$-TLCL<br>$NO_2$-TLCL<br>$(NO_2)_2$-TLCL<br>$(NO_2)$(NO)-TLCL<br>(NO)O-TLCL<br>$(NO)_2$(2O)-TLCL<br>$(NO_2)$(NO)O-TLCL | Incubation of TLCL (1 mg) with $NO_2BF_4$ (1 mg) in $CHCl_3$ (1 mL) for 1h, r.t. at 750 rpm | C30-RP-LC-ESI-MS and HCD-MS/MS using Ultimate U3000R LC system coupled online to Q-Exactive hybrid quadrupole Orbitrap® mass spectrometer, in negative-ion mode | 70 |
| $NO_2$-cLA-TAG<br>$NO_2$-oxo-OA-TAG<br>$NO_2$-OH-OA-TAG<br>$NO_2$-OOH-OA-TAG<br>Other nitrated products | Nitration of 100 µM 3-cLA-TAG or 2-cLA-TAG with 2 mM $NaNO_2$ in artificial gastric fluid, 1h at 37 °C under continuous agitation | C18-HPLC-HR-MS/MS and $MS^3$ using LTQ Orbitrap Velos equipped with HESI-II source, in positive-ion mode<br>C18-HPLC-APCI-MS/MS using API 4000 Q-trap triple quadrupole, in positive-ion mode | 62 |

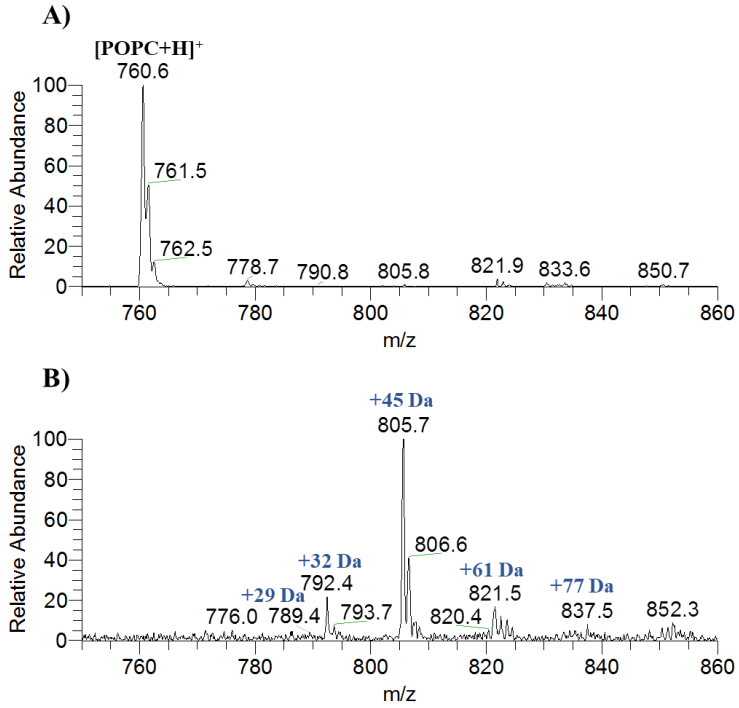


**Figure I.4.** ESI-MS spectra of POPC before **(A)** and after **(B)** nitration reaction with $NO_2BF_4$ acquired in a LXQ Linear Ion Trap mass spectrometer, in positive-ion mode. Nitrated and nitroxidized derivatives in **(B)** were identified based on specific mass shifts depending on the type of modification.

Nitrated and nitroxidized derivatives of PC, PE and PS were initially characterized by MS/MS in positive ($[M+H]^+$) and negative-ion mode ($[M-H]^-$ for PE and PS; $[M+OAc]^-$ for PC) using collision-induced dissociation (CID) in LXQ-LIT instrument[60,61,68]. This allowed to pinpoint a fragmentation fingerprint and define a set of reporter ions that can be used to design target analysis, as summarized in Table I.2. Typical fragmentation pathways included: (a) neutral loss (NL) of $HNO_2$ (47 Da) or HNO (31 Da) for nitro or nitroso derivatives, respectively; (b) formation of ionized nitrated and nitroxidized FA ($[R'COOH+H]^+$ and $R'COO^-$); (c) fragmentation of the FA backbone in the vicinity of the $NO_2$ group allowing to pinpoint the position of the modification within the fatty acyl chain; and (d) product ions arising from the combined loss of $HNO_2$ or HNO and the polar head groups of each PL. Nevertheless, liquid chromatographic (LC) methods combined with MS (and MS/MS) are necessary to confirm the presence of distinct nitrated and nitroxidized modifications in PLs. Reverse phase (RP)-LC-MS has been the most used. The insertion of the modified moiety increases the polarity of the modified PLs derivative which elute earlier than the non-modified species. Moreover, species with more modifications eluted at shorter retention times.

RP-LC-ESI-MS/MS analysis using C5 column (Discovery Bio Wide Pore 15 cm × 0.5 mm internal diameter, 5 µm particle size) allowed to identify and discriminate functional isomers of nitrated PC and nitrated PE[61], namely nitro and nitro-hydroxy derivatives. Product ions of modified PC and PE molecular species assigned as nitro ($NO_2$-PLs), dinitro ($(NO_2)_2$-PLs), nitroso (NO-PLs) and nitronitroso ($(NO_2)(NO)$-PLs) derivatives were discriminated, as well as the nitroxidized derivatives of PC and PE with hydroxy or hydroperoxy moieties such as (NO)O-PLs, $(NO_2)$O-PLs, $(NO_2)$(2O)-PLs, $(NO_2)$2O-PLs and $(NO_2)_2$(2O)-PLs were also identified (Tables I.1. and I.2).

More recently, nitrated and nitroxidized PS[68] and CL[70] were characterized using higher energy CID (higher energy collision-induced dissociation, HCD) in Q-Exactive Orbitrap instrument, with or without C30-RP-LC[68,70]. Indeed, RP-LC-ESI-MS using Accucore C30 column (150 mm x 2.1 mm internal diameter, 2.6 µm particle size, 150 Å pore size) allowed the separation and identification of 11 different nitrated and nitroxidized CL products[70] (Table I.1.). This MS-based lipidomic approach allows to discriminate four nitroso CL derivatives comprising distinct mass increments relative to the native CL namely, NO-CL (+29 Da), $(NO)_2$-CL (+58 Da), $(NO)_3$-CL (+87 Da) and $(NO)_4$-CL (+116 Da); and two nitro-CL derivatives assigned as $NO_2$-CL (+45 Da) and $(NO_2)_2$-CL (+90 Da). CL products bearing concomitantly NO with $NO_2$ groups were also identified as nitronitroso derivative ($(NO_2)(NO)$-CL) with a mass shift of 74 Da. Nitroxidized CL derivatives were also capable to be identified, namely two hydroxy-CL assigned as (NO)O-CL and $(NO_2)$(NO)O-CL with mass increments of 45 Da and 90 Da, respectively, and one hydroperoxy-TLCL with two nitroso moieties assigned as $(NO)_2$(2O)-CL (+90 Da). Besides that, for the same mass shift it was possible to identify distinct isomeric structures, as is the case of dinitro, nitronitroso-hydroxy and dinitroso-hydroperoxy CL derivatives.

**Table I.2.** Typical neutral losses and product ions observed in tandem mass spectra of nitrated and nitroxidized PLs obtained using LXQ-LIT both in positive- ($[M+H]^+$) and negative-ion mode ($[M-H]^-$ and $[M+OAc]^-$)[60,61,68].

| Nitrated derivatives | | Mass shift to unmodified PLs | Neutral losses for diagnostic scan in MS/MS | |
|---|---|---|---|---|
| **Nitroso** | NO-PLs | +29 Da | HNO | -31 Da |
| **Nitro** | $NO_2$-PLs | +45 Da | $HNO_2$ | -47 Da |
| **Dinitroso** | $(NO)_2$-PLs | +58 Da | HNO | -31 Da |
| | | | 2HNO | -62 Da |
| **Nitronitroso** | $(NO_2)(NO)$-PLs | +74 Da | $HNO_2$ | -47 Da |
| | | | HNO | -31 Da |
| **Dinitro** | $(NO_2)_2$-PLs | +90 Da | $HNO_2$ | - 47 Da |
| | | | $2HNO_2$ | -94 Da |
| **Nitroxidized derivatives** | | **Mass shift to unmodified PLs** | **Neutral losses for diagnostic scan in MS/MS** | |
| **Nitrosohydroxy** | (NO)O-PLs | +45 Da | $H_2O$ | -18 Da |
| | | | HNO | -31 Da |
| **Nitrohydroxy** | $(NO_2)$O-PLs | +61 Da | $H_2O$ | -18 Da |
| | | | $HNO_2$ | -47 Da |
| **Nitrohydroperoxy** | $(NO_2)(2O)$-PLs | +77 Da | $H_2O$ | -18 Da |
| | | | $O_2$ | -32 Da |
| | | | $HNO_2$ | -47 Da |
| **Dinitrihydroxy** | $(NO_2)_2$O-PLs | +106 Da | $H_2O$ | -18 Da |
| | | | $HNO_2$ | -47 Da |
| | | | $2HNO_2$ | -94 Da |
| **Dinitrohydroperoxy** | $(NO_2)_2(2O)$-PLs | +122 Da | $H_2O$ | -18 Da |
| | | | $O_2$ | -32 Da |
| | | | $HNO_2$ | -47 Da |
| | | | $2HNO_2$ | -94 Da |
| **$HNO_2$ + Head Group** | | **Mass shift to unmodified PLs** | **Neutral losses for diagnostic scan in MS/MS** | |
| PC | | $HNO_2$ +59 $[-N(CH_3)_3]$ | -106 Da | |
| | | $HNO_2$ +183 $[-HPO_4(CH_2)_2N(CH_3)_3]$ | -230 Da | |
| PE | | $HNO_2$ +43 $[-CH_2CH_2NH]$ | -90 Da | |
| | | $HNO_2$ +141 $[-HPO_4CH_2CH_2NH_3]$ | -188 Da | |
| PS | | $HNO_2$ +87 $[-C_3H_5NO_2]$ | -134 Da | |
| | | $HNO_2$ +185 $[-C_3H_8PO_6N]$ | -232 Da | |

Besides that, these two studies showed that HCD-MS/MS conditions lead to differences in the fragmentation patterns. In HCD-MS/MS spectra from Q-Exactive hybrid quadrupole Orbitrap high yields of low *m/z* reporter ions were found, namely the carboxylate anions ($R'COO^-$) of nitrated fatty acyl chain. The typical NL of $HNO_2$ or HNO for nitro and nitroso derivatives, respectively, were found in very low relative abundance or were reported

to be absent[68,70]. In an opposite trend, product ions with high *m/z* values, including the ones formed due to the characteristic NL of $HNO_2$ or HNO, were detected in high relative abundance in CID-MS/MS spectra from LXQ-LIT[60,61,68] (Figure I.5.). Thereby, it becomes essential carry out more studies to compare the fragmentation fingerprinting obtained when different ion activation techniques are used for MS/MS namely for PC and PE. This unveils the importance of the knowledge on the most relevant fragmentation patterns and reporter ions to enable an accurate identification of nitrated and nitroxidized PLs species.

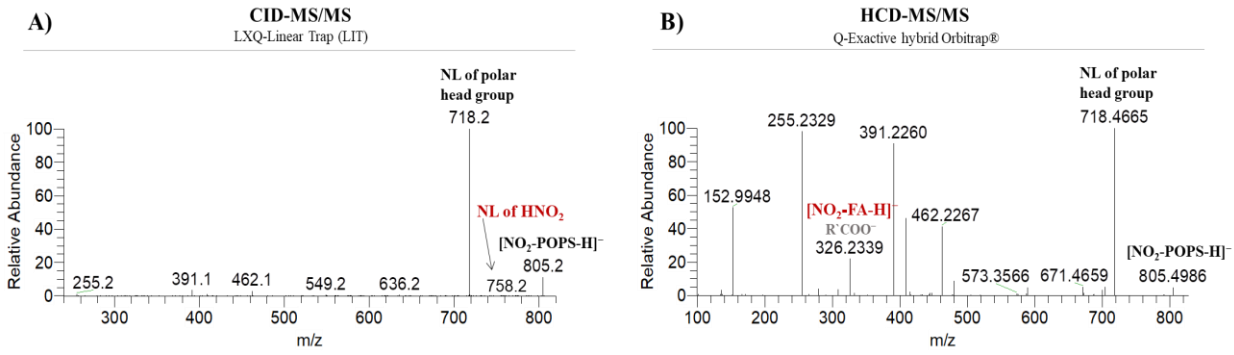


**Figure I.5.** MS/MS spectra of $NO_2$-POPS obtained using CID **(B)** and HCD **(C)** as ion activation techniques[68].

The MS-based lipidomics approaches developed using nitrated PLs generated under nitroxidative conditions in biomimetic model systems allowed to detect nitroalkene derivatives of PC ($NO_2$-PC) and PE ($NO_2$-PE) in biological samples including in cardiac mitochondria from type 1 diabetic rats[60] and cardiomyoblasts H9c2 under starvation[61], where other nitrated and nitroxidized PC were also found, using hydrophilic interaction liquid chromatography (HILIC)-ESI-MS and CID-MS/MS-based lipidomic approaches (Table I.3.). $NO_2$-PC with monounsaturated FA where found to be present in higher relative amount and to have higher percentage of conversion from their unmodified precursors[60]. This suggested that increase in FA's unsaturation degree decrease the susceptibility to nitration, which was previous verified for free $NO_2$-FA generated by mimetic nitration mediated by $NO_2^+$ [12]. Also, $NO_2$-PC derivatives were detected in high relative abundance, which suggested their further modification to yield nitroso and nitroxidized derivatives[61]. Fazzari and collaborators[20] through C18-LC-ESI-MS/MS found that regardless the type of $NO_2$-FA, either $NO_2$-FA, its reduced products or β-oxidation metabolites were preferentially incorporated in PC class in adipocytes supplemented with different $NO_2$-FA. This was suggested to be due to the high

abundance of this phospholipid class in biological membranes. Nevertheless, incorporation of $NO_2$-FA in PE, PS and PI was also verified.

Overall, esterified $NO_2$-FA were already detected *in vivo* and *in vitro* in several PLs classes. It the next section it will be described the MS and MS/MS-based lipidomics approaches used to identify and structurally characterize $NO_2$-FA incorporated into TAG.

### I.2.2. Nitrated triacylglycerides detected by MS

$NO_2$-FA esterified in TAG ($NO_2$-TAG) were detected in adipocytes supplemented with 10-$NO_2$-OA and rat plasma after oral administration of 10-$NO_2$-OA[62]; in adipocytes supplemented with different $NO_2$-FA[20]; in adipose tissue of high-fat diet-fed mice after subcutaneous administration of $NO_2$-OA[20]; in plasma of dogs after oral administration of 10-$NO_2$-OA[19]; and after *in vitro* mimetic nitration under acidic conditions using artificial gastric fluid[62]. These studies also showed electrophilic $NO_2$-FA to be preferentially incorporated in mono (MAG) and diacylglyceride (DAG), while non-electrophilic nitroalkanes (as $NO_2$-FA's reduced products and β-oxidation metabolites) are more efficiently distributed in TAG [19,20,62].

Nitrated TAG from *in vitro* and *in vivo* sources has been identified by C18-LC-ESI-MS and MS/MS-based lipidomic approaches in positive-ion mode as $[NO_2\text{-TAG}+NH_4]^+$ ions, based on specific mass shifts and odd mass *m/z* values when compared to $[TAG+NH_4]^+$ ions[62] (Tables I.1 and I.3.). Fragmentation pattern under both CID[62] and HCD-MS/MS conditions[19] include the formation of two even and one odd diacylglyceride (DAG) ions, which correspond to the NL of unmodified FA and ammonia ($[M\text{-}FA\text{-}NH_3]^+$) and $NO_2$-FA moiety plus ammonia ($[M\text{-}NO_2\text{-}FA\text{-}NH_3]^+$), respectively. CID-$MS^3$ analysis of DAG ions can give further structural information as specific NL with formation of nitrosamine and aldehyde ions to pinpoint the position of $NO_2$ group, as well as the monoacylglyceride (MAG) ions ($[RCO+74]^+$), the acylium ions ($[RCO]^+$), and their correspondent dehydrated products, which allowed to confirm the position of each FA within TAG glycerol backbone[62]. Fragmentation of non-electrophilic (nitroalkane) $NO_2$-FA-TAG also yield the three likely DAG ions, two with even *m/z* values carrying unmodified FA at *sn*-1/*sn*-3 positions and one odd bearing the nitroalkane moiety at *sn*-2. CID-$MS^3$ of DAG ions yield the product ions already reported for electrophilic $NO_2$-FA-TAG under the same conditions, like MAG ($[RCO+74]^+$) and acylium ions ($[RCO]^+$) (Table I.3.). However, new fragments ions derived from NL of HNO and $HNO_2$ from even and odd DAG ions, respectively, were also found for the non-electrophilic $NO_2$-FA-TAG[62].

Incorporation of (non-)electrophilic $NO_2$-FA was found to preferentially occur at *sn*-2 position of the glycerol backbone of TAG[19,62], which was determined by the lower relative abundance of DAG product ions with odd *m/z* values in MS/MS spectrum as the loss of FA from *sn*-1/*sn*-3 positions of TAG was reported to be energetically favored. This preference for the *sn*-2 position can impact the deliver upon lipase hydrolysis; metabolism; distribution and signaling activities of the esterified $NO_2$-FA[19]. Thereby, becomes essential carry out more studies that focus on the identification and characterization of esterified $NO_2$-FA by MS and MS/MS-based lipidomics approaches in different MS-platforms, which can also contribute to disclose their biochemical, metabolic and signaling pathways.

Esterification in complex lipids is viewed as a mechanism to shield the electrophilic potential of $NO_2$-FA. Incorporation of 10-$NO_2$-OA at *sn*-2 position of TAG was established to protect the electrophilic character of $NO_2$-FA from inactivation namely by PGR-1[19]. Hydrophobic compartmentalization in membrane or lipoprotein lipids indeed contribute to $NO_2$-FA stabilization, but this may also limit nucleophilic-adduction reactions. Thus, with a possible impact in $NO_2$-FA's biological actions and signaling roles until its further release. Nevertheless, recent research work has demonstrated that complex nitrated lipid emerged as potential novel electrophilic lipid mediators, able to interact with lipoxidation targets *in vitro*, potentially via cysteine residues, as it will be described in the next section.

**Table I.3.** Nitrated complex lipids identified in biological samples.

| Biological samples | | | |
|---|---|---|---|
| **Nitrated species** | **Experimental model** | **Method** | **Ref.** |
| NO-PC 18:0/18:1<br>$NO_2$-PC 16:0/18:1<br>($NO_2$)(NO)-PC 16:0/20:3<br>($NO_2$)$_2$-PC 16:0/16:1<br>($NO_2$)$_2$-PC 16:0/18:1<br>($NO_2$)(2O)-PC 16:0/18:1<br>$NO_2$-PE 16:0/18:1<br>$NO_2$-PE 18:0/18:1 | Lipid extracts of cardiomyoblast cell line H9c2 under starvation conditions obtained using Bligh and Dyer method | HILIC-ESI-MS and CID-MS/MS performed on Waters Alliance 2690 HPLC system coupled online to LXQ-LIT mass spectrometer, in positive-ion mode | 61 |
| $NO_2$-PC 16:0/18:2<br>$NO_2$-PC 16:0/18:1<br>$NO_2$-PC 18:2/20:4<br>$NO_2$-PC 16:0/22:5<br>$NO_2$-PC 18:0/20:5<br>$NO_2$-PC 18:1/20:4<br>$NO_2$-PC 18:0/20:4<br>$NO_2$-PC 18:2/20:1<br>$NO_2$-PC 18:0/22:6<br>$NO_2$-PE 18:0/22:6 | Lipid extracts of cardiac mitochondria from a well-characterized animal model of type 1 diabetes mellitus (T1DM) obtained using Bligh and Dyer method | HILIC-ESI-MS and CID-MS/MS performed on Waters Alliance 2690 HPLC system coupled online to LXQ-LIT mass spectrometer, in positive-ion mode | 60 |
| $NO_2$-PC 18:2/20:1 | Lipid extracts of cardiac mitochondria from control group obtained using Bligh and Dyer method | HILIC-LC-MS and CID-MS/MS performed on a Waters Alliance 2690 HPLC system coupled online to LXQ-LIT mass spectrometer, in positive-ion mode | 60 |
| $NO_2$-PC<br>$NO_2$-PE<br>$NO_2$-PS<br>$NO_2$-PI<br>$NO_2$-FA-TAG<br>$NO_2$-FA-MAG<br>$NO_2$-FA-DAG<br>$NO_2$-Cholestrol esters<br>$NO_2$-FA-derived β-oxidation products | Lipid extracts of 3T3-L1-derived adipocytes supplemented with 5 µM of 10-$NO_2$-OA, $NO_2$-cLA, $NO_2$-LA and $NO_2$-SA for 24h obtained using Bligh and Dyer method<br>Lipid classes fractionation by SPE using $NH_2$ columns | C18-HPLC-ESI-MS/MS using API 4000 Q-Trap triple quadrupole mass spectrometer, in negative-ion mode, before and after acid hydrolysis of esterified FAs | 20 |

| | | | |
|---|---|---|---|
| $NO_2$-FA-TAG<br>$NO_2$-FA-MAG<br>$NO_2$-FA-DAG<br>$NO_2$-Cholestrol esters | Lipid extracts of adipose tissue from high-fat diet-fed male C57Bl/6j mice after subcutaneous deliver of 8 mg/Kg/day $NO_2$-OA for 6.5 weeks obtained using Bligh and Dyer method<br>Lipid classes fractionation by SPE using $NH_2$ columns | C18-HPLC-ESI-MS/MS using API 4000 Q-Trap triple quadrupole mass spectrometer, in negative-ion mode, before and after acid hydrolysis of esterified FAs | 20 |
| (Non)-Electrophilic $NO_2$-FA-TAG bearing 10-$NO_2$-OA including:<br>$NO_2$-FA-TAG 54:3<br>$NO_2$-FA-TAG 54:4<br>$NO_2$-FA-TAG 54:5<br>$NO_2$-FA-TAG 52:2<br>$NO_2$-FA-TAG 52:3 | Lipid extracts of plasma from male Beagle dogs orally dosed with 31.25 mg/Kg 10-$NO_2$-OA, twice a day and 6h apart, for 14 days obtained using Bligh and Dyer method | C18-HPLC-ESI-HR-MS/MS using Q-Exactive hybrid quadrupole Orbitrap® mass spectrometer equipped with HESI-II source, in positive-ion mode, before and after acid hydrolysis of esterified FA | 19 |
| (Non)-Electrophilic $NO_2$-FA-TAG | Lipid extracts of 3T3-L1-derived adipocyte treated with 5 µM $NO_2$-OA for 24h obtained using Bligh and Dyer method<br>Lipid classes fractionation by SPE using $NH_2$ columns | C18-HPLC-ESI-HR-MS/MS and $MS^3$ using LTQ Orbitrap Velos equipped with HESI-II source, in positive-ion mode, before enzymatic hydrolysis of esterified FA<br>C18-HPLC-ESI-MS/MS using API 4000 Q-Trap triple quadrupole mass spectrometer, in negative-ion mode, after enzymatic hydrolysis of esterified FA | 62 |
| (Non)-Electrophilic $NO_2$-FA-TAG | Lipid extracts of plasma from male Sprague-Dawley rats gavaged with 100 mg/Kg $NO_2$-OA obtained using Bligh and Dyer method<br>Lipid classes fractionation by SPE using $NH_2$ columns | C18-HPLC-APCI-MS/MS using API 4000 Q-trap triple quadrupole, in positive-ion mode, before enzymatic hydrolysis of esterified FA<br>C18-HPLC-ESI-MS/MS using an API 4000 Q-Trap triple quadrupole mass spectrometer, in negative-ion mode, after enzymatic hydrolysis of esterified FA | 62 |

### I.2.3. Lipoxidation products of esterified nitro-fatty acids

The electrophilic nature of free $NO_2$-FA and ability to undergo reversible reactions with key proteins forming nitro-lipoxidation adducts are considered the key components for their plethora of biological roles and signaling actions. Despite being a challenging task, detection and characterization of lipoxidation adducts of $NO_2$-FA with proteins and peptides has been accomplished by using LC-MS based approaches[13,52] (Table I.4). In the same way, esterified $NO_2$-FA in PLs could also undergo nucleophilic-adduction reactions with cysteine or histidine residues through S-nitroalkylation or Michael addition, respectively (Figure I.6.). Nevertheless, there is a notorious lack of knowledge on the electrophilic properties of esterified $NO_2$-FA and the identification and characterization of their lipoxidation products remains poorly explored.

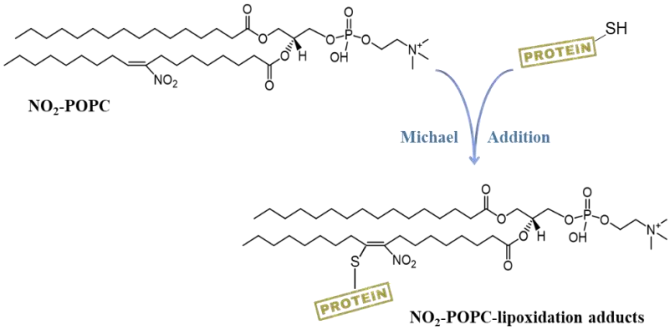


**Figure I.6.** Representative mechanism of the reversible S-nitroalkylation of proteins by esterified $NO_2$-FA. Nitrated phosphatidylcholine containing the nitro-oleic acid ($NO_2$-POPC) was selected as an example of esterified $NO_2$-FA.

The formation of lipoxidation adducts of nitroalkene derivative of POPC ($NO_2$-POPC) with glutathione (GSH), generated using *in vitro* biomimetic model systems to synthetize both nitrated POPC and $NO_2$-POPC-GSH adducts, was recently demonstrated by using ESI-MS-based lipidomic approaches[40] (Table I.4). $NO_2$-POPC-GSH adduct was formed via S-nitroalkylation of the thiol moiety of cysteine residues and its identification was performed by direct infusion ESI-MS as singly and doubly charged ions ($[M+H]^+$ and $[M+2H]^{2+}$, respectively) in positive-ion mode. Its characterization and structural elucidation was addressed by ESI-MS/MS using both low and higher energy CID (CID *versus* HCD) in three different MS platforms (*i.e.* LXQ-LIT, Q-TOF 2 and Q-Exactive Orbitrap)[40].

Montero-Bullón and co-authors [40] disclose the typical fragmentation pathways of $NO_2$-POPC-GSH under MS/MS conditions, which allowed to pinpoint the adduction site and the structural features of the $NO_2$-POPC moiety covalently bound to the GSH, thus confirming

the identity of the nitro-lipoxidation adduct. Fragmentation pattern of $NO_2$-POPC-GSH included: (a) the product ions at *m/z* 184 or NL of 183 Da that confirm the presence of PC polar head group; (b) the modified b, y and C ions ($^{*}y_2^{+}$,$^{*}y_2^{2+}$, $^{*}b_2^{2+}$ and $^{*}C_1^{2+}$) corresponding to the typical peptide fragment ions bearing the $NO_2$-POPC moiety covalently adducted, which unequivocally confirms a $NO_2$-PLs covalently linked to the peptide and the presence of the lipid-peptide adduct; and (c) the $[NO_2\text{-POPC+H}]^+$ ions and the typical NL of $HNO_2$ confirming the presence of $NO_2$-PLs species, which in this case were only observed in the MS/MS of the mono charged $[M+H]^+$ ions. The knowledge on the typical MS/MS fingerprinting of lipoxidation adducts of esterified $NO_2$-FA and their characteristics reporter ions can be used to design target analysis strategies based on MS approaches. This will aid the detection of $NO_2$-PLs-peptide/proteins adducts in complex biological samples. As so, it is essential carry out more studies under this topic in order to unveil the potential protein targets of $NO_2$-PLs, especially those with a closer relationship with the membrane.

In another study, the potential interaction between nitrated POPC with two known lipoxidation targets namely vimentin, which is an intermediate filament protein that possesses a single cysteine residue (C328), and the ligand binding domain (LBD) of PPARγ that contains a reactive cysteine (C285) was indirectly evaluated *in vitro* by using a gel-based competition assay with biotinylated iodoacetamide (Iac-B)[71] (Table I.4). Through this strategy it was possible to find a decrease in the modification of both cysteine residues by Iac-B in the presence of nitrated POPC. Incubation with unmodified POPC was not able to block the labeling of C328 in vimentin with Iac-B, and only partially diminished its incorporation in PPARγ-LBD. Moreover, nitrated POPC was more effective in the reduction of Iac-B labeling in PPARγ-LBD than the prostaglandin 15d-$PGJ_2$, which is a PPARγ agonist acting via modification of C285[71]. However, the direct covalent adduction of nitrated POPC was not possible to be confirmed. Despite do not being completely superimposable, the effects of nitrated POPC on C328 of vimentin were reported to be more similar to the ones obtained after treatment with 9-$NO_2$-OA, a well-known electrophilic $NO_2$-FA, than the ones got with the •NO donors (S-nitrosogluthatione-GSNO, or sodium nitroprusside-SNP), using adrenal carcinoma (SW13/cl.2) cell based assays[71]. These findings suggested the effects of nitrated POPC involves a direct or indirect modification of vimentin's reactive cysteine residue at position 328.

Incorporation of electrophilic $NO_2$-FA into TAG was found in plasma of dogs orally dosed with 10-$NO_2$-OA by using C18-LC-HR-MS/MS in Q-Exactive Orbitrap, in positive-ion mode. Reaction of plasma samples with BME followed by C18-LC-MS/MS in Q-TRAP 6500

triple quadrupole in negative-ion mode allowed to discriminate between (non)-electrophilic species[19].

**Table I.4.** Potential lipoxidation adducts of nitrated phosphatidylcholine containing the nitro-oleic acid ($NO_2$-POPC) identified in biological samples and *in vitro* biomimetic model systems

| ***In vitro* biomimetic model systems** | | | |
|---|---|---|---|
| **Peptide/ protein** | **Experimental model** | **Method** | **Ref.** |
| GSH | Incubation of nitrated POPC (0.25 µmol) and GSH (1.25 µmol) in $NH_4HCO_3$ buffer (5 mM, pH 7.4) at 37 °C for 6 h at 750 rpm | Direct infusion ESI-MS and MS/MS in LXQ-LIT, Q-TOF 2 hybrid quadrupole time-of-flight, and high-resolution Q-Exactive hybrid quadrupole Orbitrap® mass spectrometer, in positive-ion mode | 40 |
| Vimentin C328 | Incubation of 100 µM nitrated POPC and 3 µM vimentin in PIPES (5 mM, pH 7.0) with 0.1 mM DTT at r.t. for 2h, followed by the addition of 20 µM Iac-B and 30 min of incubation | Gel-based competition assay using 10% SDS-PAGE, HRP-streptavidin to detect the biotin signal of Iac-B incorporated in vimentin, and Western blot to evaluate vimentin levels | 71 |
| PPARγ-LBD C285 | Incubation of 100 µM nitrated POPC and 1 µM PPARγ-LBD in PIPES (5 mM, pH 7.0) with 0.1 mM DTT at r.t. for 2h, followed by the addition of 20 µM Iac-B and 30 min of incubation | Gel-based competition assay using 12.5% SDS-PAGE, HRP-streptavidin to detect the biotin signal of Iac-B incorporated in PPARγ-LBD, and Western blot to evaluate PPARγ-LBD levels | |
| **Biological samples** | | | |
| **Peptide/ protein** | **Experimental model** | **Method** | **Ref.** |
| Vimentin C328 | SW13/cl.2 cells stably transfected with GFP-vimentin wild type treated with 10 or 30 µM nitrated POPC for 75 min in serum-free medium at 37 °C, 5 % $CO_2$ | Direct visualization of cells by live cell imaging confocal microscopy | 71 |
| | SW13/cl.2 stably transfected with RFP//vimentin wild type or C328S treated with 10 µM nitrated POPC for 6h in serum-free medium at 37 °C, 5 % $CO_2$ | Cells were fixed and visualized by confocal microscopy | |

These studies provide evidence that adducts formed between $NO_2$-PLs and peptide/protein can occur *in vivo* and can be part of the mechanism by which $NO_2$-PLs can display their actions.

### I.2.4. Biological activities of Esterified Nitro-fatty acids

Besides their role as free FA, esterified $NO_2$-FA can also have high relevance at biological level, with similar or novel biological activities. However, the available knowledge on biological actions and health protective effects of esterified $NO_2$-FA is scarce. The few research works already performed suggest the potential relevance of esterified $NO_2$-FA in nitrated PLs as anti-inflammatory[72] and antioxidant species[68,72]. Nitrated PLs were recently

reported to act through a pleiotropic mechanisms of action including the possibility of electrophilic actions, which not completely overlap the ones displayed by $NO_2$-FA and were also different from those obtained using •NO donors[71]. Most of the research work on biological actions of nitrated PLs are focused on the effects of nitrated POPC[71,72], since PC is the most predominant PLs class constituent of cellular membranes and lipoproteins[73], while $NO_2$-OA is the most studied derivative of free $NO_2$-FA[72,74], and nitrated derivatives of PC including nitrated POPC were recently detected *in vitro*[60,61] and *in vivo* in H9c2 cardiomyoblasts[61] and cardiac mitochondria from streptozotocin-induced diabetic rats[60].

Nitrated POPC and nitrated POPS were reported to have antioxidant properties using non-physiological radicals as 2,2-diphenyl-1-picrylhydrazyl (DPPH•) and 2,20-azino-bis-3-ethylbenzothiazoline-6-sulfonic acid cation ($ABTS^{•+}$), which are methods commonly used to evaluate the free radical scavenging ability of antioxidant candidate compounds[68,72].The scavenging activity of both nitrated POPC and nitrated POPS was related to their ability to donate H atoms to trap harmful radicals than to its ability to act as an electron-donating agents, in a nonlinear concentration-dependent way[68,72]. These studies unveiled a higher H-donating and quenching ability, and thus a larger reactivity in aqueous media ($ABTS^{•+}$ assay) than in ethanolic (hydrophobic) media (DPPH• assay). This can be related with the stabilization and shielding of the $NO_2$-FA moiety in hydrophobic environments and with the possibility to undergo decay reactions in aqueous medium to yield •NO and other biologically relevant species to exert its biological roles. Moreover, nitrated POPC showed antioxidant potential in the same order of magnitude as the one previously reported for the 10-$NO_2$-LA isomer[72]. Nitrated POPS demonstrated higher scavenging potential than nitrated POPC in the same conditions[68,72], which was suggested to be a combination of different mechanisms of antioxidant (inter)actions by synergic effect between the POPS polar head group, acting as an active electron donator, and the $NO_2$ moiety, acting as an H-atom donor.

The antioxidant potential of nitrated POPC was also evaluated against oxygen-derived radicals that mediates oxidation associated with physiological disturbance by using the oxygen radical absorbance capacity (ORAC) assay[72]. Nitrated POPC conferred a relevant initial protection against oxygen-derived radicals-induced oxidation, in a concentration-dependent way, indicating a faster reaction with oxygen-derived radicals and thus, providing a more relevant initial protection against oxidation[72]. Radical scavenging activity of nitrated POPC against the •OH, generated under Fenton reaction conditions, was also reported [72]. Nitrated POPC was able to inhibit the lipid peroxidation of PLPC liposomes

used as a model of cell membrane, being more effective at lower concentrations. This was suggested to be due to the generation of reactive radicals derived from oxidative modifications of nitrated POPC itself that can contribute to the oxidation of PLPC through the propagation of free-radical chain reactions[72].

Nitrated POPC was also reported to display anti-inflammatory properties in a well-described *in vitro* model of inflammation[72] through the inhibition of the expression of the inducible nitric oxide synthase (iNOS), evaluated using Western blotting analysis, in a mouse leukemic monocyte cell line (Raw 264.7 macrophages) activated by the incubation with the Toll-like receptor 4 (TLR4) agonist lipopolysaccharide (LPS). Nevertheless, knowledge about the biological actions and signaling roles of esterified $NO_2$-FA is still very limited. Moreover, the recognition of the electrophilic character of esterified $NO_2$-FA and its role on their properties needs to be the subject of further studies. In this regard, more *in vitro* and *in vivo* studies are needed to highlight the biochemical mechanisms by which esterified $NO_2$-FA, both in PLs and TAG, can exert their biologically relevant roles.

### I.3. Aim of the work

Mass spectrometry, usually coupled to LC, has become the essential analytical tool for the screening of nitrated and nitroxidized PLs and TAG. These modified species have been identified based on specific mass shifts under MS conditions and typical fragmentation pattern and characteristic reporter ions under MS/MS. Earlier studies on nitrated derivatives of PLs were performed using a LIT instrument, which allowed to establish a set of reporter ions presents in a typical fragmentation pattern. Advances in MS tools, namely the high resolution and great sensitivity of the most recent mass spectrometers, have opened new horizons in the field of lipid nitration. However, two recent studies on $NO_2$-PLs structural characterization performed using a high-resolution Q-Exactive Orbitrap instrument unveiled a dissimilar fragmentation profile for these nitrated derivatives, suggesting that fragmentation patterns and the typical reporter ions can vary depending on the type of mass spectrometer and the dissociation technique used to induce fragmentation. This is a key issue since it can hinder the detection of these modified derivatives. Thus, it is fundamental new methodological developments to get knowledge on the typical fragmentation patterns obtained when different ion activation techniques are used for MS/MS, and it is essential to define what parameters are best to obtain the most useful and reproductively information, in order to improve the detection of nitrated complex lipids. This will allow to define a set of reporter product ions that can be used to design target analysis strategies to unveil these

modified species in biological samples. Moreover, further insights in biological roles and signaling properties of complex nitrated lipids are needed. In this way, the aims of this work are: (a) the identification of typical fragmentation patterns using different MS instrumental platforms to improve the accurate detection of the nitrated and nitroxidized derivatives of complex lipids obtained from *in vitro* biomimetic model systems, and (b) the development of lipidomic strategies to improve their identification in complex biological samples using the optimized high-throughput MS-based methodologies. Nitrated and nitroxidized derivatives of PLs (PE, PC, PS, CL) and also TAG will be synthesize using *in vitro* mimetic nitration with $NO_2BF_4$ to be analyzed by ESI-MS, through direct infusion or coupled to LC, and structurally characterized by MS/MS, both in positive-ion mode (as $[M+H]^+$ ions for PC, PE and PS, and $[M+NH_4]^+$ ions for TAG) and negative-ion mode (as $[M-H]^-$ ions for PS, PE and CL, and $[M+OAc]^-$ ions for PC). Information on fragmentation pattern and reporter product ions gathered with lipid standards will be used to identify these modified species in complex biological samples. Cell-based assays will be used to screen the presence of $NO_2$-PLs using lipidomics approaches. The optimization of MS and MS/MS-based lipidomic approaches is required to simultaneously obtain high accurate and confident identification of nitrated and nitroxidized PLs. Besides that, the knowledge of their typical fragmentation pathways and what parameters are best to obtain the most useful and reproductively information, are key issues for an unambiguous identification and structural characterization of the esterified $NO_2$-FA in biological matrices.

# Chapter II. MATERIAL AND METHODS

### II.1. Chemicals and Reagents

The phospholipids (PLs) standards 1-palmitoyl-2-oleoyl-*sn*-glycero-3-phosphocholine (POPC, C16:0/C18:1), 1-palmitoyl-2-linoleoyl-*sn*-glycero-3-phosphocholine (PLPC, C16:0/C18:2), 1-palmitoyl-2-arachidonoyl-*sn*-glycero-3-phosphocholine (PAPC, C16:0/C20:4) 1-palmitoyl-2-oleoyl-*sn*-glycero-3-phosphoethanolamine (POPE, C16.0/C18:1), 1-palmitoyl-2-linoleoyl-*sn*-glycero-3-phosphoethanolamine (PLPE, C16:0/C18:2), 1-palmitoyl-2-arachidonoyl-*sn*-glycero-3-phosphoethanolamine (PAPE, C16:0/C20:4), 1-palmitoyl-2-oleoyl-*sn*-glycero-3-phosphoserine (POPS, C16.0/C18:1), 3′-Bis[1,2-Di-(9Z-12Z-octadecadienoyl)-*sn*-glycero-3-phospho]-*sn*-glycerol or tetralinoleoyl cardiolipin (TLCL), 1,2,3-tri-(9Z-octadecenoyl)-glycerol or triolein (TAG C18:1/C18:1/C18:1) and phospholipid internal standards for HPLC-MS 1,2-dimyristoyl-*sn*-glycero-3-phosphocholine (dMPC; PC C14:0/C14:0) and 1,2-dimyristoyl-*sn*-glycero-3 phosphoethanolamine (dMPE; PE C14:0/C14:0) were obtained from Avanti® Polar Lipids, Inc. (Alabaster, AL, USA). These PLs had a purity of >99% and were used without further purification. Milli-Q water was used for all experiments, filtered through a 0.22-mm filter, and obtained using a Milli-Q Millipore system (Synergy®, Millipore Corporation, Billerica, MA, USA). HPLC grade chloroform ($CHCl_3$), methanol (MeOH) and acetonitrile were purchased from Fisher Scientific Ltd. (Leicestershire, UK). Formic acid, ammonium acetate and solid nitronium tetrafluoroborate ($NO_2BF_4$) were purchased from Sigma-Aldrich (St. Louis, MO, USA). Ammonium molybdate and sodium dihydrogen phosphate dihydrate ($NaH_2PO_4.2H_2O$) were purchased from Riedel-de Haën (Seelze, Germany). Perchloric acid 70% was purchased from Panreac (Barcelona, Spain). Ascorbic acid was purchased from VWR International (Leicestershire, UK). Penicillin and streptomycin were purchased from Gibco Life Technologies (Paisley, UK). Dulbecco's Modified Eagle Medium (DMEM) was purchased from Invitrogen (Carlsbad, USA). Fetal bovine serum (FBS) was purchased from Lonza Inc. (Walkersville, USA). Glass bottom dishes were purchased from MatTek Corporation (Ashland, USA). All chemicals and reagents used were of the highest grade of purity commercially available and were used without further purification.

### II.2. Nitration of phospholipids in biomimetic systems

PL standards nitration was carried out with $NO_2BF_4$ as previously described[60,61,68]. A solution of each PL standard (1 mg) in chloroform (1 mL) was prepared in an amber vial tube. Then, an excess of solid $NO_2BF_4$ (~1 mg) was added. The reaction mixture was

incubated at room temperature during 1 h and was maintained under orbital shaking at 750 rpm. After incubation, the mixture was transferred to a centrifuge glass tube, and the reaction was stopped by solvent extraction with Milli-Q water. The water was added to hydrolyze unreacted $NO_2BF_4$ and/or to separate contaminating anions from PLs, such as nitrite ($NO_2^-$), nitrated ($NO_3^-$), tetrafluoroborate anion ($BF_4^-$) [75,76]. The mixture was vortexed for 30 s and then centrifuged at 2000 rpm for 10 min at room temperature using a Mixtasel Centrifuge (Selecta, Barcelona, Spain). The organic layer containing the phospholipid products was collected, evaporated under a nitrogen stream, and stored at −20 °C to be further quantified using phosphorous assay[63] and analyzed by direct infusion using a high-resolution mass spectrometer (Q-Exactive Orbitrap).

### II.3. Phospholipids quantification by phosphorous measurement assay

The total amount of nitrated products of PLs recovered after extraction was quantified with the phosphorus assay as previously described by Bartlett and Lewis[77] with modifications. Briefly, 125 µL of concentrated perchloric acid (70% w/v) was added to an aliquot of 10 µL of nitrated PLs (lipid extracts were dissolved in 1 mL of $CHCl_3$; the 10 µL of each sample was dried under a nitrogen stream before the addition of perchloric acid). Samples were then incubated for 1h at 180 °C in the heating block (Stuart, UK). Afterwards, 825 µL of $H_2O$, 125 µL of 2.5% ammonium molybdate (m/v; 2.5 g of $NaMoO_4 \cdot H_2O$ in 100 mL of $H_2O$) and 125 µL of 10% ascorbic acid (m/v; 0.1 g in 1 mL $H_2O$) were added to all samples. The reaction mixture was homogenized in a vortex mixer after each addition followed by incubation for 10 min at 100 °C in a water bath. Samples were put on cold water afterwards. Standards from 0.1 to 2 µg of phosphate (sodium dihydrogen phosphate dihydrate ($NaH_2PO_4.2H_2O$), 100 µg of phosphorus per mL) underwent the same sample treatment except for the heating block phase. Finally, 200 µL of each standard and sample were added to the 96-multiwell plate and the absorbance was measured at 797 nm in a Multiskan GO Microplate Spectrophotometer (Thermo Fisher Scientific, Waltham, MA, USA). The amount of phosphorus present in each sample was calculated by linear regression through the graph which relates the amount of phosphorus present in the standards (X-axis) and absorbance obtained from duplicates of various concentrations (Y-axis). For lipid extracts, the amount of phospholipid was directly calculated by multiplying the amount of determined phosphorus by 25[60,61,68].

### II.4. CID-Trap instrumental conditions for PLs analysis

Analysis of nitrated PLs were carried out both in positive- and negative-ion mode in a LXQ-Linear Ion Trap (LIT) mass spectrometer (Thermo Finnigan, San Jose, CA, USA), as previously described[60,61]. An aliquot (4 µg) of each PL dissolved in methanol with 1% formic acid (2:100, v/v) was introduced through direct infusion. For the MS analysis of PCs in the negative-ion mode, 5 mM ammonium acetate in methanol was used instead of methanol with 0.1% formic acid. The ESI conditions were as follows: flow rate of 8 µL $min^{-1}$; electrospray voltage of 5 kV in positive-ion mode and 4.7 kV in negative-ion mode; capillary temperature of 275 ºC and the sheath gas flow of 8 units. An isolation width of 1 Da was used with a 30 ms activation time for MS/MS experiments. Full scan MS spectra and MS/MS spectra were acquired with a 50 ms and 200 ms maximum ion injection time, respectively. Low energy CID-MS/MS experiments were conducted using collision energy (CE) between 16 and 25 (arbitrary units) for CID-MS/MS analysis. The MS/MS spectra were acquired by CID using helium as the collision gas. Data acquisition and results treatment were carried out with an Xcalibur Data System (version 2.0, Thermo Finnigan, San Jose, CA, USA).

### II.5. HCD-Orbitrap instrumental conditions for PLs analysis

High-mass-resolving ESI-MS used for the accurate mass measurements and optimization of HCD-MS/MS experiment conditions were conducted in a Q-Exactive hybrid quadrupole Orbitrap mass spectrometer (Thermo Fisher Scientific, Bremen, Germany). The instrument was operated in both positive and negative ion mode, with a spray voltage at 3.0 kV and −2.7 kV, respectively, and interfaced with a HESI II ion source. Samples of nitrated PLs were diluted from 1 mg $mL^{-1}$ stock solutions (in chloroform) using MeOH with 1 % (*v/v*) formic acid to a final concentration of 1, 2 and 4 µg $mL^{-1}$. For the MS analysis of PCs in the negative-ion mode, 5 mM ammonium acetate in methanol was used instead of MeOH with 1% formic acid. The analysis was performed through the direct infusion of the prepared solutions at a flow rate of 12 µL $min^{-1}$ into the ESI source, and the operating conditions were as follows: sheath gas (nitrogen) flow rate 5 (arbitrary units); auxiliary gas (nitrogen) 1 (arbitrary); capillary temperature 250 °C; and S-lens RF level 50. The acquisition method was set with a full scan at a resolution of 70 000; the *m/z* ranges were set to 100-1500 in both negative and positive ion mode; the automatic gain control (AGC) target was set at 3e6; maximum injection time (IT) was 250 ms; maximum spray current was 100; and probe heater temperature was 50 °C. Full MS spectra were acquired during 20 s in profile mode. The Q Exactive system was tuned and calibrated using peaks of known mass from a

calibration solution (Thermo Scientific) to achieve a mass accuracy of <0.5 ppm RMS. Spectra were analyzed using the acquisition software Xcalibur (V3.3, Thermo Scientific, San Jose, CA, USA)[68,70]. To obtain the product ion spectra (HCD-MS/MS) of nitrated derivatives of PLs during ESI-MS experiments, the selected precursor ions were isolated by the quadrupole and sent to the HCD cell for fragmentation via the C-trap. In the MS/MS mode, the mass resolution of the Orbitrap analyzer was set at 70 000, AGC target was set at 3e6; maximum IT was 250 ms; isolation window of 1.0 *m/z*; MS/MS spectra were acquired in centroid mode; and three different normalized collision energy (NCE) were used: 20, 25 and 30 (arbitrary units). Nitrogen was also used as the collision gas. Each MS/MS spectra were acquired during 20 s. All experiments were repeated three times.

### II.6. HCD-Orbitrap instrumental conditions for TAG analysis

High-mass-resolving ESI-MS used for the accurate mass measurements and optimization of HCD-MS/MS experiment conditions were conducted in a Q-Exactive hybrid quadrupole Orbitrap mass spectrometer (Thermo Fisher Scientific, Bremen, Germany). The instrument was operated in positive ion mode, with a spray voltage at 3.0 kV and interfaced with a HESI II ion source. Samples of nitrated triolein (TAG, C18:1/C18:1/C18:1) were diluted from 1 mg $mL^{-1}$ stock solutions (in chloroform) using MeOH with 5 mM of ammonium acetate to a final concentration of 6 µg $mL^{-1}$. The analysis was performed through the direct infusion of the prepared solutions at a flow rate of 12 µL $min^{-1}$ into the ESI source, and the operating conditions were as follows: sheath gas (nitrogen) flow rate 5 (arbitrary units); auxiliary gas (nitrogen) 1 (arbitrary); capillary temperature 250 °C; and S-lens RF level 50. The acquisition method was set with a full scan at a resolution of 70 000; the *m/z* ranges were set to 100-1500 in positive ion mode; the automatic gain control (AGC) target was set at 5e6; maximum injection time (IT) was 250 ms; maximum spray current was 100; and probe heater temperature was 100 °C. Full HCD-MS spectra were acquired during 20 s in profile mode. The Q Exactive system was tuned and calibrated using peaks of known mass from a calibration solution (Thermo Scientific) to achieve a mass accuracy of <0.5 ppm RMS. Spectra were analyzed using the acquisition software Xcalibur (V3.3, Thermo Scientific, San Jose, CA, USA)[68,70]. To obtain the product ion spectra (HCD-MS/MS) of nitrated and nitroxidized derivatives of triolein during ESI-MS experiments, the selected precursor ions were isolated by the quadrupole and sent to the HCD cell for fragmentation via the C-trap. In the HCD-MS/MS mode, the mass resolution of the Orbitrap analyzer was set at 70 000, AGC target was set at 5e6; maximum IT was 250 ms; isolation window of 1.0 *m/z*; ESI-HR-HCD-MS/MS spectra were acquired during 20 s in profile mode; and collision

energy (CE) was between 14 and 20 (arbitrary units). Nitrogen was also used as the collision gas.

### II.7. Cell culture and Treatments of Adrenal Carcinoma SW13/cl.2 cells

The cell line SW13/cl.2 (SW13) was stably transfected with an expression plasmid coding for GFP-vimentin wild type (wt) as previously described by Peréz-Sala and co-authors[78]. In these cells, GFP-vimentin constructs form an extended meshwork of squiggles and short filaments. GFP-vimentin wt SW13/cl.2 cells were cultured in p-60 plates in Dulbecco's Modified Eagle Medium (DMEM) supplemented with 10 % (v/v) fetal bovine serum (FBS) and 1 % antibiotics (100 U $mL^{-1}$ penicillin and 100 µg $mL^{-1}$ streptomycin) at 37 °C under 5 % $CO_2$. Experiments were performed on confluent monolayers in serum-free medium. Cells were treated with 10 µmol $L^{-1}$ nitrated POPC (from 3.67 mmol/L stock solution in DMSO) for 6h. Control cells received an equivalent volume of vehicle (DMSO), as required. At the time point, cells were collected by scraping in PBS on ice and centrifuged at 1000 rpm for 5 min. Cell pellets were stored at −80 °C until used[71]. All experiments were repeated three times.

### II.8. Lipid Extraction from SW13/cl.2 cells

Lipid extraction of both untreated (control cells) and nitrated POPC-treated SW13/cl.2 cells was performed according to the method of Bligh and Dyer[77] with modifications[79]. Briefly, 3.75 mL chloroform:methanol 1:2 (v/v) was added to each cell pellet previously resuspended in 1 mL of Milli-Q $H_2O$. Samples were well vortexed and incubated on ice for 30 min. An additional volume of 1.25 mL of chloroform and 1.25 mL of Milli-Q $H_2O$ were added followed by vortex for 1 min between each addition. The samples were centrifuged at 1000 rpm for 5 min at room temperature using a Mixtasel Centrifuge (Selecta) to obtain a two-phase system: an aqueous top phase and an organic bottom phase. The lipid extract was recovered from the organic bottom phase. In order to guarantee full extraction, 1.88 mL of chloroform were added to the remaining aqueous phase followed by vortex and new centrifugation. The organic phase was recovered to the same tube as before and dried under a nitrogen stream. After drying, the total lipid extracts were resuspended in 300 µL of chloroform, transferred to an amber glass vial. This step was repeated twice to ensure the full recovery of lipid extracts. The phospholipid amount in each lipid extract was determined by phosphorous measurement performed according to Bartlett and Lewis, as previously described[60,61,63,68].

### II.9. HPLC-ESI-MS and MS/MS analysis

Lipid extracts from SW13/cl.2 cells (untreated and treated with 10 µmol $L^{-1}$ of nitrated POPC during culture phase) were separated by hydrophilic interaction liquid chromatography (HILIC-LC-MS) using a high performance-LC (HPLC) system (Ultimate 3000 Dionex, Thermo Fisher Scientific, Bremen, Germany) with an autosampler (sampler chamber temperature was set at 5 °C) and a 20 µL sample loop. HPLC system was coupled online to the Q-Exactive® hybrid quadrupole Orbitrap® mass spectrometer (Thermo Fisher Scientific, Bremen, Germany)[79]. The solvent system consisted of two mobile phases as follows: mobile phase A (acetonitrile:methanol:water 50:25:25 (v/v/v) with 1 mM ammonium acetate) and mobile phase B (acetonitrile:methanol 60:40 (v/v) with 1 mM ammonium acetate). Initially, 40 % of mobile phase A was held isocratically for 8 min, followed by a linear increase to 60 % of A within 7 min and a maintenance period of 5 min, returning to the initial conditions in 15 min (5 min to decrease to 40 % of A and a re-equilibration period of 10 min prior next injection). For untreated cells (control cells), a volume of 5 µL of each sample containing 5 µg of phospholipid extract, 4 µL of phospholipid standards mix (dMPC - 0.02 µg and dMPE - 0.02 µg), 1, 2, 4 and 8 ng of nitrated POPC (1µg $mL^{-1}$) and an appropriate volume of eluent B (final volume 100 µL) were introduced into the Ascentis® Si column (15 cm × 1 mm, 3 µm, Sigma-Aldrich) with a flow rate of 40 µL $min^{-1}$ and at 30 °C. These samples were labelled as treated extracts. For nitrated POPC-treated cells, a volume of 5 µL containing 5 µg of phospholipid extracts, 4 µL of phospholipid standards mix (dMPC - 0.02 µg and dMPE - 0.02 µg) and 91 µL of eluent B (final volume of 100 µL) was used. These samples were labelled as treated cells. The mass spectrometer with Orbitrap® technology operated simultaneously in positive (electrospray voltage 3.0 kV) and negative (electrospray voltage −2.7 kV) modes with high resolution with 70 000 and AGC target of 1e6, the capillary temperature was 250 °C, sheath gas flow was 15 U, the auxiliary gas flow was 5 U, maximum spray current was 100, probe heater temperature was 130 °C, S-lens RF level was 50, maximum injection time was 100 ms, scan range was 200-1600 *m/z* (profile). In MS/MS experiments, a resolution of 17 500, AGC target of 1e5, maximum injection time of 50 ms, the scan range of 200-2000 *m/z* (centroid), and an isolation width of 1.0 *m/z* were used and the cycles consisted of one full scan mass spectrum and ten data-dependent MS/MS scans that were repeated continuously throughout the experiments, with the dynamic exclusion of 60 seconds and intensity threshold of 2e4. Samples were analysed using stepped energy which effectively combines fragmentation at energies of 20, 23 and 25 or 25, 30 and 35. Data acquisition was carried out using the Xcalibur data system

(V3.3, Thermo Fisher Scientific, USA). Experiments were performed using three biological replicates, acquired in two different days.

### II.10. Data and statistical analysis

The peak area integration and assignments of $NO_2$-POPC and minor dinitro and nitroxidized species were performed using MzMine 2.42[80]. The software allows for filtering, peak detection ($[M+H]^+$ ions), peak processing, peak alignment, and assignment against an in-house made database. A *m/z* tolerance of +/- 5 ppm and a retention time (RT) tolerance of +/- 2 min was used. The validation of all assignments was made by manual analysis of the MS/MS data, whenever was possible. For the relative quantitation, we use bioinformatics tools (Excel, Microsoft, Redmond, WA) to exported integrated peak areas values. Statistical analysis was performed using one-way analysis of variance (ANOVA) and Tukey's multiple comparison tests in PRISM® GraphPad Software, Inc (GraphPad Prism 5.0, La Jolla, CA, USA).

# Chapter III. RESULTS AND DISCUSSION

# Chapter III. RESULTS AND DISCUSSION

## III.1. ADVANCING TARGET IDENTIFICATION OF NITRATED PHOSPHOLIPIDS IN BIOLOGICAL SYSTEMS BY HCD SPECIFIC FRAGMENTATION FINGERPRINTING IN ORBITRAP PLATFORMS

---

The results and discussion presented in this section were integrally published as follow:

Neves, B., Duarte, S., Domingues, P., Pérez-Sala, D., Oliveira, M.M., Domingues, R. and Melo, T. Advancing target identification of nitrated phospholipids in biological systems by HCD specific fragmentation fingerprinting in Orbitrap platforms. *Molecules*. 25, 1-19 (2020).

### III.1.1. Background and Aim of the Study

Nitrated phospholipids ($NO_2$-PLs) have recently been detected *in vitro* and *in vivo* and associated with beneficial health effects. They were identified and quantified in biological samples by lipidomics methodologies using liquid chromatography-collision-induced dissociation (CID) tandem mass spectrometry (MS/MS) acquired with the Linear Ion Trap mass spectrometer. Only few studies have used higher energy-collision dissociation (HCD)-MS/MS in high-resolution Orbitraps to characterize nitrated phosphatidylserines and nitrated cardiolipins, highlighting marked differences in the fragmentation pattern when using CID or HCD fragmentation methods. Therefore, this study aims to identify reliable reporter ions and fragmentation patterns of nitrated and nitroxidized PC and PE using lipidomic approaches based on electrospray (ESI) high resolution (HR) HCD-MS/MS performed on a Q-Exactive hybrid mass spectrometer. The analysis using ESI-HR-HCD-MS/MS experiments was carried out using nitrated PC and PE standards generated in an *in vitro* model of nitration and it was validated for the qualitative and quantitative determination of the nitrated PLs in lipid extracts from human adrenal cortex adenocarcinoma cells (SW13/cl.2 cells) treated with nitrated 1-palmitoyl-2-oleoyl-*sn*-glycero-3-phosphocholine (POPC). In this study, we also evaluated the impact of different NCE on the relative abundance of reporter product ions which are used to identify nitrated and nitroxidized PLs in *in vitro* model systems and in the lipid extracts from cells.

### III.1.2. Results

The nitrated and nitroxidized derivatives of PC and PE, the two main classes of PLs found in biological samples, were obtained using nitronium tetrafluoroborate ($NO_2BF_4$) in a mimetic model of nitration mediated by RNS which occurs in the hydrophobic environment of biological membranes[60,61]. This reaction leads to the formation of different PLs nitration products with high yields, of which, nitro PLs ($NO_2$-PLs) are one of the main species [60,61]. These modified lipids were analyzed using ESI-MS both in positive (for PC and PE) and negative ionization modes (for PE). The structural characterization was carried out by ESI-HR-HCD-MS/MS using three different NCE to evaluate the effects on the relative abundance of reporter fragment ions used for the detection of nitrated and nitroxidized PLs. In all the experiments, only NCE was modified. All the other procedures namely the preparation of samples, the additional acquisition parameters in the MS and MS/MS modes, and the methods of processing data were maintained between acquisitions. The additional MS and MS/MS parameters used in this work, such as gas flow, capillary temperature, automatic gain control, maximum injection time, and resolution, were selected taking into

account the recommendations of the manufactures during the setup of the instrument but also based on our previous lipidomic studies that allowed us to develop several optimization steps to retrieve the most useful information during data acquisition. Using this approach, we assessed whether the relative abundance of the different product ions, namely the typical reporter ions and the carboxylate anions of the modified fatty acyl chain, is different between molecular species and depends on the HCD-MS/MS parameters.

### III.1.2.1. Optimization of the normalized collision energy for the study of nitrated PLs standards

PC and PE standards carrying different unsaturated fatty acyl chains (OA-oleic acid, LA-linoleic acid and AA-arachidonic acid), namely POPC, 1-palmitoyl-2-linoleoyl-*sn*-glycero-3-phosphocholine (PLPC) and 1-palmitoyl-2-arachidonoyl-*sn*-glycero-3-phosphocholine (PAPC) for the PC class and 1-palmitoyl-2-oleoyl-*sn*-glycero-3-phosphoethanolamine (POPE), 1-palmitoyl-2-linoleoyl-*sn*-glycero-3-phosphoethanolamine (PLPE) and 1-palmitoyl-2-arachidonoyl-*sn*-glycero-3-phosphoethanolamine (PAPE) for the PE class were nitrated and analyzed. They are generally among the most abundant PLs in cells[60,61]. The nitrated PC and PE species generated using an *in vitro* model system were identified by ESI-MS and the fragmentation obtained under ESI-HR-HCD-MS/MS was analyzed. Modified PC were analyzed in positive-ion mode ($[M+H]^+$ ions), while modified PE were analyzed in positive ($[M+H]^+$ ions) and negative-ion modes ($[M-H]^-$ ions). All the data were acquired using different concentrations (1 µg $mL^{-1}$, 2 µg $mL^{-1}$ and 4 µg $mL^{-1}$) of the nitrated/nitroxidized PLs derivatives. The identification was confirmed by accurate mass measurement (error < 5 ppm) and the elemental composition from HR-MS data (Tables S1 to S9). Confirmation of structural features was obtained by data analysis of HCD-MS/MS experiments.

The ESI-HR-HCD-MS/MS data obtained in the Q-Exactive Orbitrap for the nitro derivatives of POPC ($NO_2$-POPC) and POPE ($NO_2$-POPE) are presented in Figure III.1. The two species were previously detected *in vivo*[60,61] and nitro OA ($NO_2$-OA) was the most abundant $NO_2$-FA found in human plasma[43,81]. The HCD-MS/MS spectrum of each nitro PLs was acquired using three different NCE: low (20), medium (25), and high (30).

Analysis of the ESI-HR-HCD-MS/MS spectrum of the $[M+H]^+$ ions of $NO_2$-POPC reveals a major product ion at *m/z* 184.073, corresponding to the cation of the phosphocholine polar head group ($[H_2PO_4(CH_2)_2N(CH_3)_3]^+$), typical of the PC class (Figure III.1 $A_1$-$A_3$, Figure S1). Besides, in the HCD-MS/MS spectrum acquired with NCE=20 (Figure III.1 $A_1$, Figure S1), it is possible to observe, at *m/z* 758.569, the reporter ion which

is characteristic of nitrated lipids, formed by the neutral loss (NL) of nitrous acid ($HNO_2$, NL of 47 Da). When comparing the MS/MS data obtained with an NCE=25 (Figure III.1 $A_2$, Figure S1), the intensity of this typical reporter ion has decreased and for NCE=30 it cannot be detected (Figure III.1 $A_3$, Figure S1). We also observed other product ions at lower *m/z* values, corresponding to the protonated molecules of $NO_2$-OA fatty acyl chain, namely $[NO_2\text{-OA+H}]^+$ ions, at *m/z* 328.248, and the $[NO_2\text{-OA}-H_2O\text{+H}]^+$ ions, at *m/z* 310.237, respectively (Figure III.1 $A_1$-$A_3$, Figure S1). The relative abundance of these ions significantly increases for higher NCE (Figure III.2 A).

Analysis of the ESI-HR-HCD-MS/MS spectra of $NO_2$-POPE in the positive ion mode (Figure III.1 $B_1$-$B_3$, Figure S2) showed the product ion at *m/z* 622.504 ($C_2H_6PO_4N$), formed due to the NL of 141 Da, corresponding to the polar head group of phosphoethanolamine. As observed for $NO_2$-POPC, the abundance of the product ions formed due to the typical NL of 47 Da, observed at *m/z* 716.504, were also inversely correlated to the increase in the NCE. Products ions of modified FA observed at *m/z* 328.248 and *m/z* 310.238, respectively $[NO_2\text{-OA+H}]^+$ and $[NO_2\text{-OA}-H_2O\text{+H}]^+$ ions, were fairly abundant and their abundance increased with NCE. However, for ions at *m/z* 328.248 a statistically significant decrease was observed when comparing NCE=25 and NCE=30 (Figure III.2 B).

In Figure III.3 is shown a representative structure of $NO_2$-POPC (Figure III.3 A) and $NO_2$-POPE (Figure III.3 B) with the assignment of the major fragmentation pathways observed in the HCD-MS/MS of the $[M+H]^+$ ions of both nitrated species.

Trends similar to those described above were observed in the HCD-MS/MS spectra of the $[M-H]^-$ ions of $NO_2$-POPE (Figure III.1 $C_1$-$C_3$ and Figure S3). In this spectrum, it is possible to detect minor ions arising from the typical NL of $HNO_2$, with a relative abundance which was inversely correlated with the increase in NCE, and abundant carboxylate anions of nitrated FAs at *m/z* 326.234 ($[NO_2\text{-OA}-H]^-$) namely for NCE=20 and NCE=25 (Figure III.2 C). These product ions at low *m/z* value can be proposed as $NO_2$-PLs reporter ions, because they are observed with a high relative abundance in the low *m/z* range.

In addition, in the mass spectra of PC and PE acquired in positive ion mode, we observed product ions of lower relative abundance, arising from the combined NL of the polar head of PLs and the NL of the nitro group ($NO_2$, 47 Da), and product ions arising from the NL of the modified fatty acyl chain as acid and ketene derivatives. These ions were also observed in the negative ion mode in the tandem mass spectrum of PE (Figures III.2 and S4, and Tables S10 and S11).

Analysis of the HCD-MS/MS spectra acquired for the nitro derivatives of the other PC and PE standard ($NO_2$-PLPC, $NO_2$-PAPC, $NO_2$-PLPE and $NO_2$-PAPE) revealed the same

trend as that described above (Tables S1-S11). In Table III.1 are summarized the main fragmentation pathways observed in the HCD-MS/MS spectra of the $[M+H]^+$ ions of all nitrated PLs analyzed in this study.

We have also studied, using HCD-MS/MS experiments, other nitrated derivatives of PC and PE such as dinitro ($2NO_2$-PLs, +90 Da) and nitronitroso ($(NO_2)(NO)$-PLs, +74 Da) derivatives, as well as with nitroxidized derivatives, such as nitro-hydroxy ($(NO_2)O$-PLs, +61 Da) and nitro-hydroperoxy ($(NO_2)2O$-PLs, +77 Da), previously characterized by CID-MS/MS[68]. For all these species, we observed the same tendency described above for $NO_2$-POPC and $NO_2$-POPE (Tables S1-S11) and the most abundant reporter ions were attributed to the modified fatty acids. Analysis of the HCD-MS/MS data also revealed that the fragmentation pattern is independent of the concentration of the nitrated PLs species studied, as shown in Tables S10 and S11.

In conclusion, we can propose that the most suitable reporter ions for the identification of nitrated and nitroxidized PLs strongly depend on the NCE rather than on the modification (nitration and nitroxidation), or the concentration of the nitrated species. Furthermore, the NCE=25 was, in our instrument, the most suitable for obtaining the proposed range of reporter ions, from the typical NL of $HNO_2$ to the product ions of nitrated FA, with an intensity suitable for being easily detected in the HCD-MS/MS spectra (Figure III.1). An NCE=30 led to the generation of high yields of fragment ions with low *m/z* values (Figures III.2 and S4), such as the product ions of nitrated fatty acyl chain. In the HCD-MS/MS spectra acquired at NCE=20, the product ions formed due to the typical NL of $HNO_2$ (47 Da) or those arising from the combined NL of the PLs polar head group and the NL of $HNO_2$ can be considered reporter ions; however, for a higher NCE, the product ions corresponding to $[mNOn\text{-}FA+Oy+H]^+$, $[mNOn\text{-}FA+On-H_2O+H]^+$, $[mNOn\text{-}FA+Oy-H]^-$ and $[mNOn\text{-}FA+Oy-H_2O-H]^-$ (m=1-2,n=1-2, y=0-2) were the most informative. Therefore, it is essential to monitor different fragment ions as potential reporter ions to find the most suitable ones, depending on the NCE selected for the analysis. These reporter ions will be useful for the confident identification of nitrated PLs in untargeted and targeted lipidomic analysis using high-resolution orbitrap instruments.

**Table III.1.** Summary of the main fragmentation pathways observed in the HCD-MS/MS spectra of the $[M+H]^+$ ions of nitro PLs ($NO_2$-PLs) formed after the reaction of PC and PE with $NO_2BF_4$, with the proposed identification and *m/z* values. POPC, PC16:0/18:1; PLPC, PC16:0/18:2; PAPC, PC16:0/20:4 and POPE, PE16:0/18:1; PLPE, PE16:0/18:2; PAPE, PE16:0/20:4.

| **Typical neutral losses and product ions observed for $NO_2$-PC and $NO_2$-PE in positive ion mode** | | | | | | | |
|---|---|---|---|---|---|---|---|
| **Neutral Losses** | **Proposed Identification** | **$[POPC+NO_2+H]^+$** | **$[POPE+NO_2+H]^+$** | **$[PLPC+NO_2+H]^+$** | **$[PLPE+NO_2+H]^+$** | **$[PAPC+NO_2+H]^+$** | **$[PAPE+NO_2+H]^+$** |
| | | 805.8 | 763.6 | 803.6 | 761.5 | 827.8 | 785.6 |
| 18 Da | $-H_2O$ | 787.6 | 745.5 | 785.5 | 743.5 | 809.6 | 767.5 |
| 43 Da | $-C_2H_5N$ | --- | 720.4 | -- | 718.4 | -- | 742.5 |
| 47 Da | $-HNO_2$ | 758.7 | 716.5 | 756.5 | 714.6 | 780.6 | 738.5 |
| 59 Da | $-C_3H_9N$ | 746.5 | -- | 744.34 | -- | 768.7 | -- |
| 90 Da (43+47) | $-(C_2H_5N+HNO_2)$ | -- | 673.4 | -- | 671.6 | -- | 695.5 |
| 106 Da (59+47) | $-(C_3H_9N+HNO_2)$ | 699.6 | --- | 697.4 | -- | 721.5 | -- |
| 141 Da | $-C_2H_8PO_4N$ | -- | 622.5 | -- | 620.5 | -- | 644.5 |
| 183 Da | $-C_5H_{14}PO_4N$ | 622.6 | -- | 620.6 | -- | 644.6 | -- |
| 188 Da (141+47) | $-(C_2H_8PO_4N+HNO_2)$ | --- | 575.4 | -- | 573.4 | -- | 597.6 |
| 230 Da (183+47) | $-(C_5H_{14}PO_4N+HNO_2)$ | 575.5 | -- | 573.6 | -- | 597.7 | -- |
| 238 Da | $-R_1C=C=O$ | 567.6 | 525.4 | 565.4 | 523.3 | 589.3 | 547.4 |
| 256 Da | $-R_1COOH$ | 549.6 | 507.4 | 547.4 | 505.5 | 571.5 | 529.5 |
| **Product Ions** | | | | | | | |
| | | **Nitro Oleic Acid ($NO_2$-OA)** | | **Nitro Linoleic Acid ($NO_2$-LA)** | | **Nitro Arachidonic Acid ($NO_2$-AA)** | |
| $[NO_2\text{-}FA+H]^+$ | | 328.3 | 328.3 | 326.4 | 326.4 | 350.3 | 350.3 |
| $[NO_2\text{-}FA\text{-}H_2O+H]^+$ | | 310.3 | 310.3 | 308.3 | 308.3 | 332.3 | 332.3 |
| $[NO_2\text{-}FA\text{-}2H_2O+H]^+$ | | 292.3 | 292.3 | 290.3 | 290.3 | 314.2 | 314.2 |
| $[NO_2\text{-}FA\text{-}NO_2+H]^+$ | | 281.3 | 281.3 | 279.3 | 279.3 | 303.3 | 303.3 |

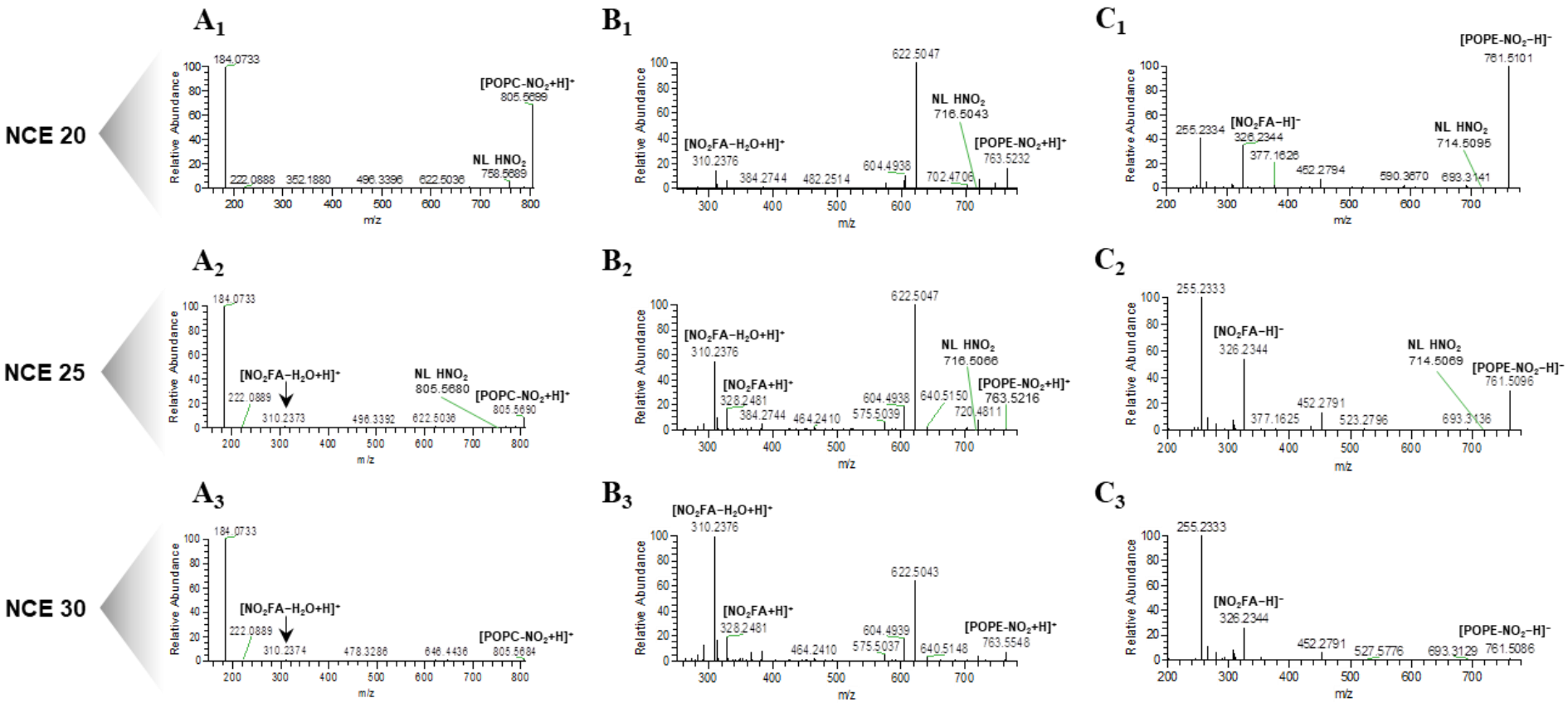


**Figure III.1.** ESI-HR-HCD-MS/MS spectra of the **(A)** $[NO_2\text{-POPC+H}]^+$ ions at *m/z* 805.6, **(B)** $[NO_2\text{-POPE+H}]^+$ ions at *m/z* 763.5 and **(C)** $[NO_2\text{-POPE−H}]^-$ ions at *m/z* 761.5, respectively, acquired in a Q-Exactive Orbitrap mass spectrometer at a concentration of 2 µg $mL^{-1}$, with low NCE (20) **A1, B1, C1** ; medium NCE (25) **A2, B2, C2** and high NCE (30) **A3, B3, C3**, respectively.

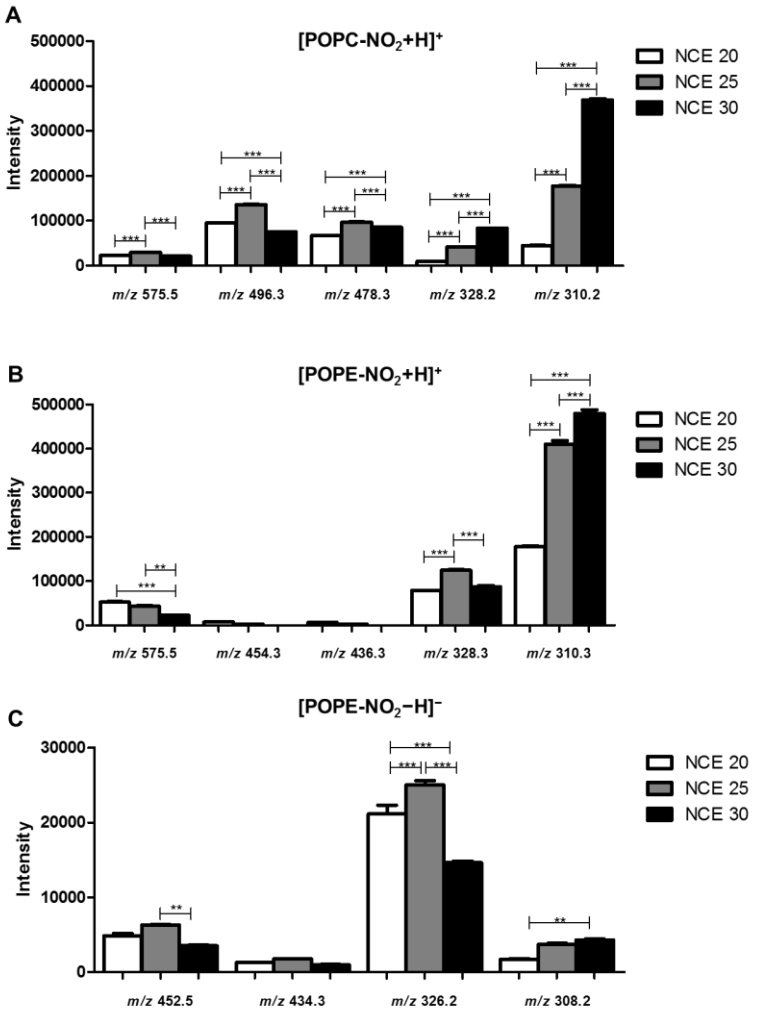


**Figure III.2.** Effect of low (20), medium (25) and high (30) NCE in the intensity of fragment ions with lower *m/z* values identified in the HCD-MS/MS spectra of: **(A)** $NO_2$-POPC ($[M+H]^+$); **(B)** $NO_2$-POPE ($[M+H]^+$); **(C)** $NO_2$-POPE ($[M-H]^-$). The identification of the fragment ions is reported in Table III.1. Fragment ions at *m/z* 575.5 are formed by the combined neutral loss of $HNO_2$ with the polar heads of phosphocholine (NL 47 plus 183 Da) or phosphoethanolamine (NL 47 plus 141 Da). The fragment ions at *m/z* 496.3 and 478.3 **(A)** and *m/z* 454.3 and *m/z* 436.3 **(B)** arise from the neutral loss of nitrated oleic acid ($NO_2$-OA) as keto (NL of 309 Da, $NO_2$-OA-$H_2O$) and acid derivatives (NL of 327 Da, $NO_2$-OA), respectively. The fragment ions at *m/z* 328.2 and 310.2 (**A** and **B**) correspond to the $[NO_2\text{-OA}+H]^+$ and $[NO_2\text{-OA}-H_2O+H]^+$ fragment ions, respectively. Fragment ions at *m/z* 452.3 and 434.3 **(C)** correspond to the neutral loss of nitrated oleic acid ($NO_2$-OA) as keto and acid derivative, respectively, and the fragment ions at *m/z* 326.3 and *m/z* 308.3 correspond to the $[NO_2\text{-OA}-H]^-$ and $[NO_2\text{-OA}-H_2O-H]^-$ ions, respectively. All the results were obtained using a concentration of 2 µg $mL^{-1}$ of the PL derivatives. Values are the means of three experiments ± standard deviation (SD). Statistical significance was determined using Anova and Tukey's multiple comparison tests (± SD, **p<0.01, ***p<0.001).

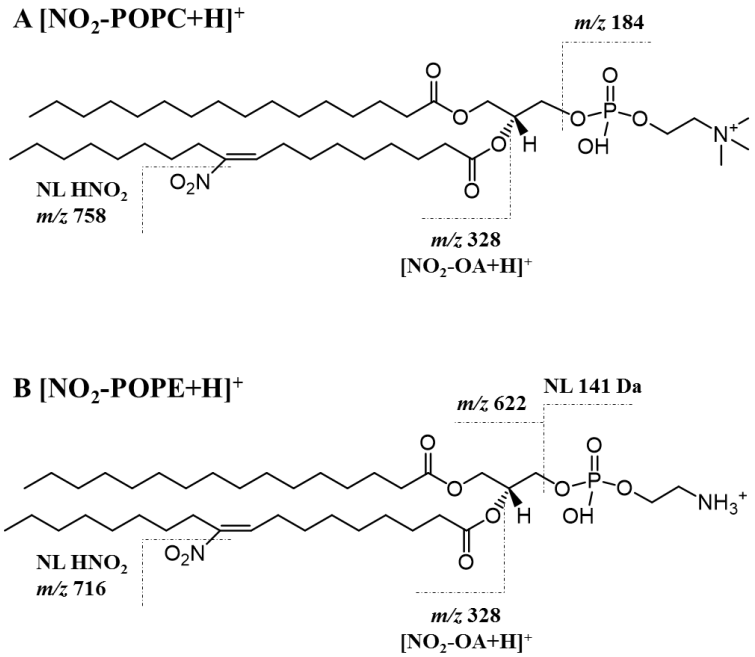


**Figure III.3.** Proposed structure of the $[M+H]^+$ ion of nitro POPC ( $[NO_2\text{-POPC+H}]^+$, **A**) and nitro POPE ($[NO_2\text{-POPE+H}]^+$, **B**) with assignment of major fragmentation pathways of nitrated phospholipids, namely the neutral loss (NL) of nitrous acid ($HNO_2$, NL 47 Da) at *m/z* 758 for $NO_2$-POPC and *m/z* 716 for $NO_2$-POPE, respectively, and the product ions of modified fatty acyl chain ($[NO_2\text{-OA+H}]^+$) at *m/z* 328. The typical fragmentation of polar head group is also assigned: product ions at *m/z* 184 for phosphocholine polar head, and NL of 141 Da for phosphoethanolamine head group. In these structures the $NO_2$ is located in C10, but it is not possible to exclude it location in C9.

### III.1.2.2. Identification of nitrated PLs in cell lipid extracts

The new findings have been validated by the identification and quantification of $NO_2$-POPC species in the analysis by hydrophilic interaction liquid chromatography (HILIC)-LC-HCD-MS/MS of cellular lipid extracts. For these experiments, SW13/cl.2 adrenal carcinoma cells stably transfected with a GFP-fusion constructs of the intermediate filament protein vimentin (GFP-vimentin wt) were used[71]. This cellular model was chosen because we recently showed that treatment of these cells with $NO_2$-POPC, but not with POPC, induced a reorganization of GFP-vimentin distribution, thus confirming a biological effect of the nitrated phospholipid[71]. Two experiments were carried out: a) the lipid extracts were obtained from GFP-vimentin SW13/cl.2 cells treated with a solution of nitrated POPC in culture (treated cells); b) the lipid extracts of the untreated cells (control cells) were treated with different volumes of nitrated POPC solution before the acquisition of the LC-ESI-MS

data (treated extracts). The $NO_2$-POPC species that were screened were previously identified *in vitro* and *in vivo* as the most abundant nitrated species[60,61].

The lipid extracts treated with different amounts of nitrated POPC (1 ng, 2 ng, 4 ng and 8 ng) were analyzed by LC-ESI-HCD-MS/MS using the data-dependent acquisition mode (DDA), as previously described in similar lipidomic studies[79,82]. MS/MS data acquisition was carried out using a stepped NCE analysis which combined information from fragment ions obtained at NCE of 20, 23 and 25 in the same spectrum. $NO_2$-POPC identification was based on retention time (RT) and exact mass measurements (error < 5 ppm), as summarized in Tables S12 and S13. Relative quantification was carried out by integrating the peak area of the extracted ion chromatograms (XIC) of $NO_2$-POPC using the MzMine software[80] and an in-house made database containing information for $NO_2$-POPC, using a mass tolerance of 5-ppm. The peak area of $NO_2$-POPC species was normalized using the peak area of the PC internal standard (dMPC, PC C14:0/C14:0). The results are presented in Figure III.4 and Tables S14 to S17. As expected, the higher the amount of nitrated POPC added to the cellular lipid extracts, the higher the relative amount of $NO_2$-POPC (Figure III.4 A). Interpretation of the MS/MS data acquired using the stepped NCE scheme made it possible to identify the fragment ions formed due to the typical NL of $HNO_2$ (Figure III.5 A). These results are in agreement with those which we described above for the standards of nitrated PC. These demonstrated that NCE lower than 25 allowed to observe the typical NL of 47 in the HCD-MS/MS spectrum of $NO_2$-POPC (Figure III.1 A).

This lipidomic approach was also applied to the identification of $NO_2$-POPC in GFP-vimentin SW13/cl.2 cells treated with nitrated POPC (Table S13). In this case, to verify the improvement acquired with the optimization of the NCE and to demonstrate the applicability of our methodology that was developed for the identification of nitrated PLs, the DDA was carried out using two different stepped NCE analyses, combining fragment ions with an NCE of 20, 23 and 25 or 25, 30 and 35. The first NCE scheme uses the range optimized with the analysis of standards and the second uses the range usually applied in our laboratory. Data analysis was performed as previously described, as well as the integration and normalization of the peak area (Table S18). We found the amount of $NO_2$-POPC in treated cells to be significantly different from treated extracts with 1 ng and 8 ng of nitrated POPC (Figure III.4 A). By using a linear regression model of the normalized peak area of $NO_2$-POPC in the treated lipid extracts, we determined that the amount of $NO_2$-POPC in treated cells was equivalent to 3.9 ng (Figure III.4 B). The HCD-MS/MS spectra obtained for treated cells (Figure III.5 B and C) were in the same trend as that observed for the $NO_2$-

POPC standards (Figure III.1): the use of the higher range of NCE leads to a decrease in the relative abundance of the product ions formed due to the NL of $HNO_2$ (*m/z* 758.58). The fragment ions formed due to the NL of $HNO_2$ were observed in the HCD-MS/MS acquired with a stepped NCE of 20, 23 and 25 (Figure III.5 B), but not in the MS/MS data obtained with a stepped NCE of 25, 30 and 35, where ions at *m/z* 310.28, corresponding to the modified fatty acyl chain ($[NO_2\text{-}OA{-}H_2O{+}H]^+$), were found (Figure III.5 C). These results highlight the need to select the most suitable reporter ions according to the experimental conditions, and that selecting the appropriate range of NCE improves the identification of nitro POPC in complex cell lipid extracts.

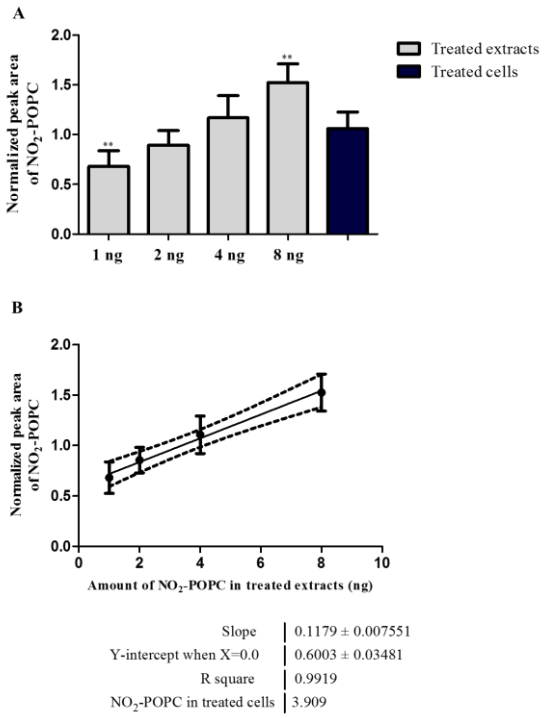


**Figure III.4. (A)** $NO_2$-POPC at *m/z* 805 detected using HILIC-MS and MS/MS analysis in GFP-vimentin SW13/cl.2 cells treated with 1 µL (1 ng), 2 µL (2 ng), 4 µL (4 ng) and 8 µL (8 ng) of nitrated POPC (1 µg $mL^{-1}$) and lipid extracts of SW13/cl.2 cells treated with nitrated POPC (10 µmol $L^{-1}$). The results were expressed as peak areas, normalized by the ratio between the peak area of $NO_2$-POPC and of the PC internal standard (dMPC, PC 14:0/14:0). The values are the means of six experiments (three biological replicas acquired in duplicate) ± standard deviation (SD). Statistical significance was determined using Anova and Tukey's multiple comparison tests (**p<0.01). **(B)** Linear regression analysis used to estimate the amount of $NO_2$-POPC in lipid extracts from cells treated with nitrated POPC (10 µmol $L^{-1}$) based on the relationship between the normalized peak area and the amount of $NO_2$-POPC in lipid extracts treated with 1 µL (1 ng), 2 µL (2 ng), 4 µL (4 ng) and 8 µL (8 ng) of nitrated POPC (1 µg $mL^{-1}$).

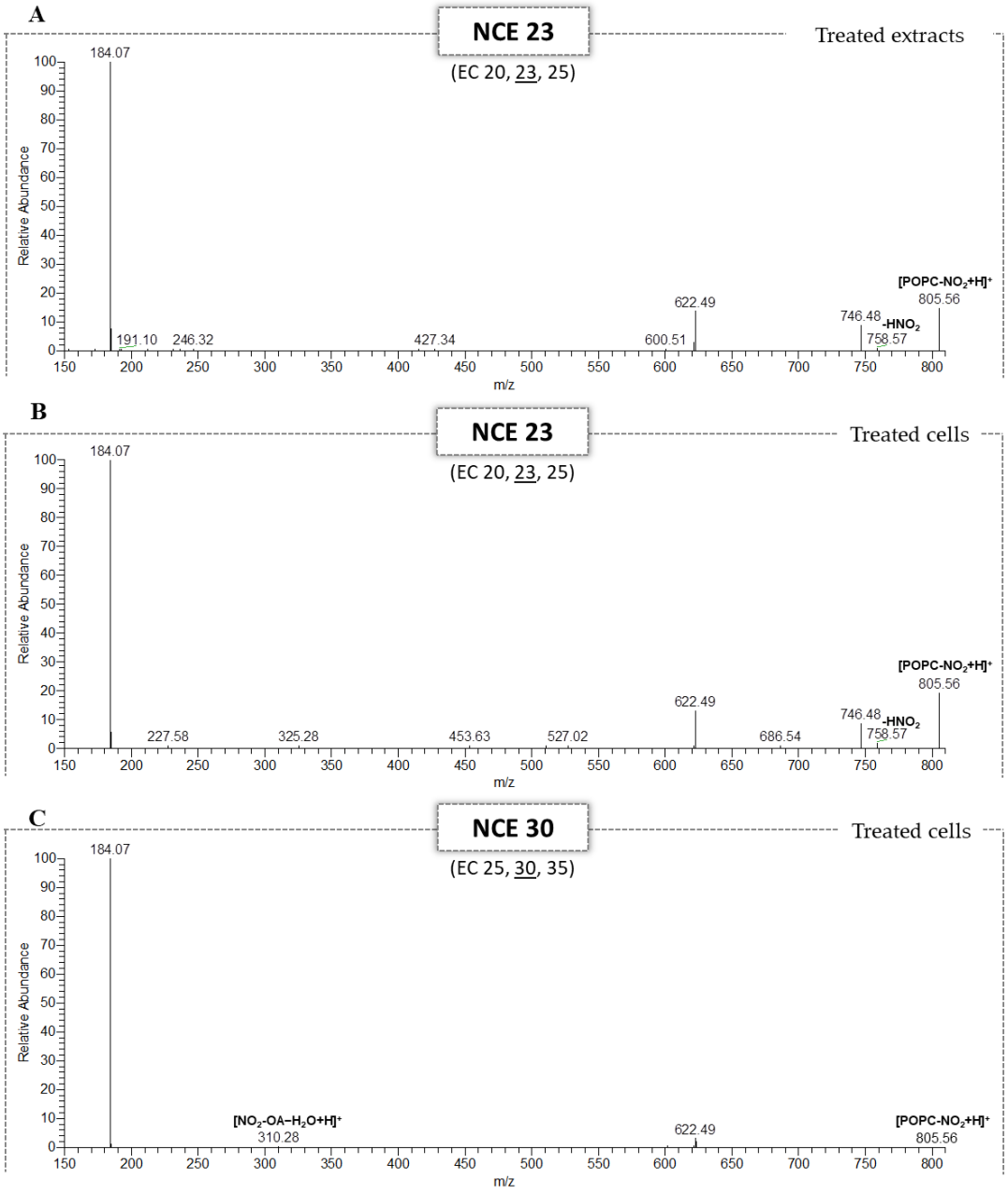


**Figure III.5.** HILIC-HCD-MS/MS spectra of $NO_2$-POPC at *m/z* 805.56 identified in the lipid extracts treated with 8 µg of nitrated POPC, obtained with an NCE=23 **(A)**. HILIC-HCD-MS/MS of $NO_2$-POPC at *m/z* 805.56 of the cellular lipid extracts from SW13/cl.2 cells treated with nitrated POPC obtained with a stepped NCE range of 20, 23, 25 (NCE 23) **(B)** and 25, 30 and 35 (NCE 30) **(C)**.

### III.1.3. Discussion

Nitrated PLs include many structurally diverse lipid species, and nitro derivatives ($NO_2$-PLs) were the main products identified in biological samples, including H9c2 cardiomyoblasts[60] and cardiac mitochondria of diabetic rats treated with streptozotocin[61]. These modified lipids showed antioxidant properties thanks to their radical scavenging potential against the $ABTS^{\bullet+}$ and $DPPH^{\bullet}$ radicals[68,72] and can also act as anti-inflammatory agents by inhibiting the expression of iNOS (at the protein level) in RAW 264.7 macrophages treated with lipopolysaccharide[72]. Also, nitrated POPC induced a series of downstream cellular effects in SW13/cl.2 cells, showing nitrated PLs as new potential electrophilic lipid mediators with selective actions[71]. However, their structural characteristics can have a great impact on their biological significance, as previously reported for $NO_2$-FA (reviewed in[13]). As such, the accurate detection and characterization of these low abundance modified lipids, in particular by using MS-based lipidomic approaches, are of the utmost importance in helping to understand their potential biological roles.

Lipidomics has been widely applied for the large-scale characterization of lipid profiles and quantification of individual lipid molecular species using either targeted or untargeted MS-based approaches that include shotgun methods and HPLC-ESI-MS based strategies. It has also applied in the study of nitrated PLs by using CID-MS/MS[60,61] and HCD-MS/MS approaches[68,70]. A very recent work on the characterization of nitrated POPS has revealed differences in the fragmentation patterns and reporter ions typical of these modified lipids under both CID- and HCD-MS/MS conditions[68]. The ion activation method and the collision energy used in tandem MS have been reported as a key step which determines the generation of structural information observed in MS/MS spectra of individual molecular species[83]. It is known that the efficiency of fragmentation of different molecular species is not equal [84] and should be adjusted to obtain the maximum intensity of the reporter fragment ions[85,86].

In this study, we outperformed, for the first time, an in-depth characterization of the fragmentation pattern of nitrated PC and nitrated PE species under HCD-MS/MS conditions in a Q-Orbitrap mass spectrometer. We assessed the alterations in the fragmentation pattern and typical reporter ions usually used to identify nitrated PLs, which were previously observed under CID conditions, using nitrated PC and nitrated PE generated from *in vitro* model systems, but also in the lipid extracts from cells treated with nitrated POPC in culture (treated cells) and in the lipid extracts treated with nitrated POPC solution before the acquisition of the LC-MS data (treated extracts). We have shown that NCE influences the

intensity of reporter ions arising from NL of $HNO_2$ (NL 47 Da), which are commonly used for the identification of nitrated and nitroxidized PLs *in vitro* and *in vivo*. Indeed, the intensity of the reporter ions formed due to the typical NL of $HNO_2$ was inversely correlated with the increase in NCE. We observed that higher NCE under HCD-MS/MS conditions is accompanied by a decrease in the relative abundance of product ions formed due to the typical NL of $HNO_2$ and, in some cases, hinders detection of these markers in the MS/MS spectra, preventing their confirmation in MS/MS analysis. The loss of $HNO_2$ has been observed with a relative high abundance, in the CID-MS/MS of nitrated PC and nitrated PE species and, until now, it was expected to be always present in all types of tandem mass spectra[60,61]. Our results have shown that it is not the case when $NO_2$-PLs are characterized by HCD-MS/MS. The absence of this typical fragmentation was recently observed for the characterization of nitrated cardiolipins (CL) under HCD-MS/MS[70].

In our study, an increase in the intensity yield of other product ions was obtained when the medium (25) and high (30) NCE ranges were applied. Some of these ions were also observed for CID-MS/MS analysis of nitrated PC and PE, namely the ions formed by the combined loss of $HNO_2$ and polar head group[60,61]. Although this seems to be desirable, these results are obtained at the expense of a decrease in the abundance of reporter ions. On the other hand, under the HCD-MS/MS conditions, the product ions with the nitrated fatty acyl moiety appear as the most dominant fragment ions, containing important information on the structural characteristics of nitrated PLs, with particular relevance in the case of nitrated PE species. These results are in agreement with the previous results reported by Neves and co-authors[68] for nitrated PS derivatives where low *m/z* reporter ions, attributed to the carboxylate anions of the modified fatty acyl chains, were seen with higher relative abundance in HCD-MS/MS spectra acquired in the orbitrap instrument, while in the CID-MS/MS the product ions with higher *m/z* values, as the ones formed by the typical NL of $HNO_2$, were the ones seen with higher relative abundance in MS/MS spectra. Montero-Bullon and co-authors[70] also found that product ions of nitrated fatty acyl arise as one of the most informative fragmentation pathways of nitrated CL. These differences are due to the higher energy dissociations in HCD (<100eV) than those used in resonant-excitation CID (<2 eV)[87]. Moreover, our results are also in agreement with those reported by Almeida and co-authors[88], who found that the same NCE is not applicable for all lipid species and is also dependent on the lipid class. These results confirmed the need for an evaluation of NCE to improve the detection of lipid molecular species, in particular those with low abundance. HCD-induced fragmentation can improve the yield of low molecular weight fragment ions

carrying important structural information due to the multiple collisions of precursor ions and fragments ions with gas molecules[75]. Moreover, HCD is a higher energy alternative to CID, and therefore a lower NCE is required to achieve the same degree of fragmentation[76,89]. This may be why it is still possible to detect the typical NL of $HNO_2$ using lower NCE.

High-resolution orbitraps have become widely used instruments for MS-based lipidomic approaches. As such, the information on the most appropriate instrument settings and parameters gathered in this study will offer new opportunities to expand the research in the field of MS analysis of nitrated PLs using orbitrap instruments, allowing accurate identification of these modified lipid species in complex biological matrices, thus facilitating the elucidation of their pathophysiological roles.

### III.1.4. Concluding Remarks

In MS/MS experiments using Orbitrap mass spectrometers, the relative abundance of the reporter ions of nitrated and nitroxidized PLs is significantly affected by the range of NCE used. This will determine which fragment ions are observed and the success of the detection of these modified lipids in biological samples. The fine-tuning of an NCE value under MS/MS experiments is necessary and extremely important to maximize the identification of nitrated and nitroxidized PLs by the generation of reporter ions with sufficient intensity to guarantee their accurate assignment.

Our results underline the importance of improving the methodology to obtain informative data in which MS/MS spectra match the typical fragmentation pattern of target compounds and allow to identify typical reporter ions. We believe that the accurate identification of these modified PLs will contribute to the understanding of their roles and signaling pathways.

# Chapter III. RESULTS AND DISCUSSION

## III.2. COMPARISON OF FRAGMENTATION PATTERNS OF NITRATED PHOSPHOLIPIDS UNDER CID AND HCD-MS/MS CONDITIONS

### III.2.1. Background and Aim of the Study

Over the past few years, MS and tandem MS strategies using soft ionization techniques namely electrospray ionization (ESI), coupled or not to liquid chromatographic (LC) techniques, has been the analytical platform chosen for the analysis (detection, characterization and quantification) of nitrated and nitroxidized PLs *in vitro* and in biological samples by using MS-based lipidomic approaches. First studies on PLs nitration/nitroxidation were performed using low collision-induced dissociation (CID) in LXQ-Linear Ion Trap (LIT) instrument[60,61]. In more recent research works, it has been used instruments with high-resolution Orbitrap technology and higher CID (higher energy collision-induced dissociation, HCD) fragmentation[68,70]. Nevertheless, fragmentation patterns and typical reporter ions can vary depending on the type of mass spectrometer and the dissociation technique used to induce the fragmentation. This is a key issue since it can hinder the detection of these modified lipid species under MS analysis. The high mass resolving power, high mass accuracy, and high sensibility of MS instruments employing Orbitrap analyzers and HCD as fragmentation method[79,82,88,90] are important features for an unambiguous detection of nitrated and nitroxidized PL species given their expected low abundance in biological samples. In this study, we aim to evaluate the differences on reliable reporter ions and fragmentation patterns of nitroso and nitro derivatives of four classes of PLs namely phosphatidylcholine (PC), phosphatidylethanolamine (PE), phosphatidylserine (PS) and cardiolipin (CL) by MS approaches based on ESI-MS/MS under both CID- and HCD-MS/MS conditions acquired in a LXQ-LIT and Q-Exactive Orbitrap, respectively, in both positive- and negative-ion modes.

### III.2.2. Results and Discussion

The PL species selected for this study were: PC C16:0/C18:1 (POPC), PE C16:0/C18:1 (POPE), PS C16:0/C18:1 (POPS), and CL $(C18:2)_4$ (tetralinoleoyl CL, TLCL). The nitroso (NO) and nitro ($NO_2$) derivatives of these PLs were generated using *in vitro* mimetic model system of nitration with $NO_2BF_4$. These species were further analyzed by MS methodologies using both CID-MS/MS and HCD-MS/MS acquired in LXQ-LIT and Q-Exactive Orbitrap mass spectrometers, respectively. The nitroso and nitro derivatives of these species were analyzed by MS and MS/MS both in positive- (as $[M+H]^+$ ions for POPC, POPE, and POPS) and negative-ion modes (as $[M-H]^-$ ions for POPE, POPS and TLCL, and $[M+OAc]^-$ ions for POPC). Despite the differences in ion activation method under CID and HCD, it was ensured that collision energy used were kept similar under both MS/MS conditions. This was performed to highlight the specific differences in the fragmentation

pattern of these modified lipid species when using distinct ion activation methods under MS/MS.

### III.2.2.1. Nitro derivatives of phospholipids

The ESI-MS/MS spectrum of nitro derivative of POPC ($NO_2$-POPC) acquired in positive-ion mode at *m/z* 805.5 and *m/z* 805.5680 upon collision-induced dissociation (CID) in a low-resolution LXQ-LIT and higher energy collision-induced dissociation (HCD)-MS/MS in high-resolution Q-Exactive Orbitrap, respectively, are depicted in Figures III.6(A) and III.6(B). The analysis of ESI-CID-MS/MS spectrum of $[NO_2\text{-POPC+H}]^+$ ions (Figures III.6(A) reveal the typical fragmentation involving PC polar head group. These fragmentations include the NL of 59 Da ($C_3H_9N$, trimethylamine) at *m/z* 746.4, and NL of 183 Da at *m/z* 622.5 ($C_5H_{14}PO_4N$, phosphocholine). Besides, the reporter ion corresponding to the typical NL of 47 Da (loss of nitrous acid, $HNO_2$), formed due to the elimination of the nitro ($NO_2$) group, was also seen at *m/z* 758.5 with a relatively high abundance. This reporter ion is characteristic of nitrated PLs and is commonly used to identify and quantify them in biological samples or in biomimetic models by MS-based lipidomic methodologies. The ions arising from combined NL of PC polar head group and NL of $HNO_2$ corresponding to the NL of 230 Da (183 Da plus 47 Da) was also observed at *m/z* 575.4.

The analysis of the ESI-HR-HCD-MS/MS spectrum of $[NO_2\text{-POPC+H}]^+$ ions at *m/z* 805.5680 (Figure III.6(B)) also reveal the common fragmentation pattern that was previously described in CID conditions, namely the product ions formed due to the NL of 183 Da (*m/z* 622.5026) and the product ion at *m/z* 575.5017 formed due to the combined fragmentation of PC polar head group with $NO_2$ group (NL of 230 Da). Other typical product ions that were observed in ESI-HCD-MS/MS spectra of the $[M+H]^+$ ions of nitrated and nitroxidized PLs are the protonated molecules of $NO_2$-FA fatty acyl chain, identified as $[NO_2\text{-FA+H}]^+$ and $[NO_2\text{-FA-}H_2O\text{+H}]^+$ ions in positive-ion mode. These product ions are formed due the cleavage between the FA and the glycerol backbone, and its observation in ESI-MS/MS spectra is favored due to charge retention in $NO_2$ group. However, they are absent or present in very low abundance in the ESI-CID-MS/MS spectra of $NO_2$-POPC.

When comparing the ESI-HR-HCD-MS/MS of $NO_2$-POPC with its ESI-CID-MS/MS, it was possible to see that the intensity of the product ions with higher *m/z* value, as the typical reporter ion at *m/z* 758.5670, have very low intensity in HCD-MS/MS spectrum. In an opposite trend, high yields of low *m/z* reporter ions were now found, namely the protonated molecules of $NO_2$-OA at *m/z* 328.2473 ($[NO_2\text{-OA+H}]^+$) and *m/z* 310.2368 ($[NO_2\text{-OA-}$

$H_2O+H]^+$). Moreover, in ESI-HR-HCD-MS/MS spectrum it was possible to observe a major product ion at *m/z* 184.0731 (base peak), corresponding to the phosphocholine polar head group ($(H_2PO_4[CH_2]_2N[CH_3]_3)^+$). In LXQ-LIT, the low mass cut-off makes difficult to attain this product ion at lower *m/z* values.

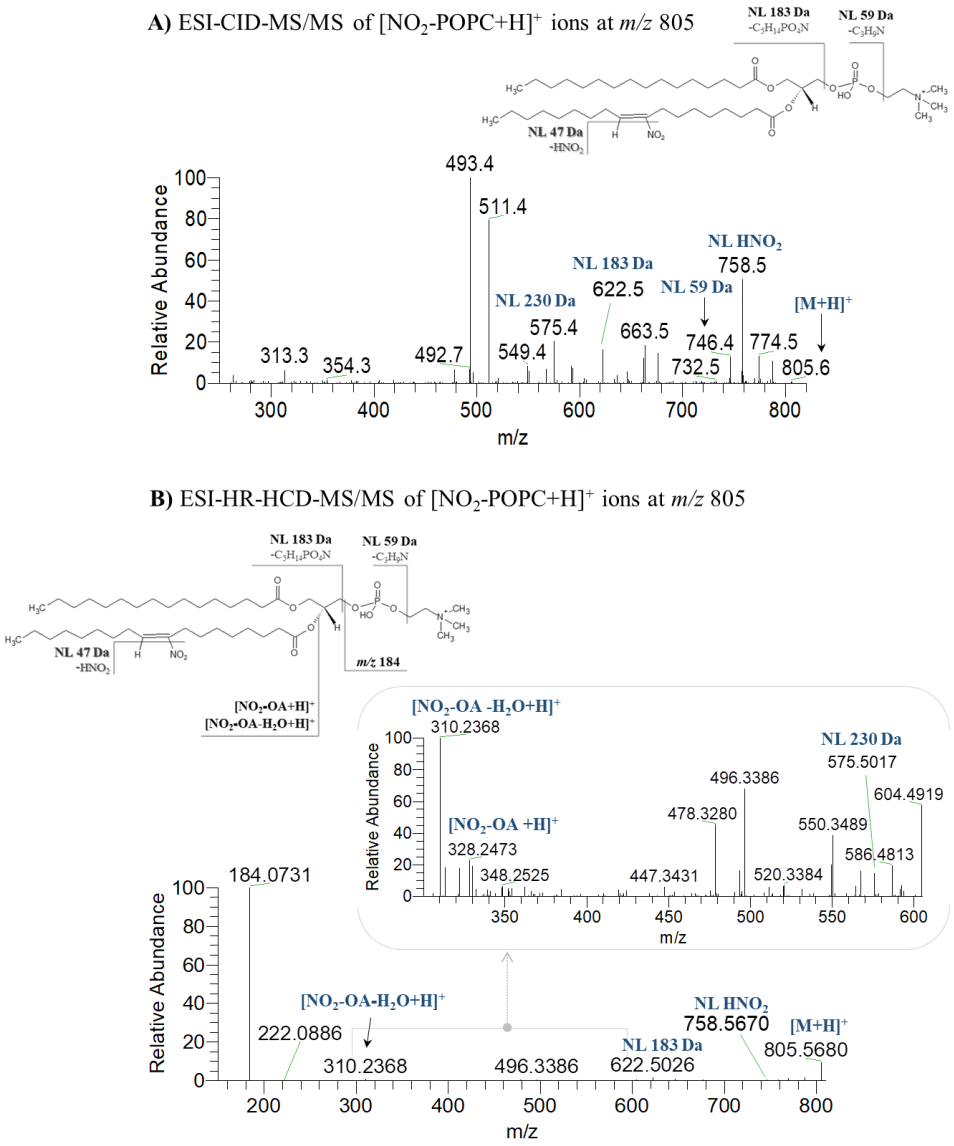


**Figure III.6. (A)** ESI-CID-MS/MS spectrum of the $[NO_2$-POPC+H]$^+$ ions at *m/z* 805.6 acquired in a Linear Ion Trap (LIT) mass spectrometer, with a collision energy (CE) of 25. **(B)** ESI-high resolution (HR)-HCD-MS/MS spectrum of the $[NO_2$-POPC+H]$^+$ ions at *m/z* 805.5680 acquired in a Q-Exactive Orbitrap, with a collision energy (CE) of 25. Inset in **(B)** illustrates the magnification of the HCD-MS/MS spectrum of $NO_2$-POPC in the *m/z* range of 300 to 600. The schematic representation of the fragmentation patterns obtained from these two different ion activation methods, CID and HCD, are also illustrated.

The analysis of the ESI-CID-MS/MS spectrum of the $[M+OAc]^-$ ions of $NO_2$-POPC, at *m/z* 863.5 (Figure III.7(A)), reveals to be not very informative as only demonstrate the reporter ion arise from the typical NL of 47 Da at *m/z* 816.6 and the product ion at *m/z* 789.3 arising from NL of 74 Da ($CH_3COOCH_3$). In an opposite trend, its ESI-HR-HCD-MS/MS (Figure III.7(B)) shows with a higher relative abundance the product ions at *m/z* 326.2328 and *m/z* 308.2224 correspond to the $[NO_2\text{-}OA\text{–}H]^-$ and $[NO_2\text{-}OA\text{–}H_2O\text{–}H]^-$ ions, respectively. The product ion at *m/z* 279.2320 was also found and corresponds to the NL of $HNO_2$ from $[NO_2\text{-}OA\text{–}H]^-$ ion. These product ions with lower *m/z* values can be used to clearly confirm the presence of $NO_2$ group.

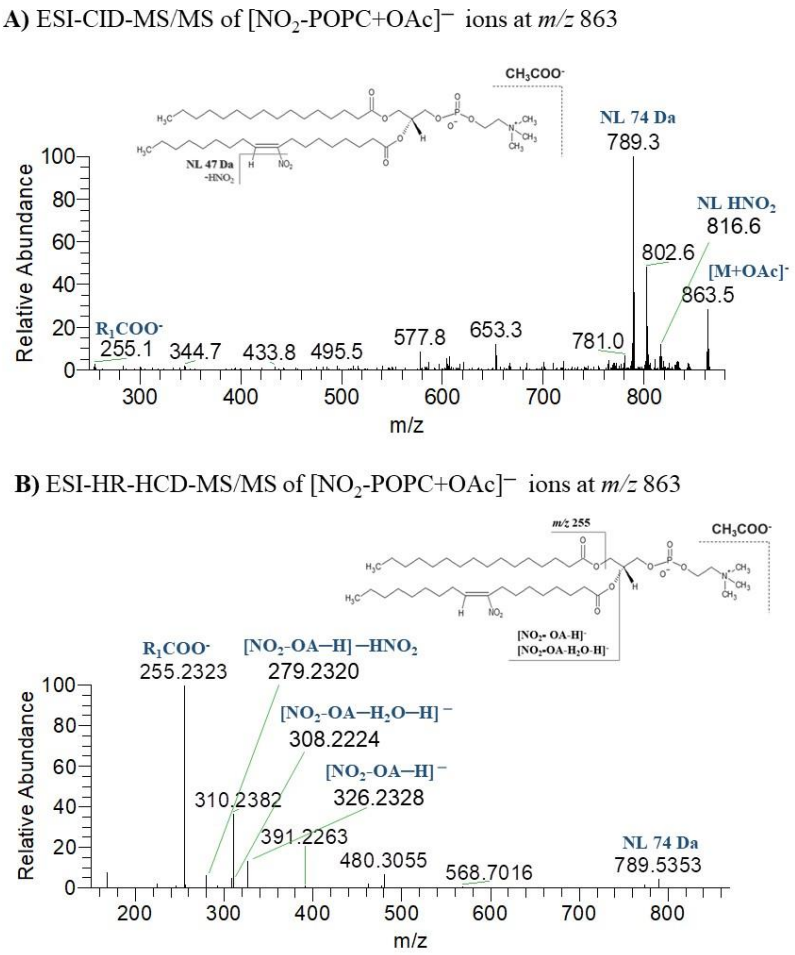


**Figure III.7**. **(A)** ESI-CID-MS/MS spectrum of the $[NO_2\text{-}POPC+OAc]^-$ ions at *m/z* 863.5 acquired in a Linear Ion Trap (LIT) mass spectrometer, with a collision energy (CE) of 25. **(B)** ESI-high resolution (HR)-HCD-MS/MS spectrum of the $[NO_2\text{-}POPC+OAc]^-$ ions at *m/z* 863.5741 acquired in a Q-Exactive Orbitrap, with a collision energy (CE) of 25. The schematic representation of the fragmentation patterns obtained from these two different ion activation methods, CID and HCD, are also illustrated.

In the same way as for $NO_2$-POPC, in Figure III.8(A) it is represented the ESI-CID-MS/MS spectrum of $[M+H]^+$ ions of nitro derivative of POPE ($NO_2$-POPE) at *m/z* 763.7. The typical fragmentation involving PE polar head group was observed through the product ions arising from NL of 43 Da ($C_2H_5N$, aziridine) at *m/z* 720.4 and the NL of 141 Da ($C_2H_8PO_4N$, phosphoethanolamine) at *m/z* 622.5 (base peak). Product ions corresponding to protonated molecule of $NO_2$-OA fatty acyl chain as the $[NO_2\text{-}OA{-}H_2O+H]^+$ ions at *m/z* 310.3 were also present. When $NO_2$-POPE was analyzed in positive-ion mode using high-resolution Orbitrap instruments, in the ESI-HR-HCD-MS/MS spectrum (Figure III.8(B)) it was possible to identify the products ions at *m/z* 720.4805 and *m/z* 622.5040 (base peak), formed due to the neutral losses of 43 Da and 141 Da, respectively. However, comparing with the information displayed in ESI-CID-MS/MS spectrum, the product ion arising from the combined fragmentation of PE polar head group with the nitro group (NL of 188 Da, i.e.141 Da plus 47 Da) at *m/z* 575.5034 was now observed. The same no longer happens for the reporter ion corresponding to the typical NL of 47 Da, which was not observed or seems to be absent in ESI-HR-HCD-MS/MS spectra of $NO_2$-POPE. On the other hand, product ions with lower *m/z* values corresponding to the protonated $NO_2$-OA at *m/z* 328.2480 ($[NO_2\text{-}OA+H]^+$) and *m/z* 310.2374 ($[NO_2\text{-}OA+H_2O+H]^+$) were observed with a higher relative abundance than those described above for CID fragmentation method.

ESI-CID-MS/MS spectrum of $[M{-}H]^-$ ions of $NO_2$-POPE at *m/z* 761.4 (Figure III.9(A)) showed the reporter ion arising from the typical NL of 47 Da at *m/z* 714.4, the carboxylate anion of $NO_2$-OA at *m/z* 326.1 ($[NO_2\text{-}OA{-}H]^-$), and the product ion at *m/z* 279.2 arising from NL of 47 Da from $[NO_2\text{-}OA{-}H]^-$**.**The ion at *m/z* 255.1 corresponds to the carboxylate anion ($R_1COO^-$) of palmitic acid.

In Figure III.9(B), the ESI-HR-HCD-MS/MS spectrum of $[NO_2\text{-}POPE{-}H]^-$ ions at *m/z* 761.5093 showed the product ions that were observed above in ESI-MS/MS data from CID, namely the product ions at *m/z* 326.2342 ($[NO_2\text{-}OA{-}H]^-$) and *m/z* 279.2333 ($[(NO_2\text{-}OA){-}HNO_2{-}H]^-$). In ESI-HR-HCD-MS/MS spectrum of $[NO_2\text{-}POPE{-}H]^-$ ions the typical reporter ion formed due the NL of $HNO_2$ was absent. In addition, the product ion at *m/z* 308.2236 correspondent to $[NO_2\text{-}OA{-}H_2O{-}H]^-$ ion was seen, which reinforces the identification of these product ions with lower *m/z* values.

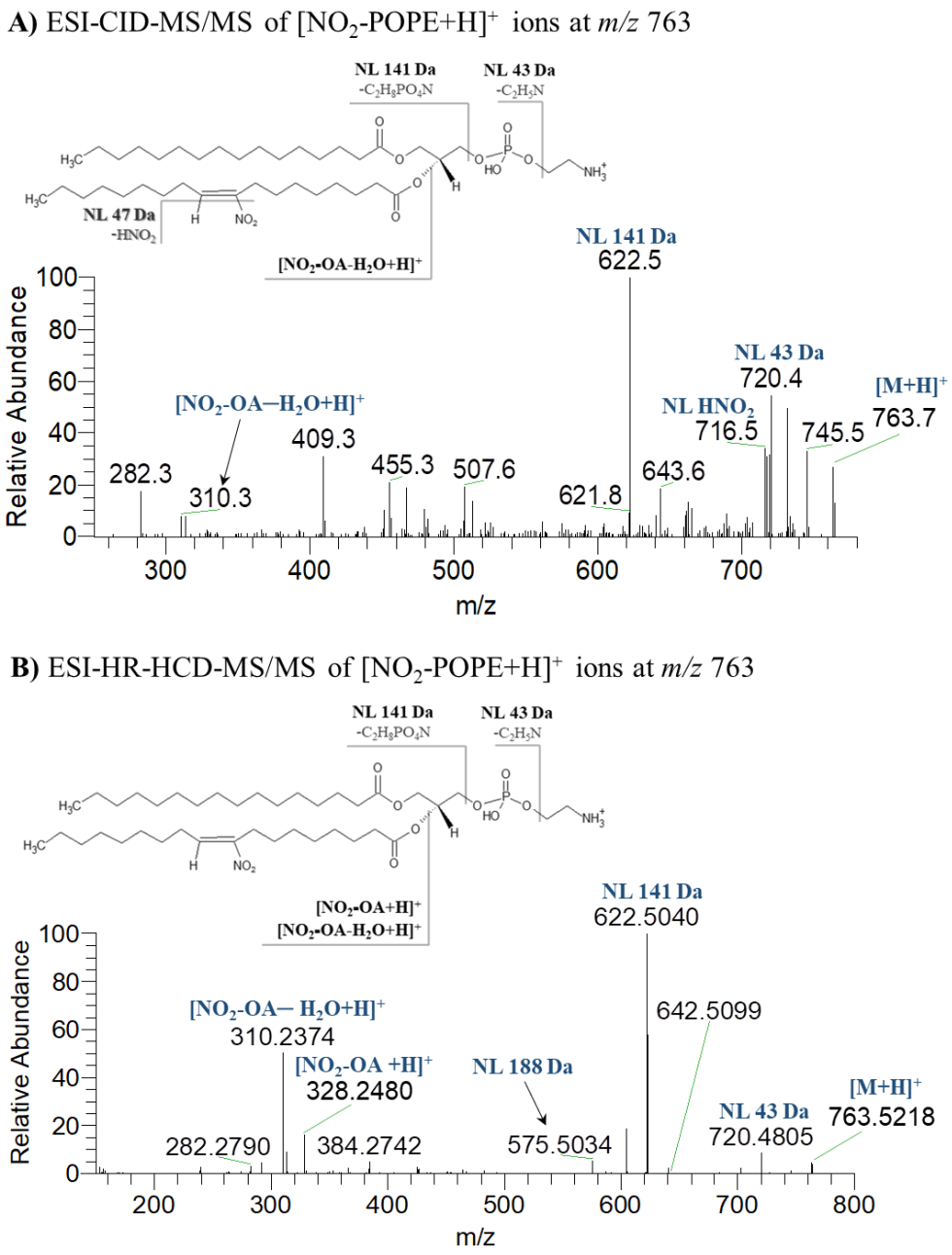


**Figure III.8. (A)** ESI-CID-MS/MS spectrum of the $[NO_2\text{-POPE+H}]^+$ ions at *m/z* 763.7 acquired in a Linear Ion Trap (LIT) mass spectrometer, with a collision energy (CE) of 25. **(B)** ESI-high resolution (HR)-HCD-MS/MS spectrum of the $[NO_2\text{-POPE+H}]^+$ ions at *m/z* 763.5218 acquired in a Q-Exactive Orbitrap, with a collision energy (CE) of 25. The schematic representation of the fragmentation patterns obtained from these two different ion activation methods, CID and HCD, are also illustrated.

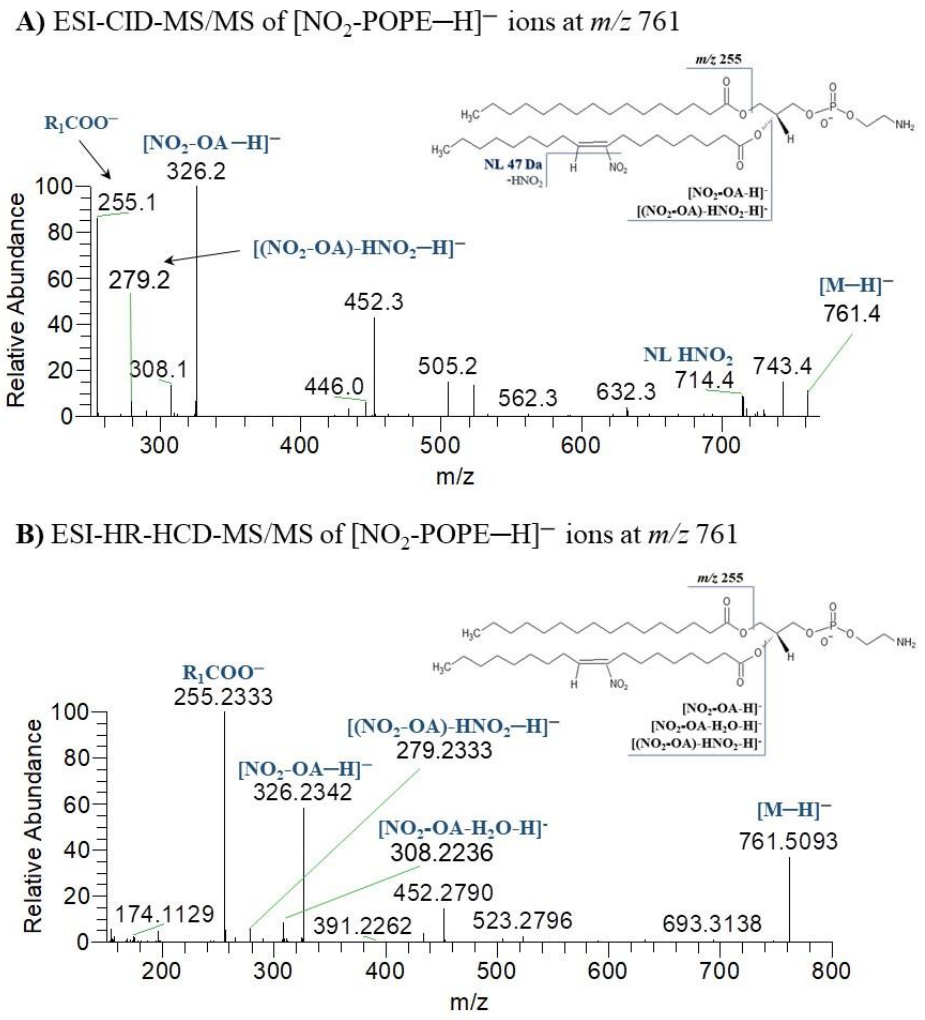


**Figure III.9. (A)** ESI-CID-MS/MS spectrum of the $[NO_2\text{-POPE–H}]^-$ ions at *m/z* 761.4 acquired in a Linear Ion Trap (LIT) mass spectrometer, with a collision energy (CE) of 25. **(B)** ESI-high resolution (HR)-HCD-MS/MS spectrum of the $[NO_2\text{-POPE–H}]^-$ ions at *m/z* 761.5093 acquired in a Q-Exactive Orbitrap, with a collision energy (CE) of 25. The schematic representation of the fragmentation patterns obtained from these two different ion activation methods, CID and HCD, are also illustrated.

ESI-CID-MS/MS spectrum of $[M+H]^+$ ions of nitro derivative of POPS ($NO_2$-POPS) at *m/z* 807.3 (Figure III.10(A)) showed product ions corresponding to the typical NL of $HNO_2$ at *m/z* 760.5, the product ions formed due the NL of 87 Da at *m/z* 720.4 occurring from the loss of PS polar head group ($C_3H_5NO_2$, serine), as well as the product ion at *m/z* 622.4 (base peak) formed due to the NL of 185 Da ($C_3H_8PO_6N$, phosphoserine). Likewise ESI-CID-MS/MS spectra of $NO_2$-POPC and $NO_2$-POPE (Figures III.6(A) and III.8(A)), here the protonated ions of the modified fatty acyl chain at *m/z* 310.2 ($[NO_2\text{-OA}+H_2O+H]^+$) was also

seen. Similarity to those described above for ESI-CID-MS/MS, in the ESI-HR-HCD-MS/MS spectrum of $[NO_2\text{-POPS+H}]^+$ ions (Figure III.10(B)) it was possible to detect product ions arising from the NL of 87 Da at *m/z* 720.4804, and the NL of 185 Da at *m/z* 622.5039. In this spectrum, the typical NL of 47 Da was absent, but the product ion at *m/z* 575.5035 arising from the NL of 232 Da (185 Da plus 47 Da), which corresponds to the combined loss of the PS polar head group with the NL of $HNO_2$, was the most abundant peak (base peak), confirming the presence of $NO_2$ group. Besides, the product ion corresponding to the protonated $NO_2$-OA at *m/z* 310.2373 ($[NO_2\text{-OA}{-}H_2O+H]^+$) was also observed with apparent high relative abundance.

In ESI-CID-MS/MS spectrum of $[NO_2\text{-POPS}{-}H]^-$ ions (Figure III.11(A)) the product ions formed due to the typical neutral losses of 47 Da and 87 Da were observed at *m/z* 758.3 and *m/z* 718.3, respectively. This abundant NL 87 Da is typically observed in the ESI-MS/MS spectra of $[M{-}H]^-$ ions of native and nitrated PS. However, ions arising from the NL of $HNO_2$ was present in very low abundance. Additionally, it is possible identify the combined NL of 87 Da plus 47 Da (NL of 134 Da) at *m/z* 671.5 and the product ions of modified oleic fatty acyl chain namely the $[NO_2\text{-OA}{-}H]^-$ ions at *m/z* 326.1 and $[(NO_2\text{-OA}){-}HNO_2{-}H]^-$ ions at *m/z* 279.3, all of them with very small relative abundance. The product ion at *m/z* 255.3 corresponds to the $R_1COO^-$. Comparing the ESI-MS/MS spectra obtained from CID (Figure III.11(A)) and HCD (Figure III.11(B)) in negative-ion mode, in ESI-HR-HCD-MS/MS spectrum of $NO_2$-POPS the same product ions at *m/z* 718.4668 (NL of 87 Da), *m/z* 671.4662 (NL of 134 Da), *m/z* 326.2339 ($[NO_2\text{-OA}{-}H]^-$) and *m/z* 279.2331 ($[(NO_2\text{-OA}){-}HNO_2{-}H]^-$) were observed but with an increase in their relative abundance. The typical NL of $HNO_2$ from the precursor ion was absent; however, the carboxylate anions at *m/z* 326.2339 ($[NO_2\text{-OA}{-}H]^-$) and *m/z* 279.2331 ($[(NO_2\text{-OA}){-}HNO_2{-}H]^-$) were found as well as one more product ion with lower *m/z* value, corresponding to the $[NO_2\text{-OA}{-}H_2O{-}H]^-$ ion at *m/z* 308.2234.

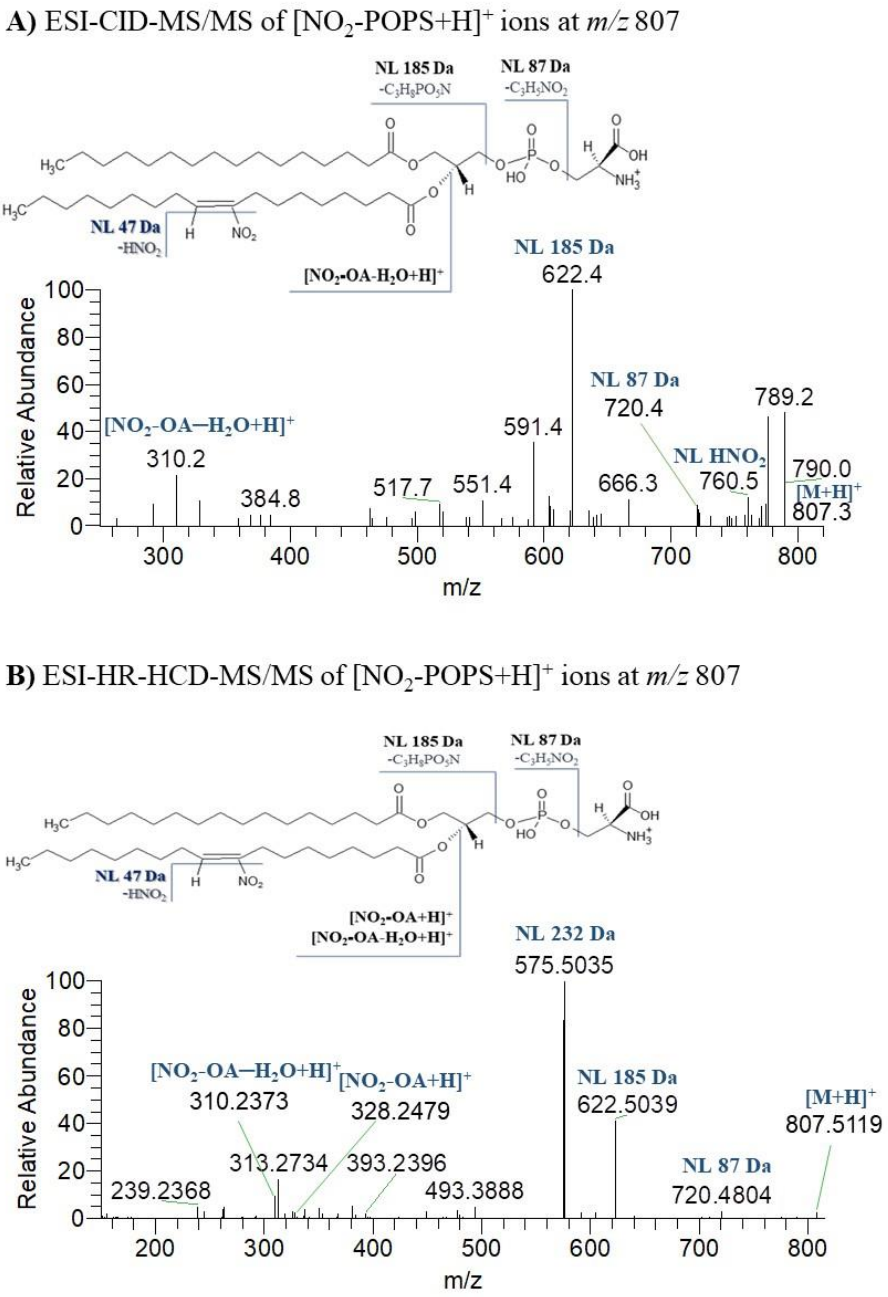


**Figure III.10. (A)** ESI-CID-MS/MS spectrum of the $[NO_2\text{-POPS+H}]^+$ ions at *m/z* 807.3 acquired in a Linear Ion Trap (LIT) mass spectrometer, with a collision energy (CE) of 16. **(B)** ESI-high resolution (HR)-HCD-MS/MS spectrum of the $[NO_2\text{-POPS+H}]^+$ ions at *m/z* 807.5119 acquired in a Q-Exactive Orbitrap, with a collision energy (CE) of 25. The schematic representation of the fragmentation patterns obtained from these two different ion activation methods, CID and HCD, are also illustrated.

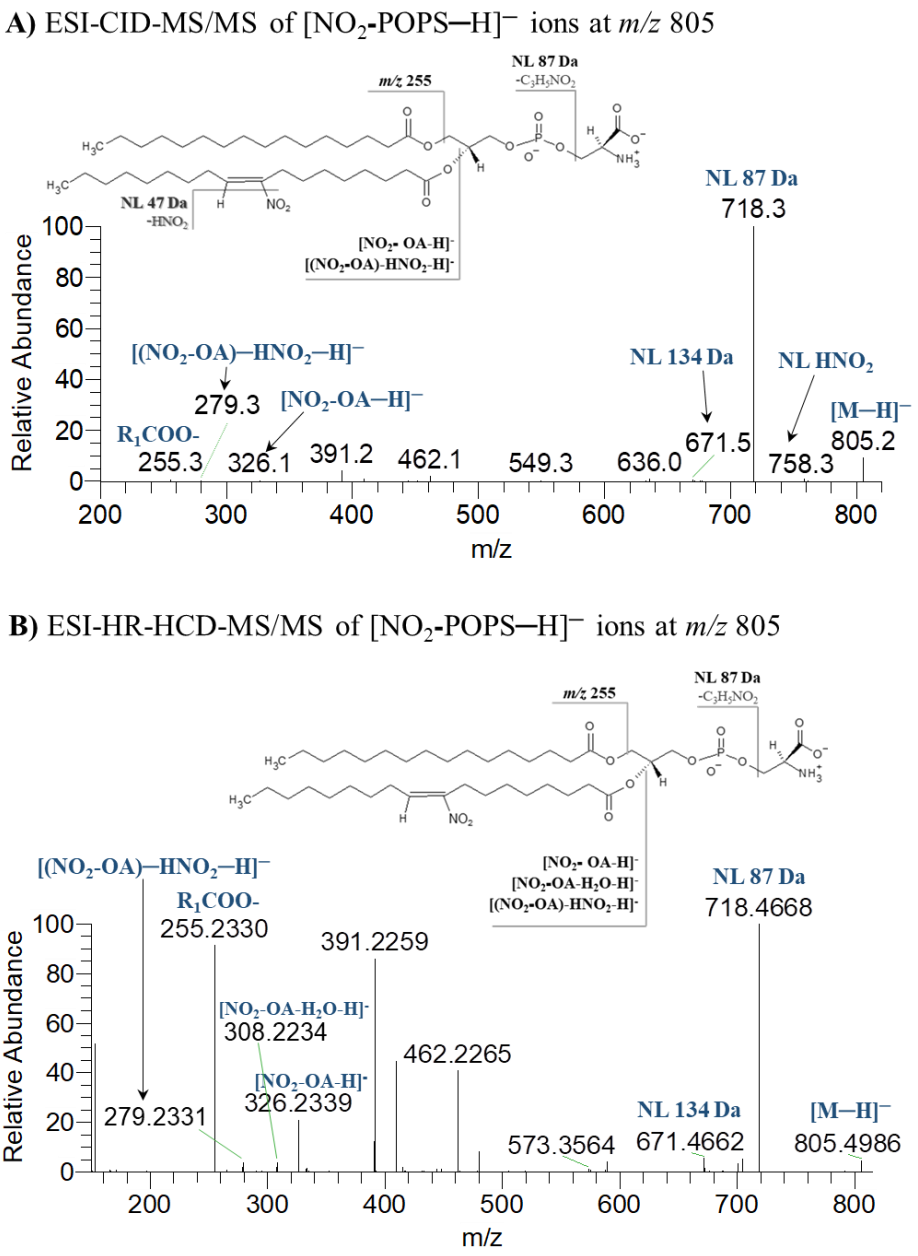


**Figure III.11. (A)** ESI-CID-MS/MS spectrum of the [$NO_2$-POPS–H]$^-$ ions at *m/z* 805.2 acquired in a Linear Ion Trap (LIT) mass spectrometer, with a collision energy (CE) of 16. **(B)** ESI-high resolution (HR)-HCD-MS/MS spectrum of the [$NO_2$-POPS–H]$^-$ ions at *m/z* 805.4983 acquired in a Q-Exactive Orbitrap, with a collision energy (CE) of 25. The schematic representation of the fragmentation patterns obtained from these two different ion activation methods, CID and HCD, are also illustrated.

Figure III.12(A) shows the ESI-CID-MS/MS spectrum of nitro tetralinoleoyl-CL ($NO_2$-TLCL) acquired in negative-ion mode where it is possible to observe the reporter ion at *m/z* 1445.8, arising from de typical NL of 47 Da, with a high relative abundance. Besides, product ions of nitro phosphatidic acid at *m/z* 740.4 ([$NO_2$-PA–H]$^-$) and nitro lysophosphatidic ([$NO_2$-LPA–H]$^-$) at *m/z* 460.1 were seen, as well as the ions at *m/z* 876.3 and *m/z* 796.6 corresponding to the [$NO_2$-PA+136–H]$^-$ and [$NO_2$-PA+56–H]$^-$, respectively. The nonmodified phosphatidic acid [PA–H]$^-$ at *m/z* 695.3 were also detected. However, the product ions corresponding to the loss of the fatty acyl substituents were not observed, since LXQ-LIT has a low mass cut-off avoiding that ions with a lower *m/z* value from being detected. In this way, the analysis of the ESI-CID-MS/MS spectrum of [M–2H]$^{2-}$ ions of $NO_2$-TLCL (Figure III.12($A_1$) at *m/z* 745.4 allows to see the product ions at *m/z* 324.3 and *m/z* 279.2 (base peak) corresponds to the nitro linoleic acid and the unmodified linoleic acid, respectively.

As observed above in ESI-CID-MS/MS spectra of $NO_2$-TLCL, its ESI-HR-HCD-MS/MS spectrum (Figure III.12(B)) also showed the main fragmentation pathways of $NO_2$-TLCL, namely the presence of the product ions corresponding to [$NO_2$-PA–H]$^-$ and [$NO_2$-LPA–H]$^-$ at *m/z* 740.4527 and 460.2119, respectively. Nevertheless, the typical NL of $HNO_2$ was not found, in contrast with described above in Figure III.12(A). Similarly, to that observed in ESI-CID-MS/MS spectrum of [$NO_2$-TLCL–2H]$^{2-}$, the product ions at *m/z* 324.2214 ($NO_2$-RCOO$^-$) and *m/z* 279.2333 (RCOO$^-$, base peak) were also observed. The product ion at *m/z* 277.2172 which arise from de NL of 47 Da from $NO_2$-RCOO$^-$ was also seen, which confirms that we are in the presence of an $NO_2$-TLCL.

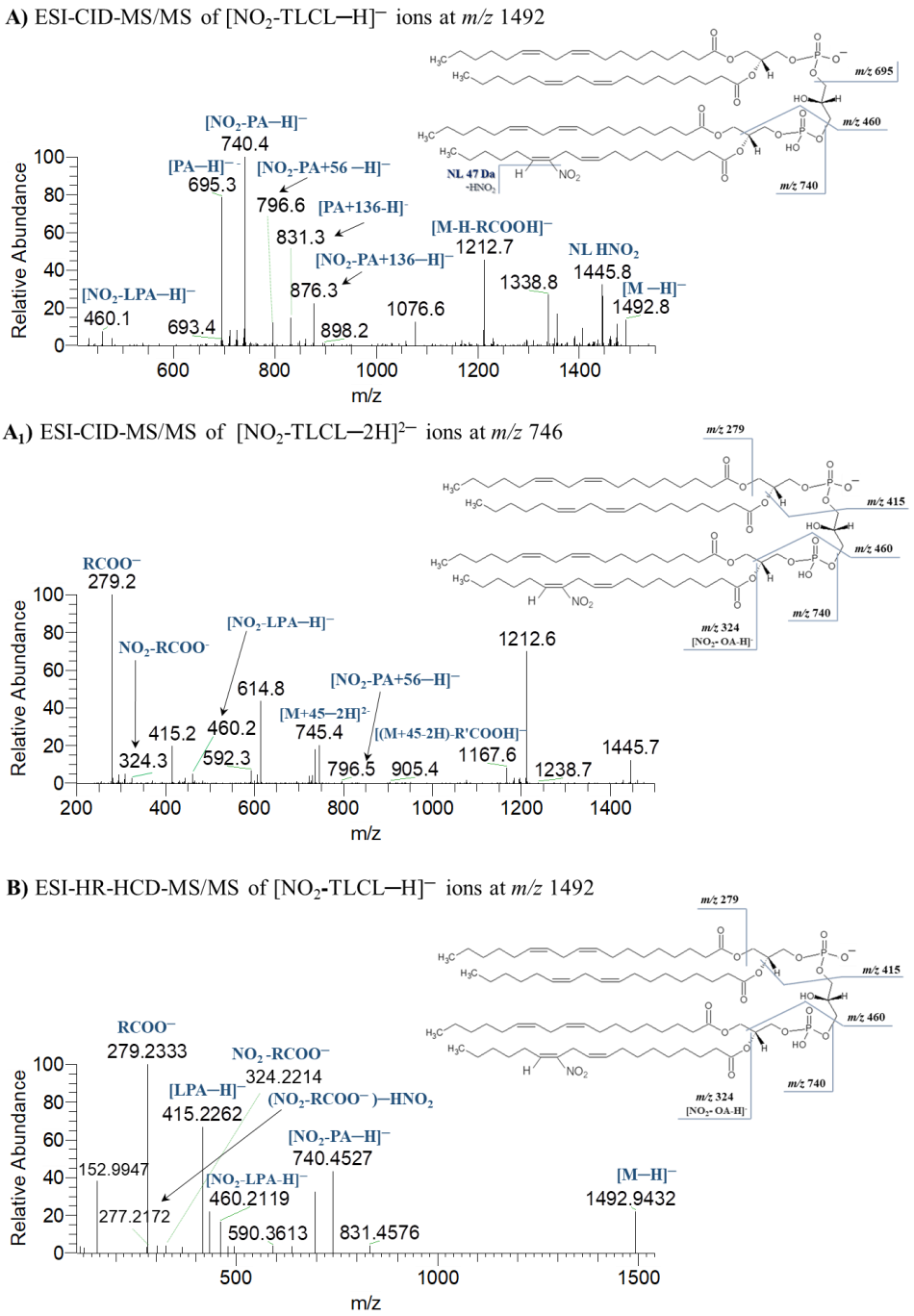


**Figure III.12. (A)** ESI-CID-MS/MS spectrum of the $[NO_2\text{-TLCL–H}]^-$ ions at *m/z* 1492.8 acquired in a Linear Ion Trap (LIT) mass spectrometer, with a collision energy (CE) of 24. **($A_1$)** ESI-CID-MS/MS spectrum of the $[NO_2\text{-TLCL–2H}]^{2-}$ ions at *m/z* 746 acquired in a Linear Ion Trap (LIT) mass spectrometer, with a collision energy (CE) of 16. **(B)** ESI-high resolution (HR)-HCD-MS/MS spectrum of the $[NO_2\text{-TLCL–H}]^-$ ions at *m/z* 1492.9432 acquired in a Q-Exactive Orbitrap, with a collision energy (CE) of 23. The schematic representation of the fragmentation patterns obtained from these two different ion activation methods, CID and HCD, are also illustrated.

### III.2.2.2. Nitroso derivatives of phospholipids

The ESI-CID-MS/MS data in LXQ-LIT in positive-ion mode for the nitroso derivatives of POPC (NO-POPC) at *m/z* 789.6, corresponding to a mass shift of 29 Da (NO) from the native POPC, is represented in Figure III.13(A). In this spectrum it was possible to identify the characteristic fragmentation pathways of PC class, namely the NL of 59 Da and NL of 183 Da (base peak) at *m/z* 730.6 and *m/z* 606.5, respectively. The reporter ion at *m/z* 758.3 arising from de typical NL of 31 Da (loss of nitroxyl group, HNO) was also observed. In Figure III.13(B) is shown the ESI-HR-HCD-MS/MS spectrum of $[NO\text{-}POPC+H]^+$ obtained in Q-Exactive Orbitrap at *m/z* 789.5742, where the product ions *m/z* 730.5009 and *m/z* 606.5090 can also be seen although they have a lower relative abundance than in ESI-CID-MS/MS. As previously describe for $[NO_2\text{-}POPC+H]^+$ ions, the ESI-HR-HCD-MS/MS of NO-POPC revealed a major product ion at *m/z* 184.0733 (base peak). However, comparing both CID and HCD fragmentation methods, the analysis of the ESI-HR-HCD-MS/MS of NO-POPC do not give information related to the typical NL of HNO, but enhance the relative abundance of the product ions with lower *m/z* value identified as $[NO\text{-}OA+H]^+$ and $[NO\text{-}OA{-}H_2O+H]^+$ at *m/z* 312.2531 and *m/z* 294.2425, respectively (Figure III.13(B)).

The ESI-CID-MS/MS spectrum of $[M+OAc]^-$ ions of NO-POPC at *m/z* 847.7, reported in Figure III.14(A), allowed to identify similar product ions as those described before for $[NO_2\text{-}POPC+OAc]^-$ (Figure III.7(A)), namely the reporter ion at *m/z* 816.3, which arises from the typical NL of HNO and the product ion at *m/z* 773.5 arising from NL of 74 Da ($CH_3COOCH_3$). The product ion at *m/z* 255.2 corresponding to the $R_1COO^-$ of palmitic acid was also observed. ESI-HR-HCD-MS/MS spectrum of $[NO\text{-}POPC+OAc]^-$ ions showed the product ions at *m/z* 255.2330 and *m/z* 773.556 (NL of 74 Da) (Figure III.14(B)). When the ESI-HR-HCD-MS/MS spectrum of NO-POPC was compared with its ESI-CID-MS/MS spectrum, the product ions arising from the carboxylate anion of NO-OA fatty acyl chain as the $[NO\text{-}OA{-}H]^-$ ion at *m/z* 310.2393 appears with a high relative abundance in opposition to the typical NL of HNO, which was not observed. The ion at *m/z* 168.0425 corresponding to the loss of methyl ($-CH_3$) from the PC polar head group was only observed in ESI-HR-HCD-MS/MS.

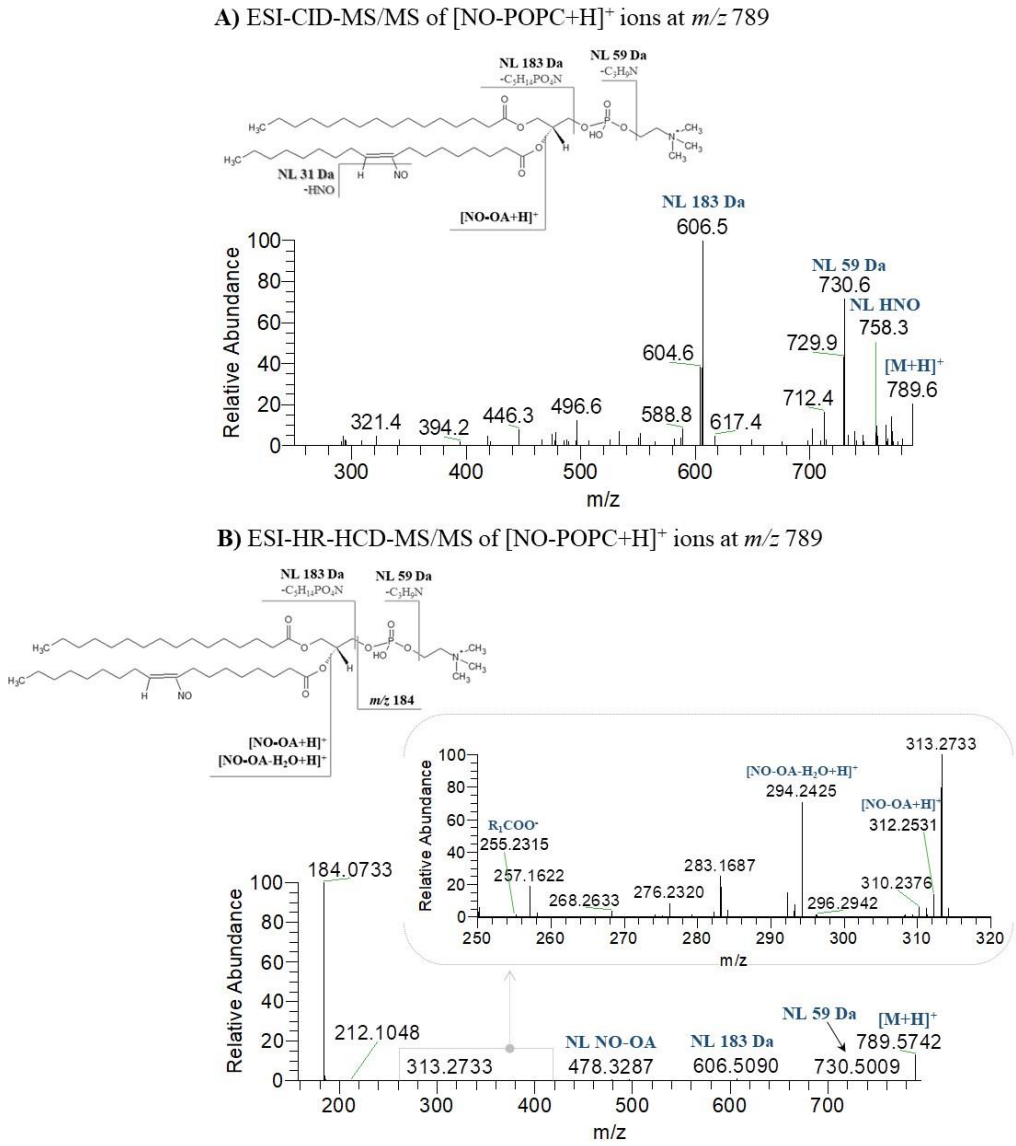


**Figure III.13. (A)** ESI-CID-MS/MS spectrum of the [NO-POPC+H]⁺ ions at *m/z* 789.6 acquired in a Linear Ion Trap (LIT) mass spectrometer, with a collision energy (CE) of 25. **(B)** ESI-high resolution (HR)-HCD-MS/MS spectrum of the [NO-POPC+H]⁺ ions at *m/z* 789.5742 acquired in a Q-Exactive Orbitrap, with a collision energy (CE) of 25. Inset in **(B)** illustrates the magnification of the HCD-MS/MS spectrum of NO-POPC in the *m/z* range of 250 to 320. The schematic representation of the fragmentation patterns obtained from these two different ion activation methods, CID and HCD, are also illustrated.

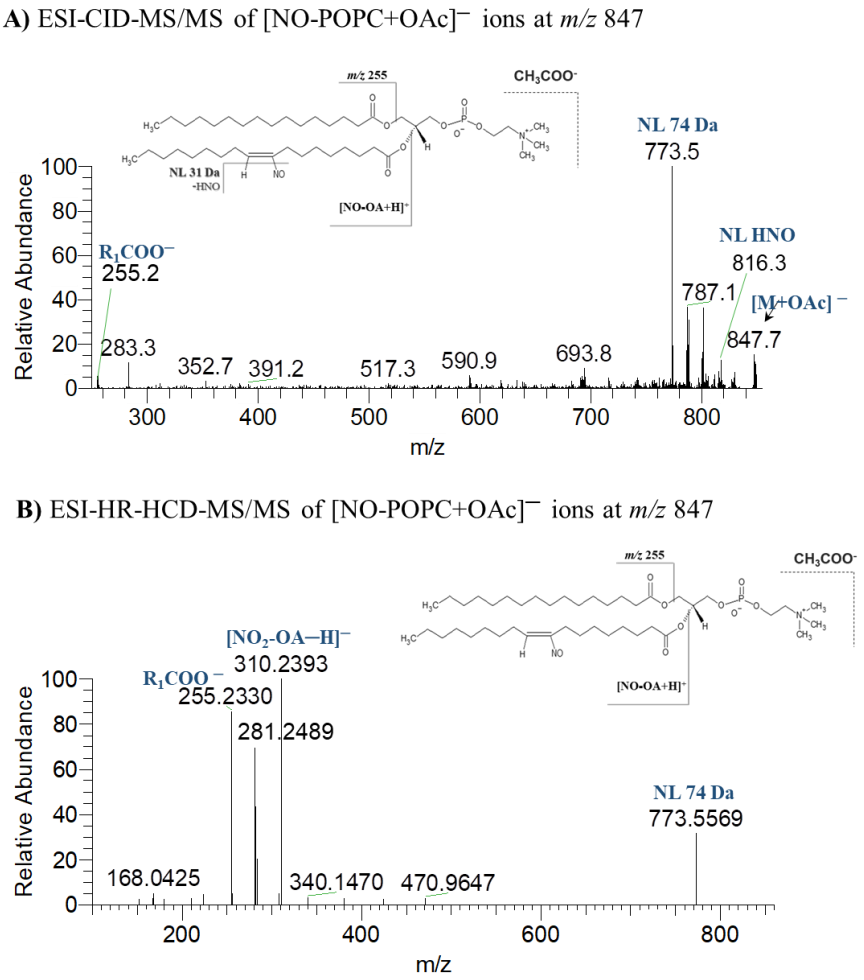


**Figure III.14. (A)** ESI-CID-MS/MS spectrum of the [NO-POPC+OAc]⁻ ions at *m/z* 847.7 acquired in a Linear Ion Trap (LIT) mass spectrometer, with a collision energy (CE) of 25. **(B)** ESI-high resolution (HR)-HCD-MS/MS spectrum of the [NO-POPC+OAc]⁻ ions at *m/z* 847.5779 acquired in a Q-Exactive Orbitrap, with a collision energy (CE) of 25. The schematic representation of the fragmentation patterns obtained from these two different ion activation methods, CID and HCD, are also illustrated.

In Figure III.15(A) is shown the ESI-CID-MS/MS spectrum of $[M+H]^+$ ions of nitroso derivatives of POPE (NO-POPE) at *m/z* 747.6. This spectrum allowed to identify the typical fragmentation of PE polar head group at *m/z* 704.6 (NL of 43 Da) and *m/z* 606.6 (NL of 141 Da, base peak). Product ions arising from the combined fragmentation of both aziridine with NO group (NL of 74 Da) at *m/z* 673.5 were also observed. The typical NL of 31 Da at *m/z* 716.5 was also found, contrary to what happens with the protonated ions of nitrated FA. On the other hand, the ESI-HR-HCD-MS/MS of $[M+H]^+$ ions of NO-POPE at *m/z* 747.5737 (Figure III.15(B)) showedthe product ions corresponding to the protonated NO-OA at *m/z* 312.2529 ($[NO\text{-}OA+H]^+$) and *m/z* 294.2424 ($[NO_2\text{-}OA–H_2O+H]^+$) were observed. As

observed in ESI-CID-MS/MS, the product ions at *m/z* 704.4779 and *m/z* 606.5084 were also present in ESI-HR-HCD-MS/MS of $[NO\text{-}POPE+H]^+$ ions. Product ions arising from the NL of HNO were absent. Since the NL of HNO and the combined fragmentation of PL polar head group plus the NO group are absent in both HCD-MS/MS data of NO-POPC and NO-POPE in positive-ion mode, the identification of the protonated ions of nitroso fatty acid can be used to validate the presence of NO group in the ESI-HR-HCD-MS/MS spectra.

The ESI-CID-MS/MS spectrum of the $[M{-}H]^-$ ions of NO-POPE at *m/z* 745.4 (Figure III.16(A)) showed the typical NL of HNO at *m/z* 714.4 as well as the product ions at *m/z* 452.2 and *m/z* 489.3 arising from the NL of the (NO-OA)$-H_2O$ and from the NL of palmitic acid, respectively. Product ion at *m/z* 255.1 corresponds to the $R_1COO^-$. The product ion with lower *m/z* value corresponding to carboxylate anion of NO-OA ($[NO\text{-}OA{-}H]^-$) at *m/z* 310.2 was also observed, with a considerable relative abundance. Likewise, the product ions at *m/z* 310.2393 and at *m/z* 452.2786 were also found in the ESI-HR-HCD-MS/MS spectrum of $[NO\text{-}POPE{-}H]^-$ ions (Figure III.16(B)). The reporter ion arising from the NL of HNO is missing.

Once again, in ESI-HCD-MS/MS of both NO-POPC and NO-POPE the presence of the product ions at lower *m/z* values and with higher abundance relative, namely the deprotonated molecules of the NO-OA allowed to confirm the presence of NO group in PLs when the NL of HNO was not observed. Trends like those described above were observed in the ESI-HR-HCD-MS/MS spectra of both $[NO_2\text{-}POPC+OAc]^-$ and $[NO_2\text{-}POPE{-}H]^-$ ions (Figures III.7(B) and III.9(B)).

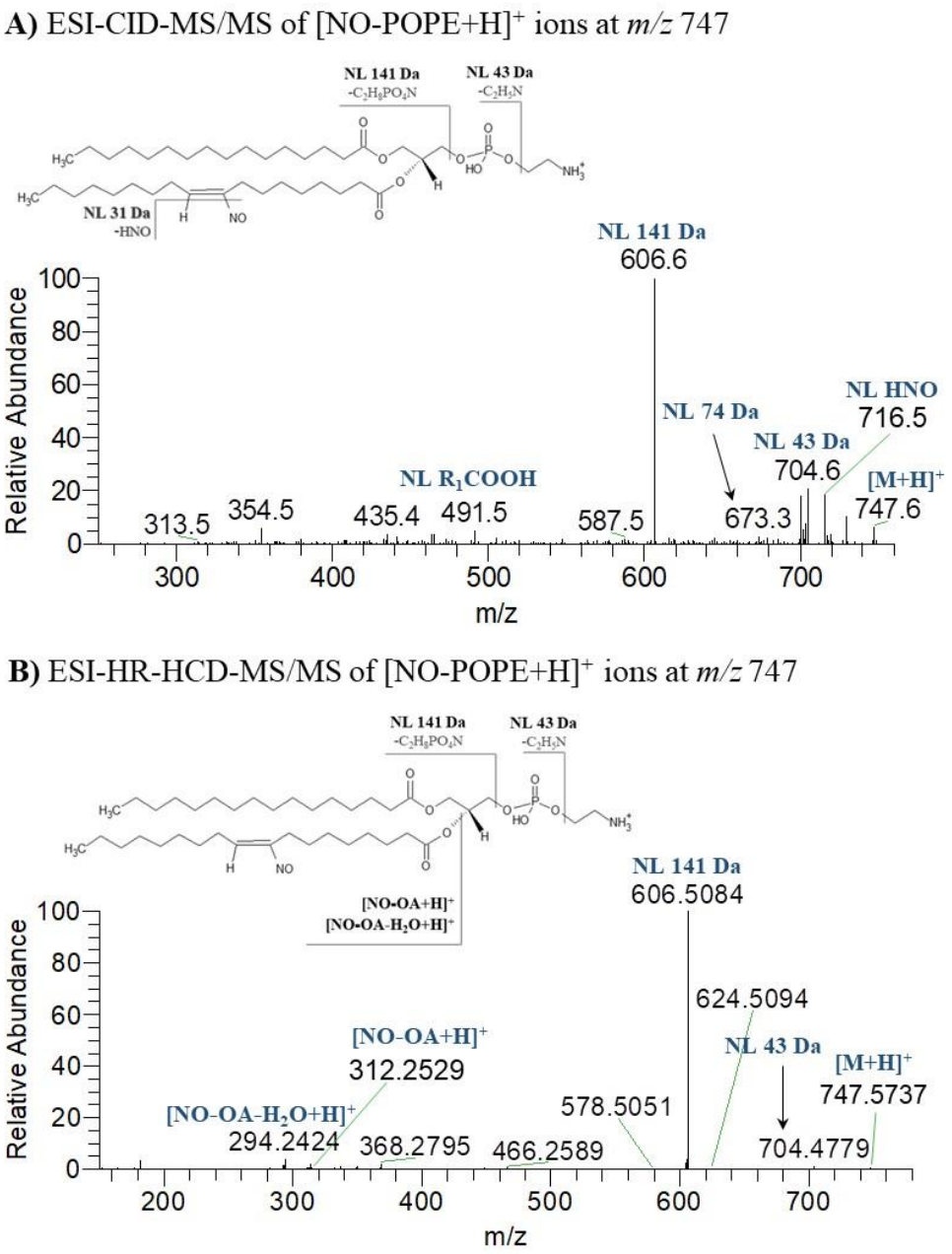


**Figure III.15. (A)** ESI-CID-MS/MS spectrum of the [NO-POPE+H]⁺ ions at *m/z* 747.6 acquired in a Linear Ion Trap (LIT) mass spectrometer, with a collision energy (CE) of 25. **(B)** ESI-high resolution (HR)-HCD-MS/MS spectrum of the [NO-POPE+H]⁺ ions at *m/z* 747.5737 acquired in a Q-Exactive Orbitrap, with a collision energy (CE) of 25. The schematic representation of the fragmentation patterns obtained from these two different ion activation methods, CID and HCD, are also illustrated.

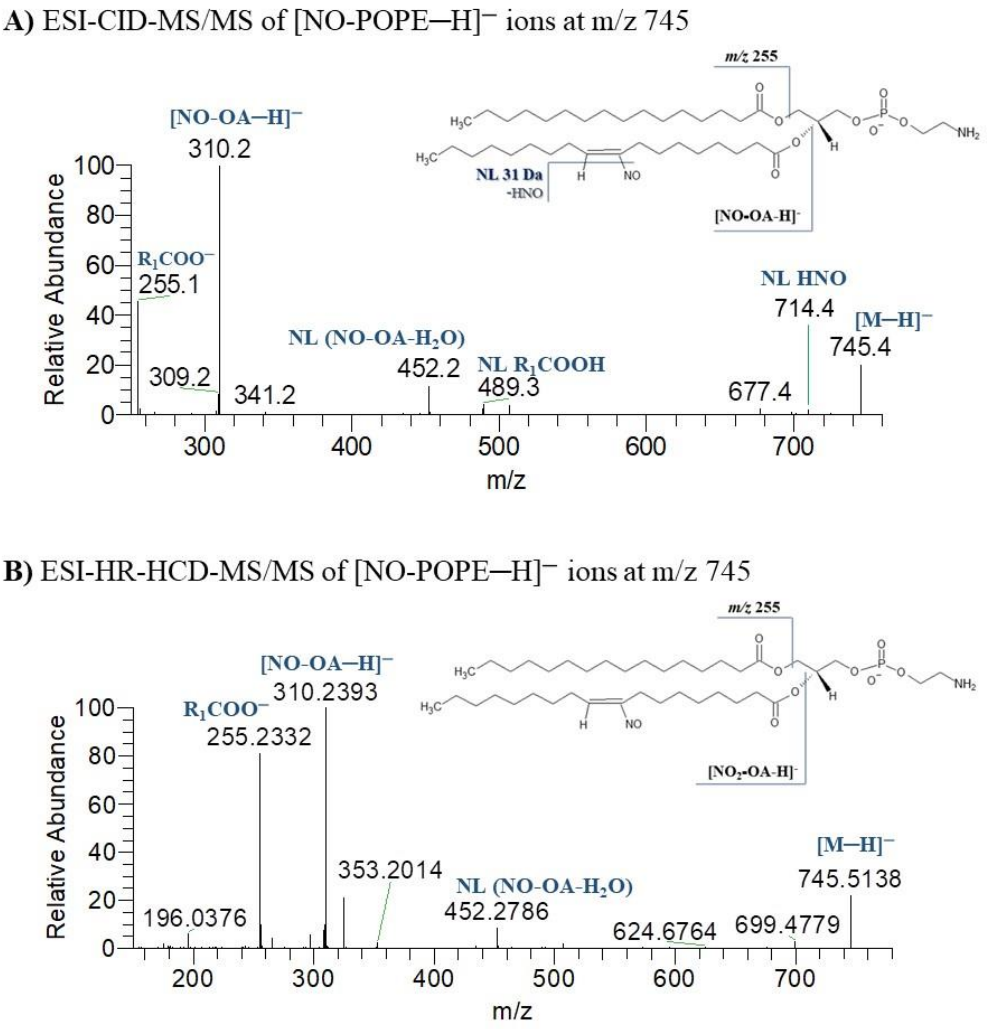


**Figure III.16. (A)** ESI-CID-MS/MS spectrum of the [NO-POPE–H]$^-$ ions at *m/z* 745.4 acquired in a Linear Ion Trap (LIT) mass spectrometer, with a collision energy (CE) of 18. **(B)** ESI-high resolution (HR)-HCD-MS/MS spectrum of the [NO-POPE–H]$^-$ ions at *m/z* 745.5138 acquired in a Q-Exactive Orbitrap, with a collision energy (CE) of 25. The schematic representation of the fragmentation patterns obtained from these two different ion activation methods, CID and HCD, are also illustrated.

As observed for $NO_2$-POPS, the analysis of the ESI-CID-MS/MS spectrum of NO-POPS acquired in positive-ion mode using a LXQ-LIT (Figure III.17(A)) reveal the characteristic fragmentation patterns of PS polar head group namely the NL of 87 Da at *m/z* 704.5 and NL of 185 Da at *m/z* 606.5 (base peak) as well as the typical reporter ion formed due the NL of HNO (31 Da) at *m/z* 760.4. However, the protonated ions of NO-OA fatty acyl were absent. In the ESI-HR-HCD-MS/MS spectrum of [NO-POPS+H]$^+$ (Figure III.17(B)), beyond the products ions with higher *m/z* values formed by NL of 87 Da (*m/z* 704.4795)

and NL of 185 Da (*m/z* 606.5095), it was also possible to see the product ion corresponding to protonated nitroso FA at *m/z* 294.2426 ([NO-OA─$H_2O$+H]$^+$). This information was also previously observed for nitro and nitroso derivatives of POPC and POPE (Figures III.6, III.8, III.15 and III.16**).**

The ESI-CID-MS/MS spectrum of the [M─H]$^-$ ions of NO-POPS (Figure III.18(A)) at *m/z* 789.3 allowed the observation of the carboxylate anion of modified OA at *m/z* 310.3 as [NO-OA─H]$^-$ ions as well as the product ions at *m/z* 446.2 and *m/z* 391.1, which were characterized as the combine loss of $R_1$COOH and NO-OA with 87 Da, respectively. The product ions formed due to the typical NL of HNO at *m/z* 758.3, the product ion arising from NL of 87 Da at *m/z* 702.3 (base peak), and the ion at *m/z* 255.3 of $R_1COO^-$ of palmitic acid were also observed. Besides the ions described above in ESI-CID-MS/MS, namely the product ions at *m/z* 702.4708 (NL of 87 Da), *m/z* 446.2321 (NL of $R_1$COOH+87 Da), *m/z* 391.2259 (NL of (NO-OA)+87 Da), *m/z* 310.2390 ([NO-OA─H]$^-$) and *m/z* 255.2330 ($R_1COO^-$, base peak), in the ESI-HR-HCD-MS/MS of [NO-POPS─H]$^-$ ions (Figure III.18(B)) it was also possible to observed another carboxylate anion of NO-OA at *m/z* 292.2979 [(NO-OA)─$H_2O$─H]$^-$). Although the reporter ion formed due the typical NL of 31 Da was absent, all the product ions with lower *m/z* values identified in this MS/MS spectrum were present with a greater relative abundance than in ESI-MS/MS using CID-LIT mass spectrometer. The same trend had already been described before, namely fort he acquisition of the nitro and nitroso derivatives of the POPC and POPE (Figures III.7, III.9, III.14 and III.16).

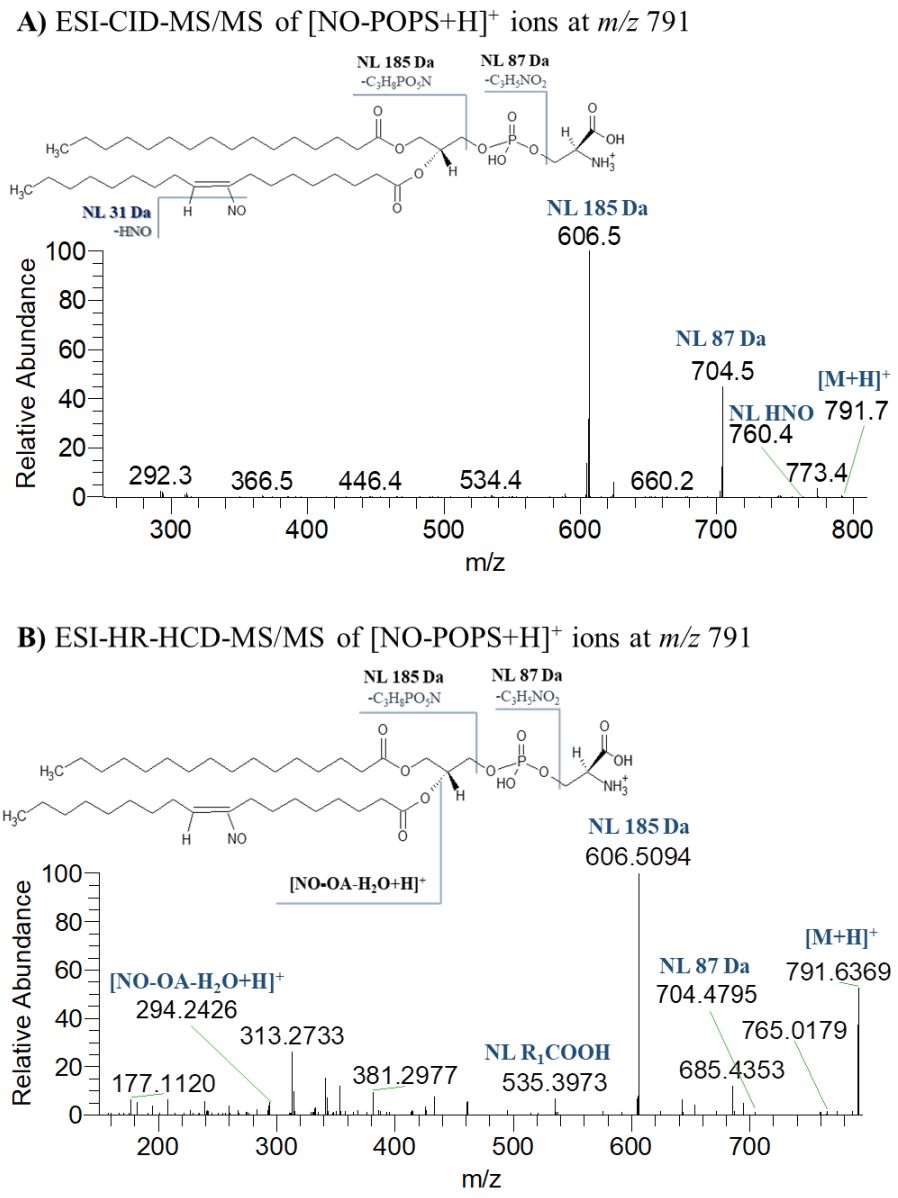


**Figure III.17. (A)** ESI-CID-MS/MS spectrum of the $[NO\text{-}POPS+H]^+$ ions at *m/z* 791.7 acquired in a Linear Ion Trap (LIT) mass spectrometer, with a collision energy (CE) of 16. **(B)** ESI-high resolution (HR)-HCD-MS/MS spectrum of the $[NO\text{-}POPS+H]^+$ ions at *m/z* 791.6369 acquired in a Q-Exactive Orbitrap, with a collision energy (CE) of 25. The schematic representation of the fragmentation patterns obtained from these two different ion activation methods, CID and HCD, are also illustrated.

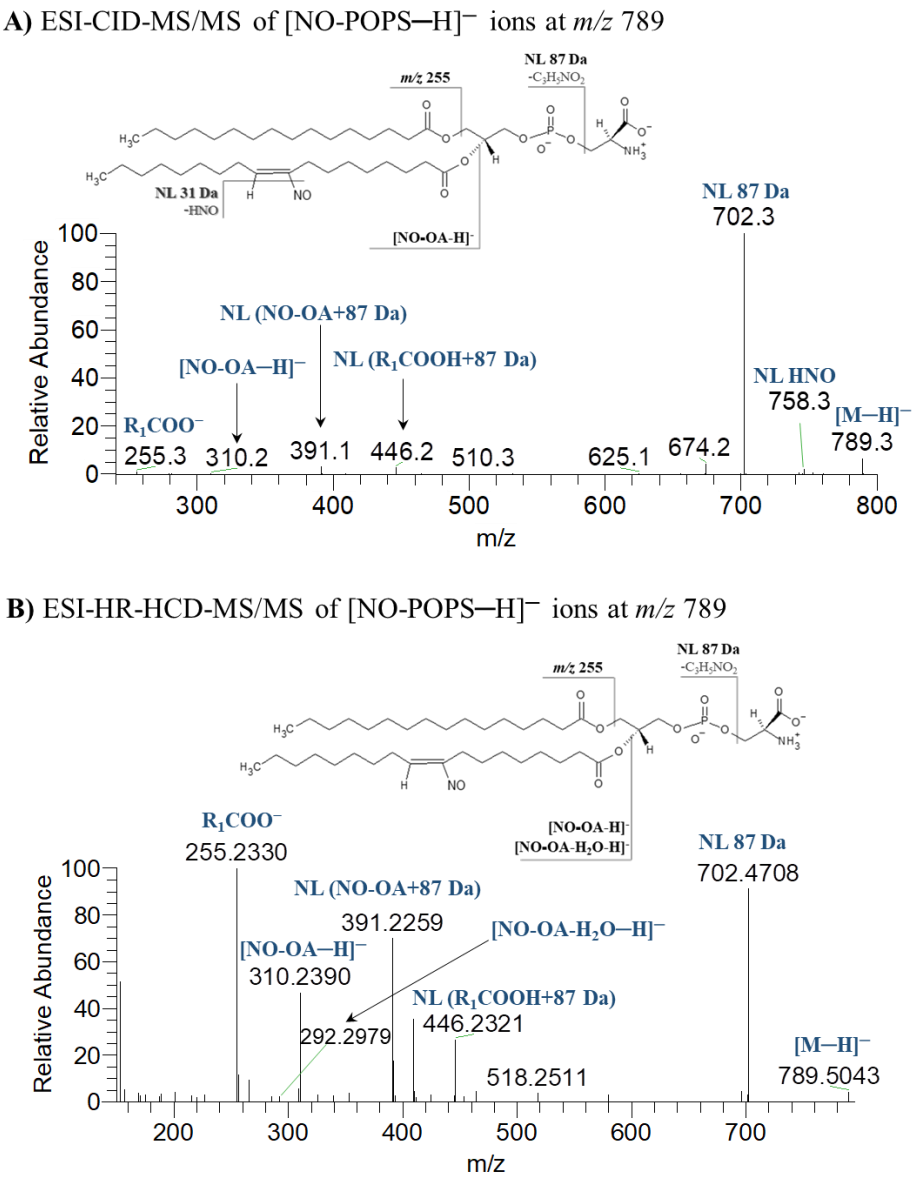


**Figure III.18. (A)** ESI-CID-MS/MS spectrum of the [NO-POPS─H]⁻ ions at *m/z* 789.3 acquired in a Linear Ion Trap (LIT) mass spectrometer, with a collision energy (CE) of 16. **(B)** ESI-high resolution (HR)-HCD-MS/MS spectrum of the [$NO_2$-POPS─H]⁻ ions at *m/z* 789.5043 acquired in a Q-Exactive Orbitrap, with a collision energy (CE) of 25. The schematic representation of the fragmentation patterns obtained from these two different ion activation methods, CID and HCD, are also illustrated.

Figure III.19 shows the ESI-MS/MS spectra of nitroso derivative of TLCL (NO-TLCL) at *m/z* 1476 acquired in negative-ion mode using CID (Figures III.19(A)) and HCD (Figure III.19(B)) fragmentation methods. In the ESI-CID-MS/MS spectrum (Figures III.19(A)), it was possible to detected the presence of the reporter product ions of nitroso phosphatidic acid [NO-PA–H]$^-$ at *m/z* 724.4 and nitroso lysophosphatidic acid [NO-LPA–H]$^-$ at *m/z* 444.2 as well as the product ions at *m/z* 860.5 and *m/z* 780.4 identify as [NO-PA+136–H]$^-$ and [NO-PA+56–H]$^-$, respectively. The product ions at *m/z* 695.3, *m/z* 751.4 and *m/z* 831.4 identified as [PA–H]$^-$, [PA+56–H]$^-$ and [PA+136–H]$^-$, respectively, were also seen. The ion at *m/z* 415.2 corresponding to [LPA–H]$^-$ ion was also observed. However, contrary to what was previously described for the $NO_2$-TLCL under CID-MS/MS conditions, the typical NL of HNO was not observed in this analysis. The product ions corresponding to of the modified fatty acyl chains were not observed. In this way, it was carried out the analysis of the ESI-CID-MS/MS spectrum of [M–2H]$^{2-}$ ions of NO-TLCL (Figures III.19($A_1$)). Like those observed on ESI-CID-MS/MS spectrum of the [$NO_2$-TLCL–2H]$^{2-}$, the product ions at *m/z* 279.3 and *m/z* 308.3 corresponding to the unmodified linoleic acid (RCOO$^-$) and nitroso-linoleic acid (NO-RCOO$^-$), respectively, were also detected in the ESI-CID-MS/MS spectrum of [NO-TLCL–2H]$^{2-}$ ions. Complementarily, the analysis of ESI-HR-HCD-MS/MS spectrum of [NO-TLCL–H]$^-$ ions (Figures III.19(B)) also shows the same product ions at *m/z* 279.2332 and *m/z* 308.2239. The latter with a greater relative abundance than that observed in Figures III.19($A_1$). Besides, both the unmodified ions of PA (*m/z* 695.4661) and LPA (*m/z* 415.2260), and the nitroso PA (*m/z* 724.4568) and LPA (*m/z* 444.2163) were detected.

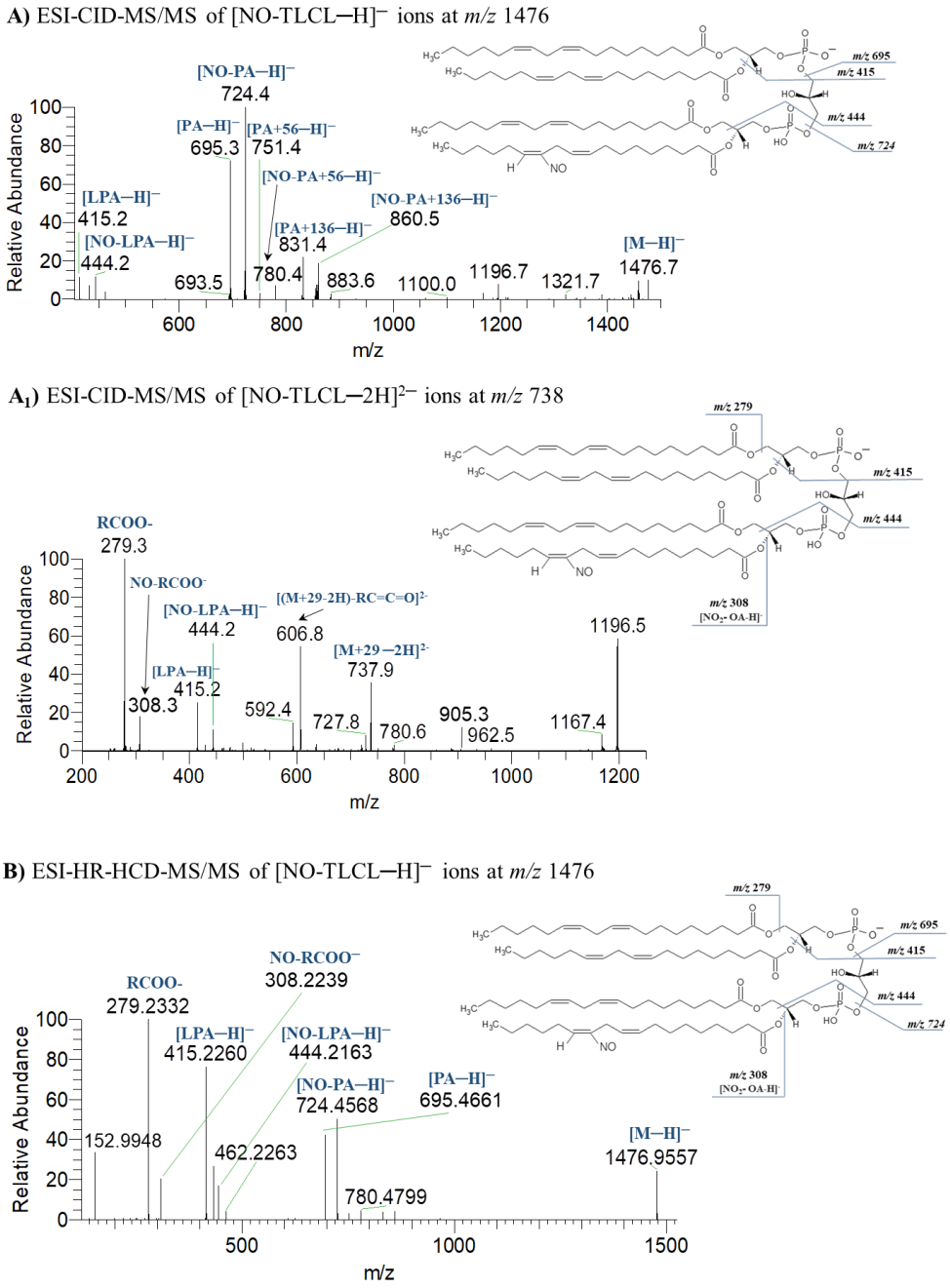


**Figure III.19. (A)** ESI-CID-MS/MS spectrum of the [NO-TLCL–H]$^{-}$ ions at *m/z* 1476.7 acquired in a Linear Ion Trap (LIT) mass spectrometer, with a collision energy (CE) of 24. **($A_1$)** ESI-CID-MS/MS spectrum of the [NO-TLCL–2H]$^{2-}$ ions at *m/z* 738.5 acquired in a Linear Ion Trap (LIT) mass spectrometer, with a collision energy (CE) of 16. **(B)** ESI-high resolution (HR)-HCD-MS/MS spectrum of the [NO-TLCL–H] $^{-}$ ions at *m/z* 1476.9557 acquired in a Q-Exactive Orbitrap, with a collision energy (CE) of 23. The schematic representation of the fragmentation patterns obtained from these two different ion activation methods, CID and HCD, are also illustrated.

### III.2.3. Concluding Remarks

Overall, herein we show that there are several differences between MS/MS spectra from LXQ-LIT and Orbitrap mass spectrometers. In ESI-CID-MS/MS spectra from LXQ-LIT the typical reporter ions used for the identification of $NO_2$-PLs and NO-PLs are the ones formed by the typical neutral losses of $HNO_2$ (47 Da) and HNO (31 Da) that are detected with high relative abundance in the high *m/z* range. In an opposite trend, in ESI-HR-HCD-MS/MS spectra from Q-Exactive Orbitrap the product ions of modified fatty acyl chain ($NO_2$-OA and NO-OA), namely the carboxylate anions or the protonated ions, were detected with a higher relative abundance in the low *m/z* range. Therefore, the product ions with the nitro and nitroso fatty acyl moiety can be selectively used as reported ions since containing important information on the structural characterization of nitrated PLs being useful for a confident identification in untargeted and targeted lipidomic analysis.

# Chapter III. RESULTS AND DISCUSSION

## III.3. FRAGMENTATION PATTERN OF NITRATED AND NITROXIDIZED TRIOLEIN UNDER HCD-MS/MS CONDITIONS

### III.3.1. Background and Aim of the Study

Recent research in the field of lipid nitration has demonstrated that $NO_2$-FA can occur as esterified forms in complex lipids as nitrated derivatives of PLs (as reported previously) as well as triacylglycerides (TAG). Nitrated TAG derivatives ($NO_2$-TAG) were recently identified and quantified in biological samples (plasma, adipocytes and adipose tissue)[19,20,62] and after *in vitro* mimetic nitration under acidic conditions using artificial gastric fluid[62] by MS and MS/MS-based lipidomics approaches. To the best of our knowledge, only one study started to unveil the structural characterization of nitrated derivatives of TAG bearing conjugated linoleic (cLA) fatty acid using HCD-MS/MS[62]. Therefore, there is a notorious lack of knowledge on the identification and detailed characterization of nitrated and nitroxidized TAG using high resolution (HR) MS and HCD-MS/MS based approaches. In this sense, this study aims to contribute to close this gap through the identification of the fragmentation pattern of nitrated and nitroxidized derivatives of triolein, using electrospray (ESI)-HR-HCD-MS/MS performed on a Q-Exactive Orbitrap, in positive-ion mode (as $[M+NH_4]^+$). Triolein is a TAG composed by three oleic acid (OA) moieties and is one of the major TAG found in vegetable and edible oils, namely in "extra virgin" olive oil, which is a key source of lipids in the Mediterranean diet. Therefore, further nitration of this oil containing triolein TAG, such as under acidic gastric digestive conditions, can lead to the generation of nitrated derivatives of esterified OA as the nitro-OA ($NO_2$-OA). This $NO_2$-FA has been associated to the multiple health benefits linked to the Mediterranean diet, including anti-inflammatory actions, anti-hypertensive and cardioprotective effects.

### III.3.2. Results and Discussion

In this study, the nitration of triolein [TAG (C18:1/C18:1/C18:1)] was induced in a mimetic system of nitration by incubation with nitronium tetrafluoroborate ($NO_2BF_4$). The reaction occurred in hydrophobic environments, mimicking the nitration that occurs in biological membranes. The formation of nitrated and nitroxidized products of triolein after this biomimetic nitration reaction was monitored by ESI-HR-HCD-MS in positive-ion mode in a Q-Exactive Orbitrap (Figure III.20(B)). Nitration TAG derivatives were observed as $[M+NH_4]^+$ ions with a total of 5 ions assigned as triolein nitrated and nitroxidized derivatives (Table III.2). These products were observed at higher *m/z* values than the nonmodified triolein ($[M+NH_4]^+$ at *m/z* 902.817). Nitro and dinitro TAG derivatives were assigned at *m/z* 947.802 ($NO_2$-TAG, +45 Da) and *m/z* 992.788 ($(NO_2)_2$-TAG, +90 Da), respectively (Figure III.20(A)). Nitroxidized TAG derivatives were also identified namely nitrohydroxy at *m/z*

963.797 ($(NO_2)$O-TAG, +61 Da), dinitrohydroxy at *m/z* 1008.785 ($(NO_2)_2$O-TAG, +106 Da) and dinitrodihydroxy derivatives at *m/z* 1024.783 ($(NO_2)_2$(2O)-TAG, +122 Da) (Figure III.20(B)). Nitrated and nitroxidized triolein derivatives shown in Table III.2 were assigned based on the mass shift compared to the nonmodified triolein as well as on the accurate mass measurement (error < 5 ppm) and elemental composition determination. The structural assignments of these nitration products were confirmed by HCD fragmentation method in Orbitrap instrument. The analysis of individual ESI-HR-HCD-MS/MS spectrum allowed to identify the specific fragmentation fingerprinting and the typical reporter ions of each TAG nitration product. All these MS/MS spectra were acquired in a Q-Exactive Orbitrap instrument using collision energies (CE) between 14 and 20.

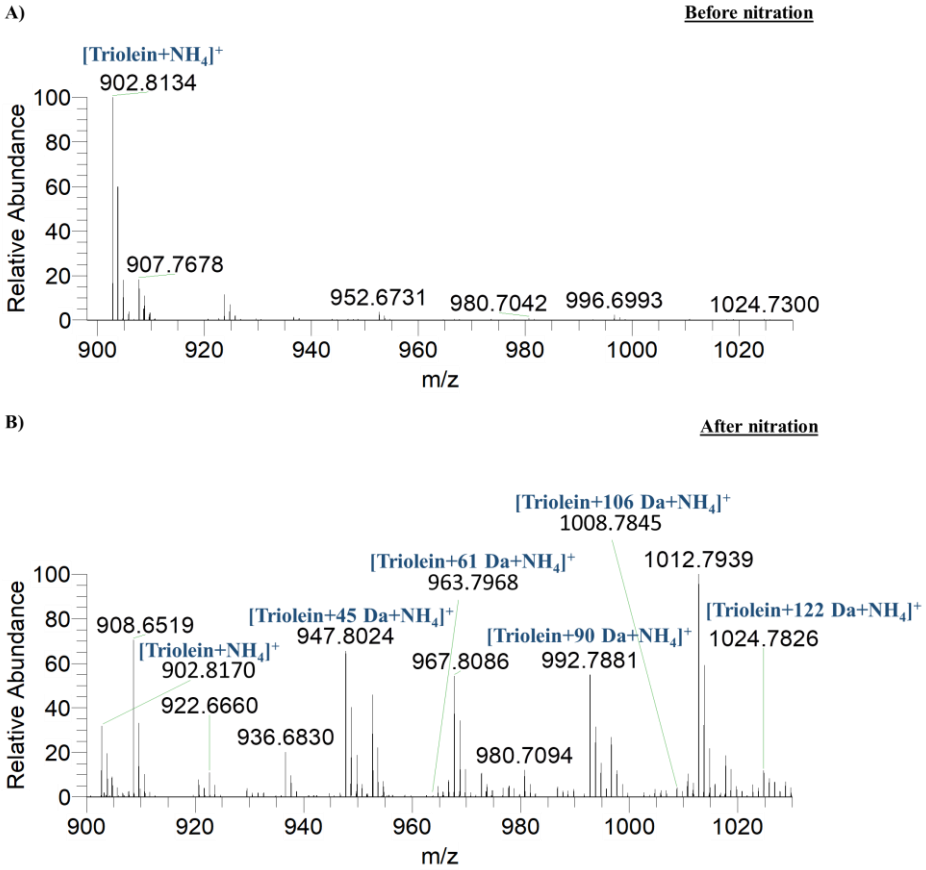


**Figure III.20.** ESI-HCD-MS spectra of the $[M+NH_4]^+$ ions of triolein before **(A)** and after **(B)** the reaction with nitronium tetrafluoroborate ($NO_2BF_4$) acquired in high-resolution Q-Exactive Orbitrap, with the proposed identification and *m/z* values of the resultant nitrated and nitroxidized derivatives.

**Table III.2.** Nitration products of triolein obtained using nitronium tetrafluoroborate ($NO_2BF_4$) in a biomimetic model of nitration identified by ESI-HR-HCD-MS in positive-ion mode as $[M+NH_4]^+$ ions. Assignments of nitrated and nitroxidized triolein derivatives were confirmed by mass accuracy. The calculated and observed mass, error, and formula of the nitrated and nitroxidized derivatives formed after reaction between $NO_2BF_4$ and triolein observed in the ESI-MS spectrum are also shown. Error (ppm) = (Observed *m/z* − Calculated *m/z*)/Calculated *m/z*) × 1 x $10^6$.

| Triolein nitration products | Calculated Mass | Observed Mass | Error (ppm) | Predicted Formula | Triolein modification | |
|---|---|---|---|---|---|---|
| $[TAG+NH_4]^+$ | 902.8177 | 902.8170 | -0.7355 | $C_{57}H_{108}NO_6$ | --- | |
| $[TAG+45Da+NH_4]^+$ | 947.8027 | 947.8024 | -0.3165 | $C_{57}H_{107}N_2O_8$ | Nitro | $NO_2$-TAG |
| $[TAG+61Da+NH_4]^+$ | 963.7977 | 963.7968 | -0.4150 | $C_{57}H_{107}N_2O_9$ | Nitrohydroxy | $(NO_2)O$-TAG |
| $[TAG+90Da+NH_4]^+$ | 992.7878 | 992.7881 | 0.3022 | $C_{57}H_{106}N_3O_{10}$ | Dinitro | $(NO_2)_2$-TAG |
| $[TAG+106Da+NH_4]^+$ | 1008.7827 | 1008.7845 | 1.7843 | $C_{57}H_{106}N_3O_{11}$ | Dinitrohydroxy | $(NO_2)_2O$-TAG |
| $[TAG+122Da+NH_4]^+$ | 1024.7777 | 1024.7826 | 4.7815 | $C_{57}H_{106}N_3O_{12}$ | Dinitrohydroperoxy | $(NO_2)_2(2O)$-TAG |

The nonmodified TAG (C18:1/C18:1/C18:1) was identified as $[M+NH_4]^+$ ions at *m/z* 902.8170 (Figure III.21) and its ESI-HR-HCD-MS/MS spectrum showed a major diacylglyceride (DAG) product ion at *m/z* 603.5352 formed due to the neutral loss (NL) of one oleic acid chain (OA, C18:1; NL 282 Da) as an acid derivative (RCOOH) plus ammonia ($NH_3$). The acylium ($RCO^+$) and monoglyceride ions ($RCO^+ + 74$) of OA acyl chain were also present at *m/z* 265.2526 and *m/z* 339.2894, respectively. As reported previously, the loss of the FA linked to the *sn-1* and *sn-3* positions in the TAG glycerol backbone is energetically favored when compared with the loss of the FA at *sn-2* position during the TAG fragmentation under MS/MS conditions[19,62]. Thus, the DAG fragment ions formed due to the NL of the fatty acyl chain at *sn-2* should be found at lower relative abundance. Taking this information into account, the proposed schematic representation and fragmentation pathways presented for the nitrated and nitroxidized triolein derivatives identified in this chapter will follow the principle that suggest the *sn-2* position to be less prone to be lost. Nonetheless, other possibilities of positional isomers of the represented derivatives cannot be excluded.

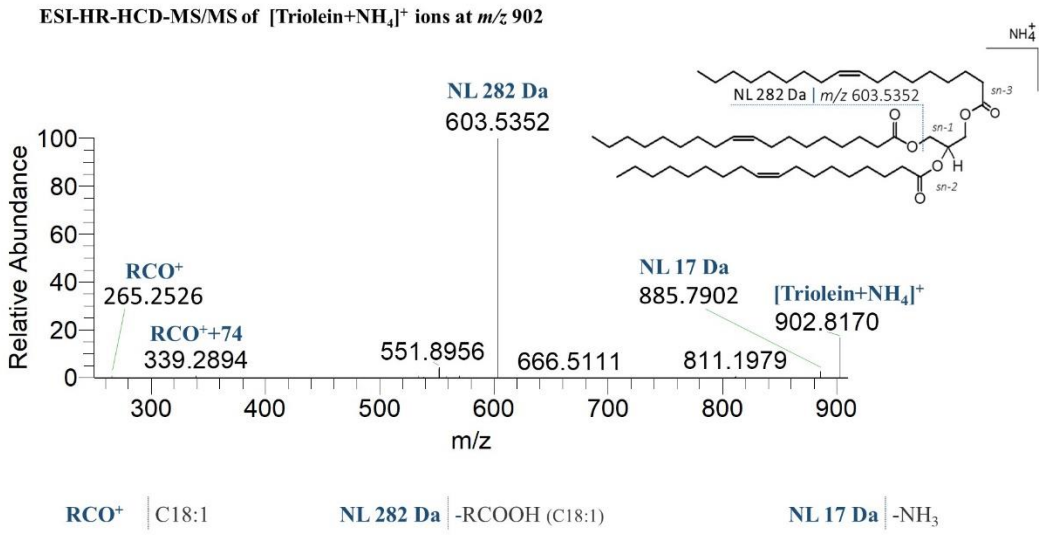


**Figure III.21.** ESI-HDC-MS/MS spectrum of the $[M+NH_4]^+$ ions of the non-modified triolein at *m/z* 902.817 acquired in a Q-Exactive Orbitrap, with a collision energy (CE) of 14. The schematic representation of the fragmentation pathways observed are also illustrated.

### III.3.2.1. Nitrated derivatives of triolein

The nitro (or nitroalkene, $NO_2$-TAG) and dinitro ($(NO_2)_2$-TAG) derivatives of triolein displayed a mass shift of + 45 Da and +90 Da, respectively, in comparison with the nonmodified triolein. In ESI-HR-HCD-MS/MS spectrum of $[M+NH_4]^+$ ions of $NO_2$-TAG at *m/z* 947.8015, showed in Figure III.22(A), it was possible to observed an abundant product ion at *m/z* 603.5349 formed by the NL of 327 Da which corresponds to the NL of OA+$NO_2$ plus $NH_3$, and the product ion at *m/z* 648.5198 formed by the NL of 282 Da, corresponding to the nonmodified OA as RCOOH, plus $NH_3$. The reporter ion related to the typical NL of 47 Da (loss of nitrous acid, $HNO_2$), formed due to the elimination of the $NO_2$ group, it was also seen at *m/z* 883.7745, with high relative abundance. This typical reporter ion commonly used to identify $NO_2$-PLs was not present in the ESI-HR-HCD-MS/MS spectrum of the nonmodified triolein (Figure III.22(B)), which confirms the presence of nitro derivative of triolein. The acylium ($RCO^+$) and monoglyceride ions ($RCO^+$+74) of nonmodified OA were also seen at *m/z* 265.2525 and 339.2893, respectively. The protonated molecules of $NO_2$-OA fatty acyl chain identified as $[NO_2\text{-OA-}H_2O+H]^+$ at *m/z* 310.2375 and $[NO_2\text{-OA+H}]^+$ at *m/z* 328.2480 were also observed, but with very low relative abundance.

ESI-HR-HCD-MS/MS spectrum of $(NO_2)_2$-TAG at *m/z* 992.7882 ((Figure III.22(B))) showed a product ion at *m/z* 601.5209 that was attributed to NL of $HNO_2$ from ion at *m/z* 648.5214 confirming the presence of two nitro moieties. The major nitro ($NO_2$)-DAG product ion observed at *m/z* 648.5214 is formed due to the NL of $NO_2$-OA (NL 327 Da) plus

$NH_3$. Besides, the NL of two $HNO_2$at *m/z* 881.7608 seen with high relative abundance corroborates the presence of two $NO_2$ groups. This indicates that this isomer of OA+90 Da derivative corresponds to a dinitro derivative, and each $NO_2$ was assigned to be present in different OA chains. Additionally, the low relative abundance of fragment ions at *m/z* 603.5362, which corresponds to the nonmodified DAG product, confirms the insertion of two $NO_2$ groups in two different OA chains. The NL of nonmodified OA plus $NH_3$ was observed at *m/z* 693.5063 (NL 282, C18:1). In an opposite trend to those described in Chapter III.2 for nitrated PLs, high yields of product ions with higher *m/z* values were now found, namely the reporter ion corresponding to the typical NL of 47 Da. On the other hand, product ions with lower *m/z* values as the ions of $NO_2$-OA fatty acyl chains identified as $[NO_2\text{-OA-}H_2O+H]^+$ at *m/z* 310.2374 and $[NO_2\text{-OA+H}]^+$ at *m/z* 328.2480 were observed, but with low relative abundance.

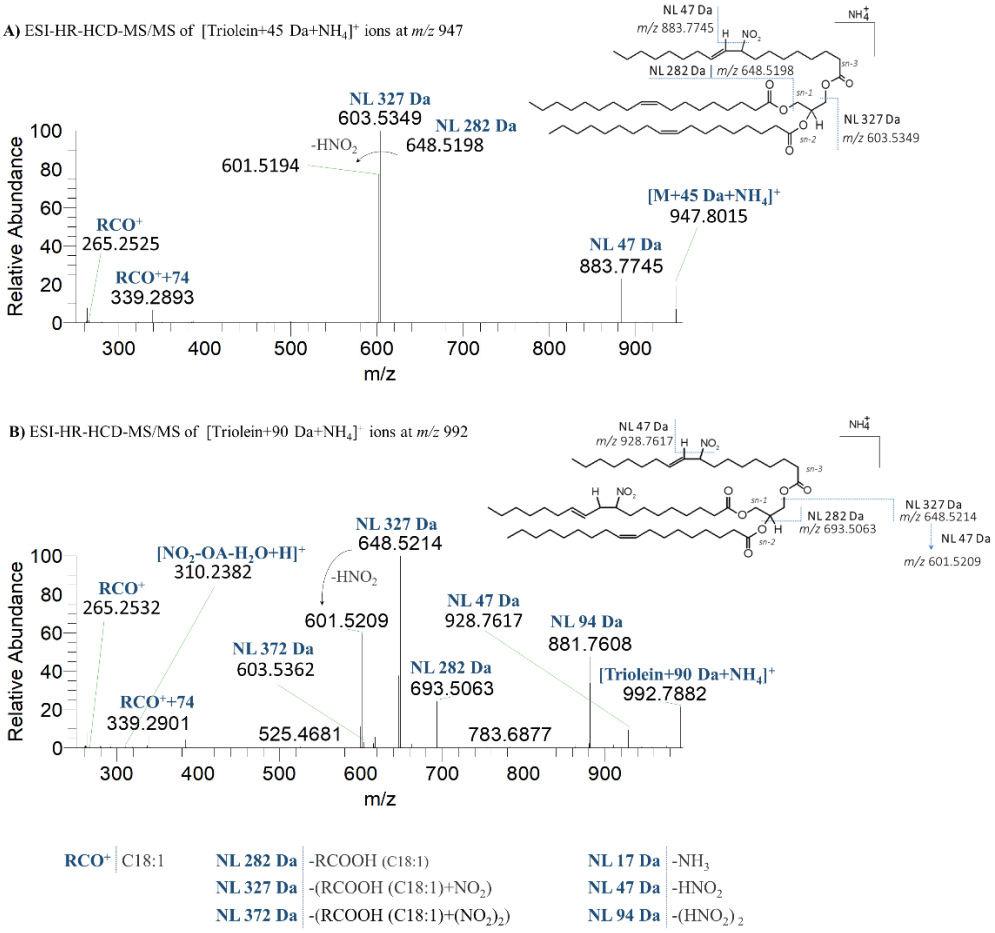


**Figure III.22.** ESI-HCD-MS/MS spectrum of the $[M+NH_4]^+$ ions of nitro **(A)** and dinitro **(B)** derivatives of triolein at *m/z* 947.8015 and *m/z* 992.7882, respectively, acquired in a Q-Exactive Orbitrap, both with a collision energy (CE) of 16. The schematic representation of the fragmentation pathways observed are also illustrated.

### III.3.2.2. Nitroxidized derivatives of triolein

In the case of $[M+NH_4]^+$ ions of $(NO_2)$O-TAG at *m/z* 963.7984 (Figure III.23(A)), it was possible to identify two isomeric structures for this derivative. On one hand, the ESI-HR-HCD-MS/MS spectrum showed, with a considerable relative abundance, the fragment ion of nonmodified DAG at *m/z* 603.5356 formed due to the NL of 343 Da (NL of OA+ 61 Da) plus $NH_3$, corresponding to the presence of $NO_2$ and hydroxy (OH) moieties in the same OA chain. The highly abundant NL of nonmodified OA (NL 282 Da) combined with $NH_3$ was seen at *m/z* 664.5153. On the other hand, this tandem MS spectrum also shown the product ion at *m/z* 619.5305, formed due to the NL of a $NO_2$-OA (NL 327 Da, NL of OA+45 Da) plus $NH_3$, and the product ion at *m/z* 648.5205, formed by the loss of a hydroxy-OA (NL 298 Da, NL of OA+16 Da) plus $NH_3$. This way, the presence of these fragment ions indicates the existence of another positional isomer where the $NO_2$ and OH groups are present in different OA chains. Moreover, the NL of $H_2O$ (18 Da) from the modified DAG ion at *m/z* 601.5198 corroborates the presence of the hydroxy-OA in a different OA chains than the one bearing the $NO_2$ group. In this MS/MS spectrum the characteristic NL of $HNO_2$ (47 Da) was found at *m/z* 899.7707, while the combined NL of $H_2O$ (18 Da) plus $HNO_2$ (i.e. NL 65 Da) was found at *m/z* 881.7585, thus corroborating the presence of nitrohydroxy derivative. Besides, the NL of $H_2O$ (18 Da) at *m/z* 928.7621 also corroborates the presence of OH group. The protonated molecules of $NO_2$-OA fatty acyl chain identified as $[NO_2\text{-OA-}H_2O+H]^+$ ion at *m/z* 310.2379 and $[NO_2\text{-OA+H}]^+$ ion at *m/z* 328.2484 were also observed, although with a low relative abundance, comparing with the product ions at higher *m/z* values.

For $(NO_2)_2$O-TAG derivatives, two major positional isomers were identified. As can be seen in Figure III.23(B), ESI-HR-HCD-MS/MS spectrum of $(NO_2)_2$O-TAG showed a major product ion at *m/z* 664.5153 formed due to NL of $NO_2$-OA chain (NL 327 Da) plus $NH_3$, which reveals the presence of each $NO_2$ group in different OA chains. The presence of the product ion at *m/z* 693.5055, formed due to the NL of a hydroxy-OA (NL 298 Da, NL of OA+16 Da) confirms the insertion of one oxygen atom in a third OA chain. This corroborates the presence of a structure with the two $NO_2$ groups and one OH group in three different OA fatty acyl chains. The product ions at *m/z* 709.5003, formed due to NL of nonmodified OA acyl chain (NL 282 Da) as an acid derivative (RCOOH) plus $NH_3$, suggests a structure in which only two of the three OA fatty acyl chains of TAG are modified. This was also corroborated by the product ion at *m/z* 648.5206 corresponding to the NL of the nitrohydroxy OA (NL of 343 Da, NL of OA+61 Da), thus proposing that both $NO_2$ and OH groups were placed in the same OA chain. Moreover, the product ions at *m/z* 897.7537 (NL

of 94 Da, corresponding to NL of $(HNO_2)_2$), at *m/z* 926.7433 (NL 65 Da, combined NL of $HNO_2$ plus $H_2O$), and at *m/z* 944.7562 (NL 47 Da, which is the NL of $HNO_2$) confirms the presence of a dinitrohydroxy derivative of triolein. As previously described, product ions at low *m/z* value identified as $[NO_2\text{-OA-}H_2O+H]^+$ and $[NO_2\text{-OA+H}]^+$ ions at *m/z* 310.2379 and *m/z* 328.2484, respectively, were also observed.

In Figure III.23(C) it is shown the ESI-HR-HCD-MS/MS spectrum of the dinitrodihydroxy derivative of triolein at *m/z* 1024.7389. Similarly to what was observed for the dinitrohydroxy derivative of triolein (Figure III.22(B), in the HCD-MS/MS spectrum of the $(NO_2)_2$(2O)-TAG it was observed the product ion at *m/z* 895.7392 (NL of 112 Da, combined NL of $(HNO_2)_2$ plus $H_2O$), at *m/z* 913.7501 (NL of 94 Da, corresponding to NL of $(HNO_2)_2$), at *m/z* 942.7404 (NL of 65 Da, combined NL of $HNO_2$ plus $H_2O$), and at *m/z* 960.7501 (NL of 47 Da, corresponding to the NL of $HNO_2$). The typical NL of hydroperoxyl group (NL 34 Da, corresponding to $H_2O_2$) was not observed, suggesting a dihydroxy derivative as well as the absence of the NL of nonmodified OA, which indicate that all the OA fatty acyl chains are modified. This tandem MS spectrum showed a product ion at *m/z* 693.5057 formed due to NL 314 Da (NL 282+32 Da) plus $NH_3$ confirming the presence of two OH moieties within the same OA chain. Additionally, the product ion at *m/z* 615.4992 also corroborate the presence of two OH moieties in the same OA chain, as it is formed due to the NL of $H_2O$ with the formation of an epoxy moiety from ions at *m/z* 633.5098, which were assigned as product ions formed due to the NL of $HNO_2$ from ions at *m/z* 680.5110. The product ion at *m/z* 680.5110, formed due NL of 327 Da (NL of OA+45 Da) plus $NH_3$ confirmed the presence of the $NO_2$ groups in different OA chains. The protonated molecules of nitrated OA identified as $[NO_2\text{-OA-}H_2O+H]^+$ at *m/z* 310.2379 was also seen with the same trends those describe above for the others derivatives of triolein.

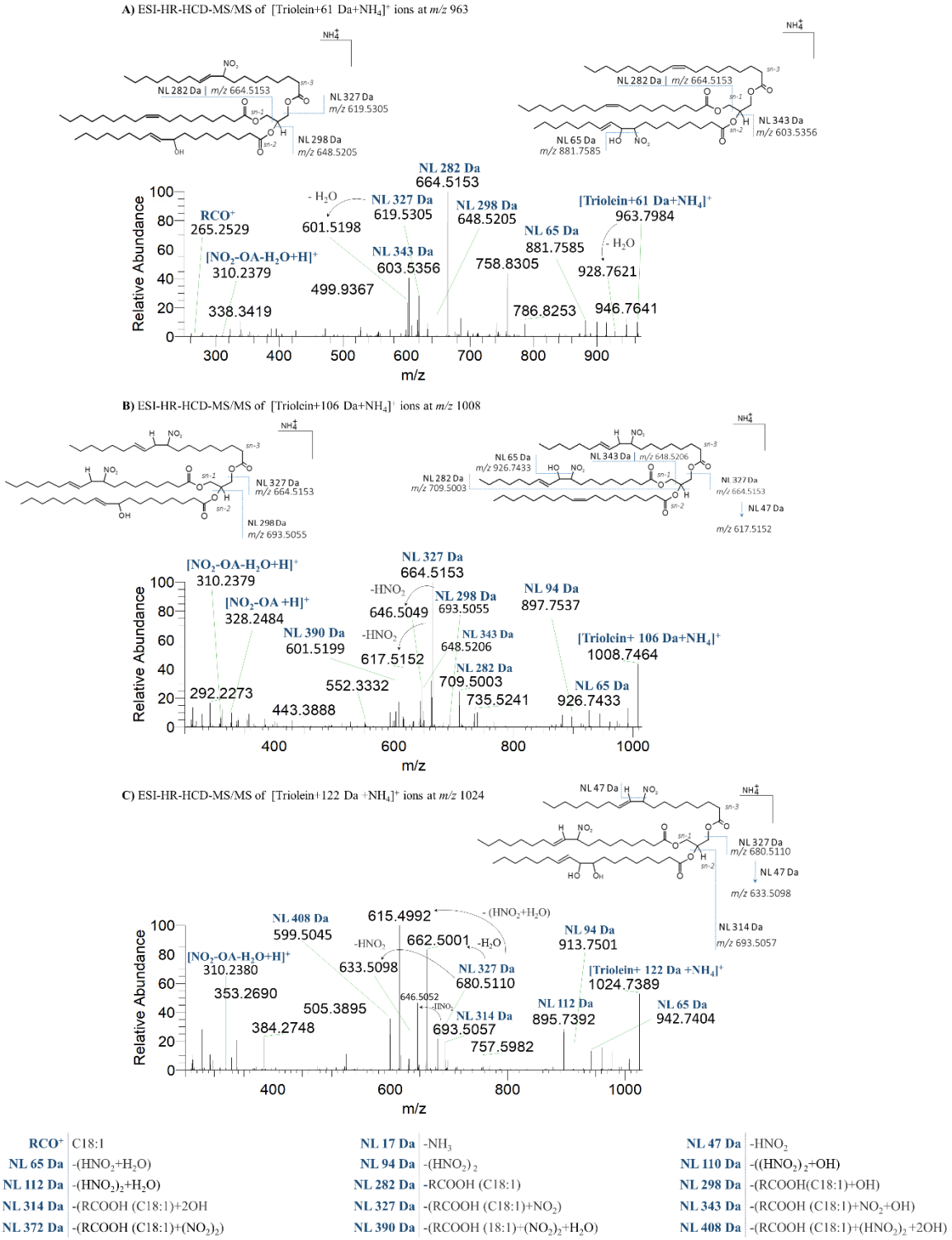


**Figure III.23.** ESI-HCD-MS/MS spectrum of the $[M+NH_4]^+$ ions of nitrohydroxy **(A)**, dinitrohydroxy **(B)** and dinitrodihydroxy **(C)** derivatives of triolein (TAG) at *m/z* 963.7984, *m/z* 1008.7464 and *m/z* 1024.7389, respectively, acquired in a Q-Exactive Orbitrap, with a collision energy (CE) of 16 for nitrohydroxy-TAG and CE of 20 for both dinitrohydroxy-TAG and dinitrodihydroxy-TAG. The schematic representation of the fragmentation pathways observed are also illustrated.

### III.3.3. Concluding Remarks

Overall, herein we show for the first time, an in-depth characterization of the fragmentation pattern of nitrated and nitroxidized TAG species under ESI-HCD-MS/MS conditions in a high-resolution Q-Exactive Orbitrap. The product ions formed due the NL of $NO_2$-OA (NL of 327 Da) plus $NH_3$ originated the most abundant product ion in the HCD-MS/MS spectra of the nitrated derivatives of triolein. Both nitrated TAG derivatives also displayed the NL of non-modified OA fatty acyl chain (NL of 282 Da) plus $NH_3$. The nitroxidized derivatives of triolein characterized in this chapter using ESI-HCD-MS/MS conditions showed the product ions formed due to NL of $HNO_2$ (NL of 47 Da), NL of $(HNO_2)_2$ (NL of 94 Da), and from the combined NL of $HNO_2$ and water (NL of 65 Da), which confirm the presence of the two nitro moieties as well as the hydroxy group. Dinitrohydroxy- and dinitrodihydroxy-triolein derivatives were discriminated due to the presence of the fragment ions arising from the NL of 298 Da (NL of OA+OH) and 314 Da (NL of OA+$(OH)_2$), respectively. In contrast to what was previously described for $NO_2$-PLs under ESI-HR-HCD-MS/MS conditions, in the HCD-MS/MS spectra of nitrated and nitroxidized TAG the typical reporter ions of nitrated lipids with higher m/z values, namely the ones formed due to the NL of $HNO_2$ (NL of 47 Da), were seen with a significantly higher relative abundance. Therefore, the analysis of HCD-MS/MS data of the $[M+NH_4]^+$ ions of nitrated and nitroxidized TAG revealed that its fragmentation pattern seems to be similar to that observed for the nitrated PLs under CID-MS/MS conditions. The information generated with this study can be useful for the detection of nitrated and nitroxidized TAG in biological samples. In the future, the characterization of these modified lipids can be further performed in negative-ion mode, for the detection of carboxylate anions of nitrated and nitroxidized fatty acyl moieties, as well as using chromatographic techniques coupled to MS to achieve the discrimination between potential functional and positional isomers.

# Chapter IV. GENERAL CONCLUDING REMARKS

Mass spectrometry, usually coupled to LC, has become the essential analytical tool for the screening and detection of free, esterified and nucleophilic-adducted $NO_2$-FA based on the identification of the typical fragmentation patterns and characteristic reporter ions under MS/MS conditions. Most of the studies on nitrated derivatives of PLs were performed using a CID-LXQ-LIT instrument based on specific mass shifts under ESI-MS conditions, which allowed to establish a set of characteristic reporter ions present in a typical fragmentation pattern after MS/MS analysis. Advances in MS tools, namely the high resolution and great sensitivity and sensibility of the most recent mass spectrometers as HCD-Orbitrap-based instruments, needed to provide information of low abundant molecules, have opened new horizons in the field of lipid nitration and their identification and role in biological samples. These properties allowed to overcome the challenging problem of the low quantity and high structural diversity of nitrated lipids. This was fundamental to improve their accurate identification in the complex mixture of lipid compounds present in samples related with health and disease conditions. However, dissimilar fragmentation patterns and new reporter ions can be observed depending on the type of mass spectrometer and the dissociation technique used to induce the fragmentation. Having this in mind, the proposed aim of this work was to give some insights on the typical fragmentation patterns of nitrated and nitroxidized PLs and TAG using different MS instrumental platforms, namely CID-LXQ-LIT and HCD-Orbitrap, to improve the accurate detection of these derivatives of complex lipids, and the development of lipidomic strategies to improve their identification in complex biological samples using the optimized high-throughput HCD-MS-based methodologies.

Nitrated and nitroxidized derivatives of PLs (PE, PC, PS, CL) and TAG were synthesized using *in vitro* biomimetic nitration with $NO_2BF_4$, and were analyzed by ESI-CID-MS and ESI-HR-HCD-MS through direct infusion and structurally characterized by MS/MS, both in positive-ion mode (as $[M+H]^+$ ions for PC, PE and PS, and $[M+NH_4]^+$ ions for TAG) and negative-ion mode (as $[M-H]^-$ ions for PS, PE and CL, and $[M+OAc]^-$ ions for PC). Information on the fragmentation pattern and reporter product ions gathered with the lipid standards was used to identify these modified species in complex biological using LC-MS based lipidomics approaches.

Distinct reporter ions were identified for CID- and HCD-MS/MS analysis of nitrated and nitroxidized PLs, where the typical NL of $HNO_2$ is found in CID-MS/MS while the nitrated fatty acyl chains were the reporter ions for HCD-MS/MS of these modified lipids. Additionally, the relative abundance of the typical reporter ions of nitrated and nitroxidized

PLs is significantly affected by the range of NCE used under HCD-MS/MS. Using the defined fragmentation HCD-MS/MS approach, it was possible to detect nitrated phosphatidylcholine derivatives in cell lipid extracts, which demonstrates the feasibility of the developed methodology for an accurate detection of these modified species in complex biological matrices.

Nitrated and nitroxidized derivatives of TAG characterized under HCD-MS/MS showed a fragmentation pattern where the typical NL of $HNO_2$ was observed with a high relative abundance. The fragmentation fingerprinting reveals to be similar to the one observed for nitrated and nitroxidized PLs under CID-MS/MS.

The optimization of MS and MS/MS-based (lipidomic) approaches, such as using *in vitro* studies, is required to simultaneously obtain a more comprehensive knowledge for a high accurate and confident identification of nitrated and nitroxidized complex lipids. This important finding combined with the most appropriate instrument settings and parameters as well as the influence of them in the fragmentation patterns will allow to define a set of reporter product ions that can be used to design target (lipidomic) analysis strategies. This will contribute to the confident and unambiguous detection of esterified $NO_2$-FA in complex biological samples and will also be relevant to infer their biological properties and signaling actions. Additionally, this underpinning information becomes even more important since it can lead to new clues for the discovery of new biomarkers or therapeutic strategies, as proposed for free $NO_2$-FA.

In line with this, it is still necessary to make an effort for the development of systematic, standardized, reproducible and sensitive analytical strategies based on MS methodologies for a more comprehensive understanding of the modification of PLs and TAG under nitration or nitroxidation conditions. More biologically relevant RNS species should be used as nitrating agents namely peroxynitrite and nitrite. The search for additional modifications induced by RNS such as the formation of short chain products, lyso derivatives, or alteration in the polar head of aminophospholipids, as previously described to occur under oxidative stress conditions and mediated by reactive oxygen species, should also be taken into account. And finally, evaluation of the potential electrophilic character of $NO_2$-PLs and their biological roles and signaling properties must continue to be explored. It will contribute to unveil their roles in health and disease states.

# Chapter V. REFERENCES

1. Dedon, P. C. & Tannenbaum, S. R. Reactive nitrogen species in the chemical biology of inflammation. *Arch Biochem Biophys.* **423**, 12–22 (2004).
2. Pacher, P., Beckman, J. S. & Liaudet, L. Nitric oxide and peroxynitrite in health and disease. *Physiol Rev.* **87**, 315–424 (2007).
3. Pryor, W. A., Kendall N. H., Christopher S. F., Jon M. F., Louis J. I., Giuseppe L. S. & Kelvin J. A. D. Free radical biology and medicine: it's a gas, man! *Am J Physiol Regul Integr Comp Physiol.* 291, 491–511 (2006).
4. Calcerrada, P., Peluffo, G. & Radi, R. Nitric oxide-derived oxidants with a focus on peroxynitrite: molecular targets, cellular responses and therapeutic implications. *Curr Pharm Desing.* **17**, 3905–3932 (2011).
5. Lancaster, J. R. Nitroxidative, nitrosative, and nitrative stress: kinetic predictions of reactive nitrogen species chemistry under biological conditions. *Chem Res Toxicol.* **19**, 1160–1174 (2006).
6. Freeman, B. A., Baker, P. R., Schopfer, F. J., Woodcock, S. R., Napolitano, A. & Ischia, M. Nitro-fatty acid formation and signaling. *J Biol Chem.* **283**, 15515–15519 (2008).
7. Rubbo, H., Trostchansky, A. & O'Donnell, V. B. Peroxynitrite-mediated lipid oxidation and nitration: mechanisms and consequences. *Arch Biochem Biophys.* **484**, 167–172 (2009).
8. Trostchansky, A., Souza, J. M., Ferreira, A., Ferrari, M., Blanco, F., Trujillo, M., Castro, D., Cerecetto, H., Baker, P. R. & O'Donnell, V. B. Synthesis, isomer characterization, and anti-Inflammatory properties of nitroarachidonate. *Biochem.* **46**, 4645–4653 (2007).
9. Napolitano, A. Panzella, L., Savarese, M., Sacchi, R., Giudicianni, I., Paolillo, L. & d'Ischia, M. Acid-induced structural modifications of unsaturated fatty acids and phenolic olive oil constituents by nitrite Ions: a chemical assessment. *Chem Res Toxicol.* **17**, 1329–1337 (2004).
10. Pereira, C., Ferreira, N. R., Rocha, B. S., Barbosa, R. M. & Laranjinha, J. The redox interplay between nitrite and nitric oxide: From the gut to the brain. *Redox Biol.* **1**, 276–284 (2013).
11. Trostchansky, A. & Rubbo, H. Nitrated fatty acids: mechanisms of formation, chemical characterization, and biological properties. *Free Radical Bio Med.* **44**, 1887–1896 (2008).
12. Milic, I., Griesser, E., Vemula, V., Ieda, N., Nakagawa, H., Miyata, N., Galano, J.M., Oger, C., Durand, T. & Fedorova, M. Profiling and relative quantification of multiply nitrated and oxidized fatty acids. *Anal Bioanal Chem.* **407**, 5587–5602 (2015).
13. Melo, T., Montero-Bullón, J.-F., Domingues, P. & Domingues, M. R. Discovery of bioactive nitrated lipids and nitro-lipid-protein adducts using mass spectrometry-based approaches. *Red Biol.* 1–16 (2019).
14. Bonacci, G., Baker, P. R., Salvatore, S. R., Shores, D., Khoo, N. K. H., Koenitzer, J. R., Vitturi, D. A., Woodcock, S. R., Golin-Bisello, F. & Cole, M. P. Conjugated linoleic acid is a preferential substrate for fatty acid nitration. *J Biol Chem.* **287**, 44071–44082 (2012).
15. Nadtochiy, S. M., Baker, P. R., Freeman, B. A. & Brookes, P. S. Mitochondrial nitroalkene formation and mild uncoupling in ischaemic preconditioning: implications for cardioprotection. *Cardiovasc Res.* **82**, 333–340 (2009).

16. Schopfer, F. J., Batthyany, C., Baker, P. R., Bonacci, G., Cole, M. P., Rudolph, V., Groeger, A. L., Rudolph, T. K., Nadtochiy, S. & Brookes, P. S. Detection and quantification of protein adduction by electrophilic fatty acids: mitochondrial generation of fatty acid nitroalkene derivatives. *Free Radical Bio Med.* **46**, 1250–1259 (2009).
17. Vitturi, D. A., Chen, C.-S., Woodcock, S. R., Salvatore, S. R., Bonacci, G., Koenitzer, J. R., Stewart, N. A., Wakabayashi, N., Kensler, T. W. & Freeman, B. A. Modulation of nitro-fatty acid signaling: prostaglandin reductase-1 is a nitroalkene reductase. *J Biol Chem.* **288**, 25626–25637 (2013).
18. Zatloukalova, M., Mojovic, M., Pavicevic, A., Kabelac, M., Freeman, B. A., Pekarova, M. & Vacek, J. Redox properties and human serum albumin binding of nitro-oleic acid. *Redox Biol.* **24**, 1-13 (2019).
19. Fazzari, M., Vitturi, D. A., Woodcock, S. R., Salvatore, S. R., Freeman, B. A. & Schopfer, F. J. Electrophilic fatty acid nitroalkenes are systemically transported and distributed upon esterification to complex lipids. *J Lipid Res.* **60**, 388–399 (2019).
20. Fazzari, M., Khoo, N. K. H., Woodcock, S. R., Jorkasky, D. K., Li, L., Schopfer, F. J. & Freeman, B. A. Nitro-fatty acid pharmacokinetics in the adipose tissue compartment. *J Lipids Res.* **58**, 375–385 (2017).
21. Schopfer, F. J., Baker, P. R., Giles, G., Chumley, P., Batthyany, C., Crawford, J., Patel, R. P., Hogg, N., Branchaud, B. P. & Lancaster, J. R.. Fatty acid transduction of nitric oxide signaling: nitrolinoleic acid is a hydrophovically stabilized nitric oxide donor. *J Biol Chem.* **280**, 19289–19297 (2005).
22. Rudolph, V., Schopfer, F. J., Khoo, N. K. H., Rudolph, T. K., Cole, M. P., Woodcock, S. R., Bonacci, G., Groeger, A. L., Golin-Bisello, F. & Chen, C. S. Nitro-fatty acid metabolome: saturation, desaturation, β-oxidation, and protein adduction. *J Biol Chem.* **284**, 1461–1473 (2009).
23. Salvatore, S. R., Vitturi, D. A., Baker, P. R., Bonacci, G., Koenitzer, J. R., Woodcock, S. R., Freeman, B. A. & Schopfer, F. J. Characterization and quantification of endogenous fatty acid nitroalkene metabolites in human urine. *J Lipid Res.* **54**, 1998–2009 (2013).
24. Mata-Pérez, C., Sánchez-Calvo, B., Padilla, M. N., Begara-Morales, J. C., Luque, F., Melguizo, M., Jiménez-Ruiz, J., Fierro-Risco, J., Peñas-Sanjuán, A. & Valderrama, R. Nitro-fatty acids in plant signaling: nitro-linolenic acid induces the molecular chaperone network in Arabidopsis. *Plant Physiol.* **170**, 686–701 (2016).
25. Mata-Pérez, C., Sánchez-Calvo, B., Padilla, M. N., Begara-Morales, J. C., Valderrama, R., Corpas, F. J. & Barroso, J. B. Nitro-fatty acids in plant signaling: new key mediators of nitric oxide metabolism. *Redox Biol.* **11**, 554–561 (2017).
26. Fazzari, M., Trostchansky, A., Schopfer, F. J., Salvatore, S. R., Sánchez-Calvo, B., Vitturi, D., Valderrama, R., Barroso, J. B. Radi, R. & Freeman, B. A. Olives and olive oil are sources of electrophilic fatty acid nitroalkenes. *PLoS ONE* **9**, 1–9 (2014).

27. Charles, R. L., Rudyk, O., Prysyazhna, O., Kamynina, A., Yang, J., Morisseau, C., Hammock, B. D., Freeman, B. A. & Eaton, P. Protection from hypertension in mice by the Mediterranean diet is mediated by nitro fatty acid inhibition of soluble epoxide hydrolase. *Proc. Natl. Acad. Sci. U.S.A.* **111**, 8167–8172 (2014).
28. Zhang, J., Villacorta, L., Chang, L., Fan, Z., Hamblin, M., Zhu, T., Chen, C. S., Cole, M. P., Schopfer, F. J. & Deng, C. X. Nitro-oleic acid inhibits angiotensin II–induced hypertension. *Circ Res.* **107**, 540–548 (2010).
29. Coles, B., Bloodsworth, A., Eiserich, J. P., Coffey, M. J., McLoughlin, R. M., Giddings, J. C., Lewis, M. J., Haslam, R. J., Freeman, B. A. & O'Donnell, V. B.. Nitrolinoleate inhibits platelet activation by attenuating calcium mobilization and inducing phosphorylation of vasodilator-stimulated phosphoprotein through elevation of cAMP. *J Biol Chem.* **277**, 5832–5840 (2002).
30. Liu, H., Jia, Z., Jia, Z., Soodvilai, S., Guan, G., Wang, M. H., Dong, Z., Symons, J. D. & Yang, T. Nitro-oleic acid protects the mouse kidney from ischemia and reperfusion injury. *Am J Physiol Renal Physiol.* **295**, 942–949 (2008).
31. Rudolph, V., Rudolph, V., Rudolph, T. K., Schopfer, F. J., Bonacci, G., Woodcock, S. R., Cole, M. P., Baker, P. R., Ramani, R. & Freeman, B. A. Endogenous generation and protective effects of nitro-fatty acids in a murine model of focal cardiac ischaemia and reperfusion. *Cardiovasc Res.* **85**, 155–166 (2010).
32. Wang, H., Liu, H., Jia, Z., Guan, G. & Yang, T. Effects of endogenous PPAR agonist nitro-oleic acid on metabolic syndrome in obese zucker rats. *PPAR Res.* 1–7 (2010)
33. Reddy, A. T., Lakshmi, S. P. & Reddy, R. C. The nitrated fatty acid 10-nitro-oleate diminishes severity of LPS-induced acute lung injury in mice. *PPAR Res.* **2012**, 1–12 (2012).
34. Khoo, N. K. H., Rudolph, V., Cole, M. P., Golin-Bisello, F., Schopfer, F. J., Woodcock, S. R., Batthyany, C. & Freeman, B. A. Activation of vascular endothelial nitric oxide synthase and heme oxygenase-1 expression by electrophilic nitro-fatty acids. *Free Radical Bio Med.* **48**, 230–239 (2010).
35. Borniquel, S., Jansson, E. A., Cole, M. P., Freeman, B. A. & Lundberg, J. O. Nitrated oleic acid up-regulates PPARgamma and attenuates experimental inflammatory bowel disease. *Free Radical Bio Med.* **48**, 499–505 (2010).
36. Arbeeny, C., Ling, H., Smith, M. M., O'Brien, S., Wawersik, S., Ledbetter, S. R., McAlexander, A., Schopfer, F. J., Willette, R. N. & Jorkasky, D. K. CXA-10, a nitrated fatty acid, Is renoprotective in decoxycorticosterone acetate-salt nephropathy. *J Pharmacol Exp Ther.* **369**, 503–510 (2019).
37. Schopfer, F. J., Vitturi, D. A., Jorkasky, D. K. & Freeman, B. A. Nitro-fatty acids: New drug candidates for chronic inflammatory and fibrotic diseases. *Nitric Oxide.* **79**, 31–37 (2018).
38. Wang, W., Li, C. & Yang, T. Protection of nitro-fatty acid against kidney diseases. *Am J Renal Physiol* **310**, 697–704 (2016).

39. Mata-Pérez, C*.,* Sánchez-Calvo, B., Begara-Morales, J. C., Carreras, A., Padilla, M. N., Melguizo, M., Valderrama, R., Corpas, F. J. & Barroso, J. B. Nitro-linolenic acid is a nitric oxide donor. *Nitric Oxide.* **57**, 57–63 (2016).
40. Montero-Bullon, J.F., Melo, T., Domingues, M. R. & Domingues, P. Characterization of nitrophospholipid-peptide covalent adducts by electrospray tandem mass spectrometry: a first screening analysis using different instrumental platforms. *Eur J Lipid Sci Tech.* **120**, 1–6 (2018).
41. Ferreira, A. M., Minarrieta, L., Lamas Bervejillo, M. & Rubbo, H. Nitro-fatty acids as novel electrophilic ligands for peroxisome proliferator-activated receptors. *Free Radical Bio Med.* **53**, 1654–1663 (2012).
42. Schopfer, F. J., Cole, M. P., Groeger, A. L., Chen, C.-S., Khoo, N. K. H., Woodcock, S. R., Golin-Bisello, F., Motanya, U. N., Li, Y. & Zhang, J. Covalent peroxisome proliferator-activated receptor gamma adduction by nitro-fatty acids: selective ligand activity and anti-diabetic signaling actions. *J Biol Chem.* **285**, 12321–12333 (2010).
43. Baker, P. R., Lin, Y., Schopfer, F. J., Woodcock, S. R., Groeger, A. L., Batthyany, C., Sweeney, S., Long, M. H., Baker, L. M. & Branchaud, B. P. Fatty acid transduction of nitric oxide signaling: multiple nitrated unsaturated fatty acid derivatives exist in human blood and urine and serve as endogenous peroxisome proliferator-activated receptor ligands. *J Biol Chem*. **30,** 42464–42475 (2005).
44. Cui, T., Schopfer, F. J., Zhang, J., Chen, K., Baker, P. R., Batthyany, C., Chacko, B. K., Feng, X., Agarwal, A. & Freeman, B. A. Nitrated fatty acids: endogenous anti-inflammatory signaling mediators. *J Bio Chem.* **281**, 1–24 (2007).
45. Lima, É. S., Bonini, M. G., Augusto, O., Barbeiro, H. V., Souza, H. P. & Abdalla, D. S. P. Nitrated lipids decompose to nitric oxide and lipid radicals and cause vasorelaxation. *Free Radic Biol Med.* **39**, 532–539 (2005).
46. Gorczynski, M. J., Huang, J., Lee, H. & King, S. B. Evaluation of nitroalkenes as nitric oxide donors. *Bioorg Med Chem Lett.* **17**, 2013–2017 (2007).
47. Rubbo, H., Parthasarathy, S., Barnes, S., Kirk, M., Kalyanaraman, B. & Freeman, B. A. Nitric oxide inhibition of lipoxygenase-dependent liposome and low-density lipoprotein oxidation: termination of radical chain propagation reactions and formation of nitrogen-containing oxidized lipid derivatives. *Arch Biochem Biophys.* **324**, 15–25 (1995).
48. Faine, L. A., Cavalcanti, D. M. H., Rudnicki, M., Ferderbar, S., Macedo, S. M. D., Souza, H. P., Farsky, S. H. P., Boscá, L. & Abdalla, D. S. P. Bioactivity of nitrolinoleate: effects on adhesion molecules and CD40-CD40L system. *J Nutr Biochem.* **21**, 125–132 (2010).
49. Mata-Pérez, C., Sánchez-Calvo, B., Begara-Morales, J. C., Padilla, M. N., Valderrama, R., Corpas F. J. & Barroso, J. B. Nitric oxide release from nitro-fatty acids in Arabidopsis roots. *Plant Signal Beh.* **11**, 1–4 (2016).
50. Sánchez-Calvo, B., Barroso, J. B. & Corpas, F. J. Hypothesis: nitro-fatty acids play a role in plant metabolism. *Plant Sci.* **200**, 1–6 (2013).

51. Geisler, A. C. & Rudolph, T. K. Nitroalkylation: a redox sensitive signaling pathway. *Biochim Biophys Acta.* **1820**, 777–784 (2012).
52. Domingues, M. R., Domingues, P. Melo, T., Pérez-Sala, D., Reis, A. & Spickett, C. M. Lipoxidation adducts with peptides and proteins: deleterious modifications or signaling mechanisms? *J Proteomics.* **92**, 110–131 (2013).
53. Hwang, J., Lee, K. E., Lim, J. Y. & Park, S. I. Nitrated fatty acids prevent TNFα-stimulated inflammatory and atherogenic responses in endothelial cells. *Biochem Bioph Res Co.* **387**, 633–640 (2009).
54. Trostchansky, A., Bonilla, L., González-Perilli, L. & Rubbo, H. Nitro-fatty acids: formation, redox signaling, and therapeutic potential. *Antioxid Redox Sign.* **19**, 1257–1265 (2013).
55. Aranda, L., Sánchez-Calvo, B., Begara-Morales, J. C., Chaki, M., Mata-Pérez , C., Padilla, M. N., Valderrama, R. & Barroso, J. B. Post-translational modification of proteins mediated by nitro-fatty acids in plants: nitroalkylation. *Plants.* **8**, 1–82 (2019).
56. Schopfer, F. J., Cipollina, C. & Freeman, B. A. Formation and signaling actions of electrophilic lipids. *Chem Rev.* **111**, 5997–6021 (2011).
57. Gorczynski, M. J., Smitherman, P. K., Akiyama, T. E., Wood, H. B., Berger, J. P., King, S. B. & Morrow, C. S Activation of peroxisome proliferator-activated receptor gamma (PPARgamma) by nitroalkene fatty acids: importance of nitration position and degree of unsaturation. *J Med Chem.* **52**, 4631–4639 (2009).
58. Woodcock, S. R., Bonacci, G., Gelhaus, S. L. & Schopfer, F. J. Nitrated fatty acids: synthesis and measurement. *Free Radical Bio Med.* **59**, 14–26 (2013).
59. Batthyany, C. , Schopfer, F. J., Baker, P. R., Durán, R., Baker, L. M. S., Huan, Y., Cerveñansky, C., Branchaud, B. P. & Freeman, B. A. Reversible post-translational modification of proteins by nitrated fatty acids in vivo. *J Bio Chem.* **281**, 1–30 (2006).
60. Melo, T., Domingues, P., Ferreira, R., Milic, I., Fedorova, M., Santos, S. M., Marcela, A. S. & Domingues. Recent advances on mass spectrometry analysis of nitrated phospholipids. *Anal Chem.* **88**, 2622–2629 (2016).
61. Melo, T. Domingues, P., Ribeiro-Rodrigues, M.T., Girão, H., Marcela, A. S. & Domingues, M. R. Characterization of phospholipid nitroxidation by LC-MS in biomimetic models and in H9c2 Myoblast using a lipidomic approach. *Free Radical Bio Med.* **106**, 219–227 (2017).
62. Fazzari, M. Khoo, N., Woodcock, S. R., Li, L., Freeman, B. A. & Schopfer, F. J. Generation and esterification of electrophilic fatty acid nitroalkenes in triacylglycerides. *Free Radical Bio Med.* **87**, 113–124 (2015).
63. Chakravartula, S. V. S. & Balazy, M. Characterization of nitro arachidonic acid and nitro linoleic acid by mass spectrometry. *Anal Lett.* **45**, 2412–2424 (2012).
64. Lima, É. S., Di Mascio, P., Rubbo, H. & Abdalla, D. S. P. Characterization of linoleic acid nitration in human blood plasma by mass spectrometry. *Biochem.* **41**, 10717–10722 (2002).
65. Rubbo, H. Nitro-fatty acids: novel anti-inflammatory lipid mediators. *Braz J Med Biol Res.* **46**, 728–734 (2013).

66. Lima, E. S., Di Mascio, P. & Abdalla, D. S. P. Cholesteryl nitrolinoleate, a nitrated lipid present in human blood plasma and lipoproteins. *J Lipid Res.* **44**, 1660–1666 (2003).
67. Bonacci, G., Asciutto, E. K., Woodcock, S. R., Salvatore, S. R., Freeman, B. A. & Schopfer, F. J. Gas-phase fragmentation analysis of nitro-fatty acids. *J Am Soc Mass Spectr.* **22**, 1534–1551 (2011).
68. Neves, B., Domingues, P., Oliveira, M., Domingues, M. R. & Melo, T. Profile of phosphatidylserine modifications under nitroxidative stress conditions using a liquid chromatography-mass spectrometry based approach. *Molecules.* **24**, 1–17 (2018).
69. Liu, X., Miller, M. J. S., Joshi, M. S., Thomas, D. D. & Lancaster, J. R. Accelerated reaction of nitric oxide with $O_2$ within the hydrophobic interior of biological membranes. *P Natl A Sci.* **95**, 2175–2179 (1998).
70. Montero-Bullon, J. F., Melo, T., Domingues, M. R. & Domingues, P. Liquid chromatography/tandem mass spectrometry characterization of nitroso, nitrated and nitroxidized cardiolipin products. *Free Radical Bio Med.* **144**, 183–191 (2019).
71. Duarte, S., Melo, T., Domingues, R., de Dios Alché, J. & Pérez-Sala, D. Insight into the cellular effects of nitrated phospholipids: evidence for pleiotropic mechanisms of action. *Free Radical Bio Med.* **144**, 192–202 (2019).
72. Melo, T., Marques, S. S., Ferreira, I., Cruz, M. T., Domingues, P., Marcela, A. S. & Domingues, M. R. New insights into the anti-Inflammatory and antioxidant properties of nitrated phospholipids. *Lipids.* **53**, 117–131 (2018).
73. Van der Veen, J. N., Lingrell, S. & Vance, D. E. The membrane lipid phosphatidylcholine is an unexpected source of triacylglycerol in the liver. *J Bio Chem.* **287**, 23418–23426 (2012).
74. Baker, P. R., Schopfer, F. J., Sweeney, S. & Freeman, B. A. Red cell membrane and plasma linoleic acid nitration products: synthesis, clinical identification, and quantitation. *Proc Natl Acad Sci.* **101**, 11577–11582 (2004).
75. Olsen, J. V. Schwartz, J. C., Griep-Raming, J., Nielsen, M. L., Damoc, E., Denisov, E., Lange, O., Remes, P., Taylor, D., Splendore, M., Wouters, E. R., Senko, M., Makarov, A., Mann, M. & Horning, S. A dual pressure linear ion trap orbitrap instrument with very high sequencing speed. *Mol Cell Proteomics.* **8**, 2759–2769 (2009).
76. Bayat, P., Lesage, D. & Cole, R. B. Ion activation in tandem mass spectrometry using ultra-high resolution instrumentation. *Mass Spectrom Rev.* **39**, 1–23 (2020)
77. Barlett, E. M. & Lewis, D. H. Spectrophotometric determination of phosphate esters in the presence and absence of orthophosphate. *Anal Biochem*. **36**, 159–167 (1970).
78. Pérez-Sala, D., Oeste, C. L., Martínez, A. E., Carrasco, M. J., Garzón, B. & Cañadas, J. Vimentin filament organization and stress sensing depend on its single cysteine residue and zinc binding. *Nat Commun.* **6**, 1–17 (2015).
79. Colombo, S., Melo, T.,Martínez-López, M., Carrasco, M.J., Domingues, M. R., Pérez-Sala, D. & Domingues, P. Phospholipidome of endothelial cells shows a different adaptation response upon oxidative, glycative and lipoxidative stress. *Sci Rep-UK.* **8**, 1–13 (2018).

80. Pluskal, T., Castillo, S., Villar-Briones, A. & Orešič, M. MZmine 2: Modular framework for processing, visualizing, and analyzing mass spectrometry-based molecular profile data. *BMC Bioinformatics.* 1–11, (2010).
81. Jones, L. H. Chemistry and biology of biomolecule nitration. *Chem Biol.* **19**, 1086–1092 (2012).
82. Anjos, S., Feiteira, F., Cerveira, F., Melo, T., Reboredo, A., Colombo, S., Dantas, R., Costa, E., Moreira, A., Santos, S., Campos, A., Ferreira, R., Domingues, P. & Domingues, M. R. Lipidomics reveals similar changes in serum phospholipid signatures of overweight and obese pediatric subjects. *J Proteome Res.* **18**, 3174–3183 (2019).
83. Chiva, C. & Sabidó, E. HCD-only fragmentation method balances peptide identification and quantitation of TMT-labeled samples in hybrid linear ion trap/orbitrap mass spectrometers. *J Proteomics.* **96**, 263–270 (2014).
84. Koivusalo, M., Haimi, P., Heikinheimo, L., Kostiainen, R. & Somerharju, P. Quantitative determination of phospholipid compositions by ESI-MS: effects of acyl chain length, unsaturation, and lipid concentration on instrument response. *J Lipid Res.* **42**, 663–672 (2001).
85. Wang, Y., Armando, A. M., Quehenberger, O., Yan, C. & Dennis, E. A. Comprehensive ultra-performance liquid chromatographic separation and mass spectrometric analysis of eicosanoid metabolites in human samples. *J Chromatogr A.* **1359**, 60–69 (2014).
86. Buré, C., Ayciriex, S., Testet, E. & Schmitter, J.-M. A single run LC-MS/MS method for phospholipidomics. *Anal Bioanal Chem.* **405**, 203–213 (2013).
87. Olsen, J. V., Macek, B., Lange, O., Makarov, A., Horning, S. & Mann, M. Higher energy C-trap dissociation for peptide modification analysis. *Nat Methods.* **4**, 709–712 (2007).
88. Almeida, R., Pauling, J. K., Sokol, E., Hannibal-Bach, H. K. & Ejsing, C. S. Comprehensive lipidome analysis by shotgun lipidomics on a hybrid quadrupole-orbitrap-linear ion trap mass spectrometer. *J Am Soc Mass Spectr.* **26**, 133–148 (2015).
89. Zuo, M.-Q., Sun, R.-X., Fang, R.-Q., He, S.-M. & Dong, M.-Q. Characterization of collision-induced dissociation of deprotonated peptides of 4–16 amino acids using high-resolution mass spectrometry. *J Am Soc Mass Spectr.* **445**, 116186 (2019).
90. Wang, M., Wang, C., Han, R. H. & Han, X. Novel advances in shotgun lipidomics for biology and medicine. *Prog Lipid Res.* **61**, 83–108 (2016).

## SUPPLEMENTARY FIGURES

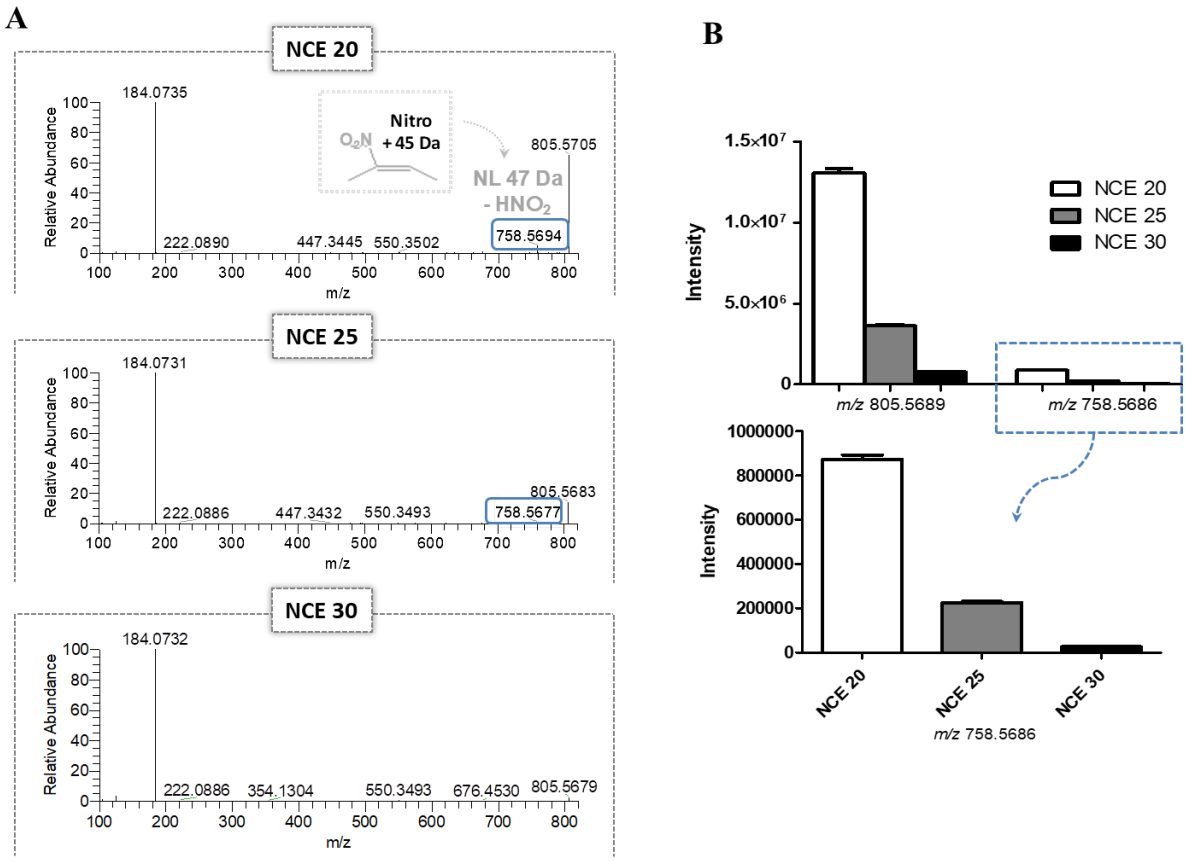


**Figure S1. (A)** HCD-MS/MS spectra of $[NO_2\text{-POPC+H}]^+$ ions at *m/z* 805.5 obtained at low (20), medium (25), and high (30) NCE for $NO_2$-POPC. Neutral loss of $HNO_2$ can be observed at *m/z* 758.5. **(B)** Effect of low (20), medium (25), and high (30) NCE in the intensity of the reporter ions of nitro POPC ($NO_2$-POPC, *m/z* 805.5) observed in positive ion mode that corresponds to the neutral loss of nitro group ($HNO_2$, *m/z* 758.5).

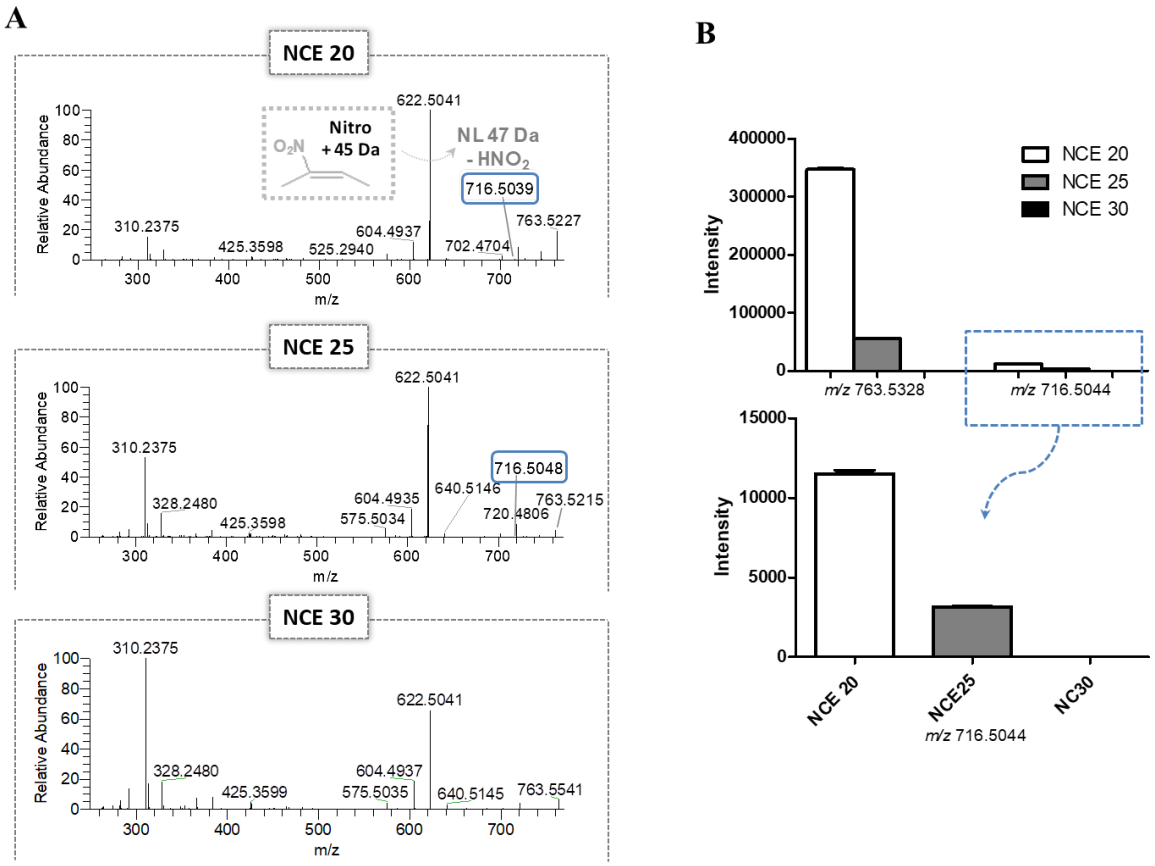


**Figure S2. (A)** HCD-MS/MS spectra of $[NO_2\text{-POPE+H}]^+$ ions at *m/z* 763.5 obtained at low (20), medium (25), and high (30) NCE for $NO_2$-POPE. Neutral loss of $HNO_2$ can be observed at *m/z* 716.5. **(B)** Effect of low (20), medium (25), and high (30) NCE in the intensity of the reporter ions of nitrated POPE ($NO_2$-POPE, *m/z* 763.5) observed in positive ion mode that corresponds to the neutral loss of nitro group ($HNO_2$, *m/z* 716.5).

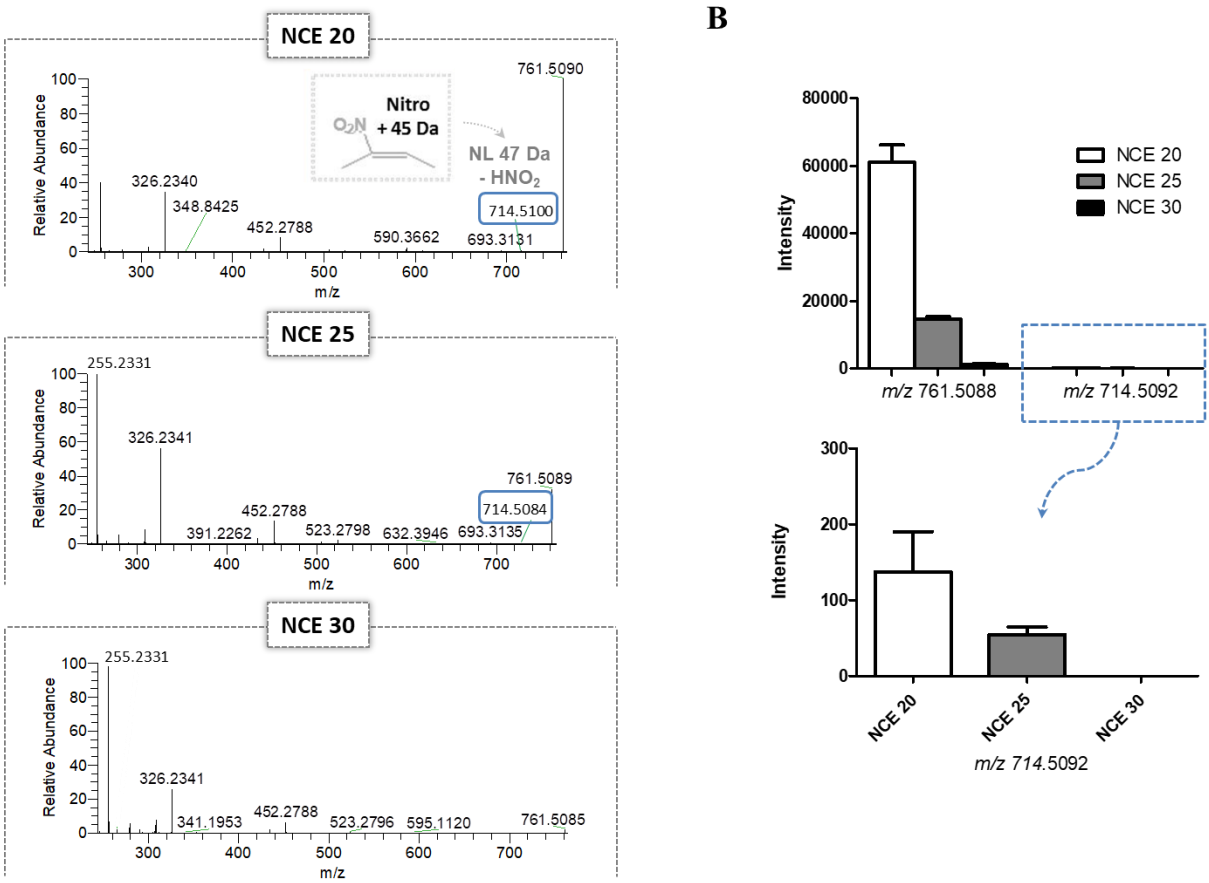


**Figure S3. (A)** HCD-MS/MS spectra of $[NO_2\text{-POPE}-H]^-$ ions at *m/z* 761.5 obtained at low (20), medium (25), and high (30) NCE for $NO_2$-POPE. Neutral loss of $HNO_2$ can be observed at *m/z* 714.5. **(B)** Effect of low (20), medium (25), and high (30) NCE in the intensity of the reporter ions of nitrated POPE ($NO_2$-POPE, *m/z* 761.5) observed in negative ion mode that corresponds to the neutral loss of nitro group ($HNO_2$, *m/z* 714.5).

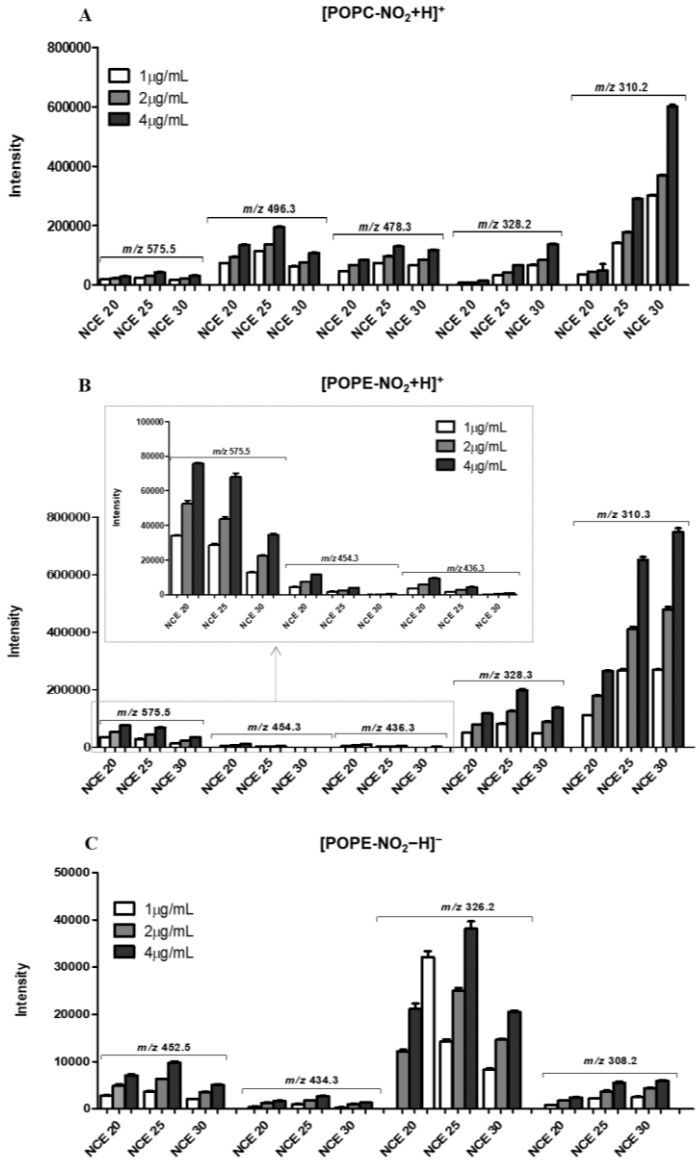


**Figure S4.** Effect of low (20), medium (25) and high (30) NCE in the intensity of the fragment ions with lower *m/z* values observed in the HCD-MS/MS spectra of $NO_2$-POPC in positive ion mode (from the $[M+H]^+$ ions, **A**) and of $NO_2$-POPE both in positive (from the $[M+H]^+$ ions, **B)** and negative ion mode (from the $[M-H]^-$ ions, **C)** obtained when using three concentrations of $NO_2$-PL (1 µg $mL^{-1}$, 2 µg $mL^{-1}$ and 4 µg $mL^{-1}$). Fragment ions at *m/z* 575.5 correspond to the combined neutral loss of $HNO_2$ with phosphocholine (NL 47 plus 183 Da) or phosphoethanolamine polar heads (NL 47 plus 141 Da). Fragment ions at *m/z* 496.3 and 478.3 **(A)** and at *m/z* 454.3 and 436.3 **(B)** correspond to the neutral loss of nitrated oleic acid ($NO_2$-OA) as keto (NL of 309 Da, ($NO_2$-OA−$H_2O$)) and acid derivatives (NL of 327 Da, $NO_2$-OA), respectively. Fragment ions at *m/z* 328.2 and 310.2 (**A** and **B**) correspond to the $[NO_2\text{-OA}+H]^+$ and $[NO_2\text{-OA}-H_2O+H]^+$ ions, respectively. Fragment ions at *m/z* 452.3 and 434.3 **(C)** correspond to the neutral loss of nitrated oleic acid ($NO_2$-OA) as keto and acid derivative, respectively, and fragment ions at *m/z* 326.3 and 308.3 correspond to the $[NO_2\text{-OA}-H]^-$ and $[NO_2\text{-OA-}H_2O-H]^-$ ions, respectively.

## SUPPLEMENTARY TABLES

**Table S1.** Formula, calculated and observed mass, and mass error of $[M+H]^+$ ions observed in the ESI-MS spectra of nitrated and nitroxidized derivatives of POPC, PLPC and PAPC formed due to reaction between $NO_2BF_4$ and each PC. Data was acquired for 20 s and in triplicate in the Q-Exactive Orbitrap mass spectrometer using a concentration of 1 µg $mL^{-1}$. POPC, PC16:0/18:1; PLPC, PC16:0/18:2; PAPC, PC16:0/20:4.

| PC nitration products | Observed Mass (Da) | Calculated Mass (Da) | Error (ppm) | Predicted Formula $[M+H]^+$ |
|---|---|---|---|---|
| $[POPC+45Da+H]^+$ | 805.5704 | 805.5707 | -0.3724 | $C_{42}H_{82}N_2O_{10}P$ |
| $[POPC+45Da+H]^+$ | 805.5701 | 805.5707 | -0.7448 | $C_{42}H_{82}N_2O_{10}P$ |
| $[POPC+45Da+H]^+$ | 805.5700 | 805.5707 | -0.8689 | $C_{42}H_{82}N_2O_{10}P$ |
| $[POPC+61Da+H]^+$ | 821.5651 | 821.5656 | -0.6086 | $C_{42}H_{82}N_2O_{11}P$ |
| $[POPC+61Da+H]^+$ | 821.5648 | 821.5656 | -0.9738 | $C_{42}H_{82}N_2O_{11}P$ |
| $[POPC+61Da+H]^+$ | 821.5647 | 821.5656 | -1.0955 | $C_{42}H_{82}N_2O_{11}P$ |
| $[POPC+74Da+H]^+$ | 834.5591 | 834.5609 | -2.1568 | $C_{42}H_{81}N_3O_{11}P$ |
| $[POPC+74Da+H]^+$ | 834.5584 | 834.5609 | -2.9956 | $C_{42}H_{81}N_3O_{11}P$ |
| $[POPC+74Da+H]^+$ | 834.5580 | 834.5609 | -3.4749 | $C_{42}H_{81}N_3O_{11}P$ |
| $[POPC+77Da+H]^+$ | 837.5598 | 837.5605 | -0.8358 | $C_{42}H_{82}N_2O_{12}P$ |
| $[POPC+77Da+H]^+$ | 837.5595 | 837.5605 | -1.1939 | $C_{42}H_{82}N_2O_{12}P$ |
| $[POPC+77Da+H]^+$ | 837.5596 | 837.5605 | -1.0745 | $C_{42}H_{82}N_2O_{12}P$ |
| $[POPC+90Da+H]^+$ | 850.5552 | 850.5558 | -0.7054 | $C_{42}H_{81}N_3O_{12}P$ |
| $[POPC+90Da+H]^+$ | 850.5551 | 850.5558 | -0.8230 | $C_{42}H_{81}N_3O_{12}P$ |
| $[POPC+90Da+H]^+$ | 850.5548 | 850.5558 | -1.1757 | $C_{42}H_{81}N_3O_{12}P$ |
| $[PLPC+45Da+H]^+$ | 803.5558 | 803.5551 | 0.8711 | $C_{42}H_{80}N_2O_{10}P$ |
| $[PLPC+45Da+H]^+$ | 803.5553 | 803.5551 | 0.2489 | $C_{42}H_{80}N_2O_{10}P$ |
| $[PLPC+45Da+H]^+$ | 803.5558 | 803.5551 | 0.8711 | $C_{42}H_{80}N_2O_{10}P$ |
| $[PLPC+61Da+H]^+$ | 819.5505 | 819.5500 | 0.6101 | $C_{42}H_{80}N_2O_{11}P$ |
| $[PLPC+61Da+H]^+$ | 819.5501 | 819.5500 | 0.1220 | $C_{42}H_{80}N_2O_{11}P$ |
| $[PLPC+61Da+H]^+$ | 819.5507 | 819.5500 | 0.8541 | $C_{42}H_{80}N_2O_{11}P$ |
| $[PLPC+74Da+H]^+$ | 832.5462 | 832.5452 | 1.2011 | $C_{42}H_{79}N_3O_{11}P$ |
| $[PLPC+74Da+H]^+$ | 832.5466 | 832.5452 | 1.6816 | $C_{42}H_{79}N_3O_{11}P$ |
| $[PLPC+74Da+H]^+$ | 832.5466 | 832.5452 | 1.6816 | $C_{42}H_{79}N_3O_{11}P$ |
| $[PLPC+77Da+H]^+$ | 835.5463 | 835.5449 | 1.6756 | $C_{42}H_{80}N_2O_{12}P$ |
| $[PLPC+77Da+H]^+$ | 835.5458 | 835.5449 | 1.0771 | $C_{42}H_{80}N_2O_{12}P$ |
| $[PLPC+77Da+H]^+$ | 835.5464 | 835.5449 | 1.7952 | $C_{42}H_{80}N_2O_{12}P$ |
| $[PLPC+90Da+H]^+$ | 848.5406 | 848.5401 | 0.5892 | $C_{42}H_{79}N_3O_{12}P$ |
| $[PLPC+90Da+H]^+$ | 848.5405 | 848.5401 | 0.4714 | $C_{42}H_{79}N_3O_{12}P$ |
| $[PLPC+90Da+H]^+$ | 848.5410 | 848.5401 | 1.0606 | $C_{42}H_{79}N_3O_{12}P$ |
| $[PAPC+45Da+H]^+$ | 827.5545 | 827.5551 | -0.7250 | $C_{44}H_{80}N_2O_{10}P$ |
| $[PAPC+45Da+H]^+$ | 827.5546 | 827.5551 | -0.6042 | $C_{44}H_{80}N_2O_{10}P$ |
| $[PAPC+45Da+H]^+$ | 827.5537 | 827.5551 | -1.6917 | $C_{44}H_{80}N_2O_{10}P$ |
| $[PAPC+61Da+H]^+$ | 843.5471 | 843.5500 | -3.4379 | $C_{44}H_{80}N_2O_{11}P$ |
| $[PAPC+61Da+H]^+$ | 843.5474 | 843.5500 | -3.0822 | $C_{44}H_{80}N_2O_{11}P$ |
| $[PAPC+61Da+H]^+$ | 843.5475 | 843.5500 | -2.9637 | $C_{44}H_{80}N_2O_{11}P$ |
| $[PAPC+74Da+H]^+$ | 856.5425 | 856.5452 | -3.1522 | $C_{44}H_{79}N_3O_{11}P$ |
| $[PAPC+74Da+H]^+$ | 856.5421 | 856.5452 | -3.6192 | $C_{44}H_{79}N_3O_{11}P$ |
| $[PAPC+74Da+H]^+$ | 856.5425 | 856.5452 | -3.1522 | $C_{44}H_{79}N_3O_{11}P$ |
| $[PAPC+77Da+H]^+$ | 859.5421 | 859.5449 | -3.2575 | $C_{44}H_{80}N_2O_{12}P$ |
| $[PAPC+77Da+H]^+$ | 859.5435 | 859.5449 | -1.6288 | $C_{44}H_{80}N_2O_{12}P$ |
| $[PAPC+77Da+H]^+$ | 859.5433 | 859.5449 | -1.8615 | $C_{44}H_{80}N_2O_{12}P$ |
| $[PAPC+90Da+H]^+$ | 872.5366 | 872.5401 | -4.0113 | $C_{44}H_{79}N_3O_{12}P$ |
| $[PAPC+90Da+H]^+$ | 872.5363 | 872.5401 | -4.3551 | $C_{44}H_{79}N_3O_{12}P$ |
| $[PAPC+90Da+H]^+$ | 872.5361 | 872.5401 | -4.5843 | $C_{44}H_{79}N_3O_{12}P$ |

**Table S2.** Formula, calculated and observed mass, and mass error of $[M+H]^+$ ions observed in the ESI-MS spectra of nitrated and nitroxidized derivatives of POPC, PLPC and PAPC formed due to reaction between $NO_2BF_4$ and each PC. Data was acquired for 20 s and in triplicate in the Q-Exactive Orbitrap mass spectrometer using a concentration of 2 µg $mL^{-1}$. POPC, PC16:0/18:1; PLPC, PC16:0/18:2; PAPC, PC16:0/20:4.

| PC nitration products | Observed Mass (Da) | Calculated Mass (Da) | Error (ppm) | Predicted Formula $[M+H]^+$ |
|---|---|---|---|---|
| $[POPC+45Da+H]^+$ | 805.5702 | 805.5707 | -0.6207 | $C_{42}H_{82}N_2O_{10}P$ |
| $[POPC+45Da+H]^+$ | 805.5704 | 805.5707 | -0.3724 | $C_{42}H_{82}N_2O_{10}P$ |
| $[POPC+45Da+H]^+$ | 805.5702 | 805.5707 | -0.6207 | $C_{42}H_{82}N_2O_{10}P$ |
| $[POPC+61Da+H]^+$ | 821.5650 | 821.5656 | -0.7303 | $C_{42}H_{82}N_2O_{11}P$ |
| $[POPC+61Da+H]^+$ | 821.5651 | 821.5656 | -0.6086 | $C_{42}H_{82}N_2O_{11}P$ |
| $[POPC+61Da+H]^+$ | 821.5648 | 821.5656 | -0.9738 | $C_{42}H_{82}N_2O_{11}P$ |
| $[POPC+74Da+H]^+$ | 834.5569 | 834.5609 | -4.7929 | $C_{42}H_{81}N_3O_{11}P$ |
| $[POPC+74Da+H]^+$ | 834.5580 | 834.5609 | -3.4749 | $C_{42}H_{81}N_3O_{11}P$ |
| $[POPC+74Da+H]^+$ | 834.5580 | 834.5609 | -3.4749 | $C_{42}H_{81}N_3O_{11}P$ |
| $[POPC+77Da+H]^+$ | 837.5601 | 837.5605 | -0.4776 | $C_{42}H_{82}N_2O_{12}P$ |
| $[POPC+77Da+H]^+$ | 837.5603 | 837.5605 | -0.2388 | $C_{42}H_{82}N_2O_{12}P$ |
| $[POPC+77Da+H]^+$ | 837.5604 | 837.5605 | -0.1194 | $C_{42}H_{82}N_2O_{12}P$ |
| $[POPC+90Da+H]^+$ | 850.5552 | 850.5558 | -0.7054 | $C_{42}H_{81}N_3O_{12}P$ |
| $[POPC+90Da+H]^+$ | 850.5556 | 850.5558 | -0.2351 | $C_{42}H_{81}N_3O_{12}P$ |
| $[POPC+90Da+H]^+$ | 850.5556 | 850.5558 | -0.2351 | $C_{42}H_{81}N_3O_{12}P$ |
| $[PLPC+45Da+H]^+$ | 803.5551 | 803.5551 | 0.0000 | $C_{42}H_{80}N_2O_{10}P$ |
| $[PLPC+45Da+H]^+$ | 803.5553 | 803.5551 | 0.2489 | $C_{42}H_{80}N_2O_{10}P$ |
| $[PLPC+45Da+H]^+$ | 803.5549 | 803.5551 | -0.2489 | $C_{42}H_{80}N_2O_{10}P$ |
| $[PLPC+61Da+H]^+$ | 819.5498 | 819.5500 | -0.2440 | $C_{42}H_{80}N_2O_{11}P$ |
| $[PLPC+61Da+H]^+$ | 819.5500 | 819.5500 | 0.0000 | $C_{42}H_{80}N_2O_{11}P$ |
| $[PLPC+61Da+H]^+$ | 819.5497 | 819.5500 | -0.3661 | $C_{42}H_{80}N_2O_{11}P$ |
| $[PLPC+74Da+H]^+$ | 832.5460 | 832.5452 | 0.9609 | $C_{42}H_{79}N_3O_{11}P$ |
| $[PLPC+74Da+H]^+$ | 832.5457 | 832.5452 | 0.6006 | $C_{42}H_{79}N_3O_{11}P$ |
| $[PLPC+74Da+H]^+$ | 832.5457 | 832.5452 | 0.6006 | $C_{42}H_{79}N_3O_{11}P$ |
| $[PLPC+77Da+H]^+$ | 835.5458 | 835.5449 | 1.0771 | $C_{42}H_{80}N_2O_{12}P$ |
| $[PLPC+77Da+H]^+$ | 835.5460 | 835.5449 | 1.3165 | $C_{42}H_{80}N_2O_{12}P$ |
| $[PLPC+77Da+H]^+$ | 835.5462 | 835.5449 | 1.5559 | $C_{42}H_{80}N_2O_{12}P$ |
| $[PLPC+90Da+H]^+$ | 848.5402 | 848.5401 | 0.1178 | $C_{42}H_{79}N_3O_{12}P$ |
| $[PLPC+90Da+H]^+$ | 848.5400 | 848.5401 | -0.1178 | $C_{42}H_{79}N_3O_{12}P$ |
| $[PLPC+90Da+H]^+$ | 848.5402 | 848.5401 | 0.1178 | $C_{42}H_{79}N_3O_{12}P$ |
| $[PAPC+45Da+H]^+$ | 827.5541 | 827.5551 | -1.2084 | $C_{44}H_{80}N_2O_{10}P$ |
| $[PAPC+45Da+H]^+$ | 827.5552 | 827.5551 | 0.1208 | $C_{44}H_{80}N_2O_{10}P$ |
| $[PAPC+45Da+H]^+$ | 827.5548 | 827.5551 | -0.3625 | $C_{44}H_{80}N_2O_{10}P$ |
| $[PAPC+61Da+H]^+$ | 843.5482 | 843.5500 | -2.1338 | $C_{44}H_{80}N_2O_{11}P$ |
| $[PAPC+61Da+H]^+$ | 843.5477 | 843.5500 | -2.7266 | $C_{44}H_{80}N_2O_{11}P$ |
| $[PAPC+61Da+H]^+$ | 843.5482 | 843.5500 | -2.1338 | $C_{44}H_{80}N_2O_{11}P$ |
| $[PAPC+74Da+H]^+$ | 856.5431 | 856.5452 | -2.4517 | $C_{44}H_{79}N_3O_{11}P$ |
| $[PAPC+74Da+H]^+$ | 856.5432 | 856.5452 | -2.3350 | $C_{44}H_{79}N_3O_{11}P$ |
| $[PAPC+74Da+H]^+$ | 856.5431 | 856.5452 | -2.4517 | $C_{44}H_{79}N_3O_{11}P$ |
| $[PAPC+77Da+H]^+$ | 859.5425 | 859.5449 | -2.7922 | $C_{44}H_{80}N_2O_{12}P$ |
| $[PAPC+77Da+H]^+$ | 859.5428 | 859.5449 | -2.4432 | $C_{44}H_{80}N_2O_{12}P$ |
| $[PAPC+77Da+H]^+$ | 859.5428 | 859.5449 | -2.4432 | $C_{44}H_{80}N_2O_{12}P$ |
| $[PAPC+90Da+H]^+$ | 872.5365 | 872.5401 | -4.1259 | $C_{44}H_{79}N_3O_{12}P$ |
| $[PAPC+90Da+H]^+$ | 872.5364 | 872.5401 | -4.2405 | $C_{44}H_{79}N_3O_{12}P$ |
| $[PAPC+90Da+H]^+$ | 872.5363 | 872.5401 | -4.3551 | $C_{44}H_{79}N_3O_{12}P$ |

**Table S3.** Formula, calculated and observed mass, and mass error of $[M+H]^+$ ions observed in the ESI-MS spectra of nitrated and nitroxidized derivatives of POPC, PLPC and PAPC formed due to reaction between $NO_2BF_4$ and each PC. Data was acquired for 20 s and in triplicate in the Q-Exactive Orbitrap mass spectrometer using a concentration of 4 μg $mL^{-1}$. POPC, PC16:0/18:1; PLPC, PC16:0/18:2; PAPC, PC16:0/20:4.

| PC nitration products | Observed Mass (Da) | Calculated Mass (Da) | Error (ppm) | Predicted Formula $[M+H]^+$ |
|---|---|---|---|---|
| $[POPC+45Da+H]^+$ | 805.5693 | 805.5707 | -1.7379 | $C_{42}H_{82}N_2O_{10}P$ |
| $[POPC+45Da+H]^+$ | 805.5693 | 805.5707 | -1.7379 | $C_{42}H_{82}N_2O_{10}P$ |
| $[POPC+45Da+H]^+$ | 805.5695 | 805.5707 | -1.4896 | $C_{42}H_{82}N_2O_{10}P$ |
| $[POPC+61Da+H]^+$ | 821.5641 | 821.5656 | -1.8258 | $C_{42}H_{82}N_2O_{11}P$ |
| $[POPC+61Da+H]^+$ | 821.5640 | 821.5656 | -1.9475 | $C_{42}H_{82}N_2O_{11}P$ |
| $[POPC+61Da+H]^+$ | 821.5642 | 821.5656 | -1.7041 | $C_{42}H_{82}N_2O_{11}P$ |
| $[POPC+74Da+H]^+$ | 834.5568 | 834.5609 | -4.9128 | $C_{42}H_{81}N_3O_{11}P$ |
| $[POPC+74Da+H]^+$ | 834.5573 | 834.5609 | -4.3136 | $C_{42}H_{81}N_3O_{11}P$ |
| $[POPC+74Da+H]^+$ | 834.5577 | 834.5609 | -3.8344 | $C_{42}H_{81}N_3O_{11}P$ |
| $[POPC+77Da+H]^+$ | 837.5594 | 837.5605 | -1.3133 | $C_{42}H_{82}N_2O_{12}P$ |
| $[POPC+77Da+H]^+$ | 837.5594 | 837.5605 | -1.3133 | $C_{42}H_{82}N_2O_{12}P$ |
| $[POPC+77Da+H]^+$ | 837.5592 | 837.5605 | -1.5521 | $C_{42}H_{82}N_2O_{12}P$ |
| $[POPC+90Da+H]^+$ | 850.5543 | 850.5558 | -1.7636 | $C_{42}H_{81}N_3O_{12}P$ |
| $[POPC+90Da+H]^+$ | 850.5544 | 850.5558 | -1.6460 | $C_{42}H_{81}N_3O_{12}P$ |
| $[POPC+90Da+H]^+$ | 850.5540 | 850.5558 | -2.1163 | $C_{42}H_{81}N_3O_{12}P$ |
| $[PLPC+45Da+H]^+$ | 803.5550 | 803.5551 | -0.1244 | $C_{42}H_{80}N_2O_{10}P$ |
| $[PLPC+45Da+H]^+$ | 803.5549 | 803.5551 | -0.2489 | $C_{42}H_{80}N_2O_{10}P$ |
| $[PLPC+45Da+H]^+$ | 803.5548 | 803.5551 | -0.3733 | $C_{42}H_{80}N_2O_{10}P$ |
| $[PLPC+61Da+H]^+$ | 819.5497 | 819.5500 | -0.3661 | $C_{42}H_{80}N_2O_{11}P$ |
| $[PLPC+61Da+H]^+$ | 819.5497 | 819.5500 | -0.3661 | $C_{42}H_{80}N_2O_{11}P$ |
| $[PLPC+61Da+H]^+$ | 819.5498 | 819.5500 | -0.2440 | $C_{42}H_{80}N_2O_{11}P$ |
| $[PLPC+74Da+H]^+$ | 832.5455 | 832.5452 | 0.3603 | $C_{42}H_{79}N_3O_{11}P$ |
| $[PLPC+74Da+H]^+$ | 832.5457 | 832.5452 | 0.6006 | $C_{42}H_{79}N_3O_{11}P$ |
| $[PLPC+74Da+H]^+$ | 832.5453 | 832.5452 | 0.1201 | $C_{42}H_{79}N_3O_{11}P$ |
| $[PLPC+77Da+H]^+$ | 835.5461 | 835.5449 | 1.4362 | $C_{42}H_{80}N_2O_{12}P$ |
| $[PLPC+77Da+H]^+$ | 835.5467 | 835.5449 | 2.1543 | $C_{42}H_{80}N_2O_{12}P$ |
| $[PLPC+77Da+H]^+$ | 835.5467 | 835.5449 | 2.1543 | $C_{42}H_{80}N_2O_{12}P$ |
| $[PLPC+90Da+H]^+$ | 848.5398 | 848.5401 | -0.3535 | $C_{42}H_{79}N_3O_{12}P$ |
| $[PLPC+90Da+H]^+$ | 848.5399 | 848.5401 | -0.2357 | $C_{42}H_{79}N_3O_{12}P$ |
| $[PLPC+90Da+H]^+$ | 848.5401 | 848.5401 | 0.0000 | $C_{42}H_{79}N_3O_{12}P$ |
| $[PAPC+45Da+H]^+$ | 827.5535 | 827.5551 | -1.9334 | $C_{44}H_{80}N_2O_{10}P$ |
| $[PAPC+45Da+H]^+$ | 827.5541 | 827.5551 | -1.2084 | $C_{44}H_{80}N_2O_{10}P$ |
| $[PAPC+45Da+H]^+$ | 827.5541 | 827.5551 | -1.2084 | $C_{44}H_{80}N_2O_{10}P$ |
| $[PAPC+61Da+H]^+$ | 843.5484 | 843.5500 | -1.8967 | $C_{44}H_{80}N_2O_{11}P$ |
| $[PAPC+61Da+H]^+$ | 843.5485 | 843.5500 | -1.7782 | $C_{44}H_{80}N_2O_{11}P$ |
| $[PAPC+61Da+H]^+$ | 843.5478 | 843.5500 | -2.6080 | $C_{44}H_{80}N_2O_{11}P$ |
| $[PAPC+74Da+H]^+$ | 856.5435 | 856.5452 | -1.9847 | $C_{44}H_{79}N_3O_{11}P$ |
| $[PAPC+74Da+H]^+$ | 856.5434 | 856.5452 | -2.1015 | $C_{44}H_{79}N_3O_{11}P$ |
| $[PAPC+74Da+H]^+$ | 856.5434 | 856.5452 | -2.1015 | $C_{44}H_{79}N_3O_{11}P$ |
| $[PAPC+77Da+H]^+$ | 859.5443 | 859.5449 | -0.6980 | $C_{44}H_{80}N_2O_{12}P$ |
| $[PAPC+77Da+H]^+$ | 859.5449 | 859.5449 | 0.0000 | $C_{44}H_{80}N_2O_{12}P$ |
| $[PAPC+77Da+H]^+$ | 859.5443 | 859.5449 | -0.6980 | $C_{44}H_{80}N_2O_{12}P$ |
| $[PAPC+90Da+H]^+$ | 872.5370 | 872.5401 | -3.5528 | $C_{44}H_{79}N_3O_{12}P$ |
| $[PAPC+90Da+H]^+$ | 872.5372 | 872.5401 | -3.3236 | $C_{44}H_{79}N_3O_{12}P$ |
| $[PAPC+90Da+H]^+$ | 872.5371 | 872.5401 | -3.4382 | $C_{44}H_{79}N_3O_{12}P$ |

**Table S4.** Formula, calculated and observed mass, and mass error of $[M+H]^+$ ions observed in the ESI-MS spectra of nitrated and nitroxidized derivatives of POPE, PLPE and PAPE formed due to reaction between $NO_2BF_4$ and each PE. Data was acquired for 20 s and in triplicate in the Q-Exactive Orbitrap mass spectrometer using a concentration of 1 µg $mL^{-1}$. POPE, PE16:0/18:1; PLPE, PE16:0/18:2; PAPE, PE16:0/20:4.

| PE nitration products | Observed Mass (Da) | Calculated Mass (Da) | Error (ppm) | Predicted Formula [M+H]+ |
|---|---|---|---|---|
| $[POPE+45Da+H]^+$ | 763.5238 | 763.5238 | 0.0000 | $C_{39}H_{76}N_2O_{10}P$ |
| $[POPE+45Da+H]^+$ | 763.5241 | 763.5238 | 0.3929 | $C_{39}H_{76}N_2O_{10}P$ |
| $[POPE+45Da+H]^+$ | 763.5236 | 763.5238 | -0.2619 | $C_{39}H_{76}N_2O_{10}P$ |
| $[POPE+61Da+H]^+$ | 779.5185 | 779.5187 | -0.2566 | $C_{39}H_{76}N_2O_{11}P$ |
| $[POPE+61Da+H]^+$ | 779.5186 | 779.5187 | -0.1283 | $C_{39}H_{76}N_2O_{11}P$ |
| $[POPE+61Da+H]^+$ | 779.5183 | 779.5187 | -0.5131 | $C_{39}H_{76}N_2O_{11}P$ |
| $[POPE+74Da+H]^+$ | 792.5101 | 792.5139 | -4.7949 | $C_{39}H_{75}N_3O_{11}P$ |
| $[POPE+74Da+H]^+$ | 792.5102 | 792.5139 | -4.6687 | $C_{39}H_{75}N_3O_{11}P$ |
| $[POPE+74Da+H]^+$ | 792.5104 | 792.5139 | -4.4163 | $C_{39}H_{75}N_3O_{11}P$ |
| $[POPE+77Da+H]^+$ | 795.5134 | 795.5136 | -0.2514 | $C_{39}H_{76}N_2O_{12}P$ |
| $[POPE+77Da+H]^+$ | 795.5133 | 795.5136 | -0.3771 | $C_{39}H_{76}N_2O_{12}P$ |
| $[POPE+77Da+H]^+$ | 795.5130 | 795.5136 | -0.7542 | $C_{39}H_{76}N_2O_{12}P$ |
| $[POPE+90Da+H]^+$ | 808.5089 | 808.5088 | 0.1237 | $C_{39}H_{75}N_3O_{12}P$ |
| $[POPE+90Da+H]^+$ | 808.5085 | 808.5088 | -0.3711 | $C_{39}H_{75}N_3O_{12}P$ |
| $[POPE+90Da+H]^+$ | 808.5090 | 808.5088 | 0.2474 | $C_{39}H_{75}N_3O_{12}P$ |
| $[PLPE+45Da+H]^+$ | 761.5070 | 761.5081 | -1.4445 | $C_{39}H_{74}N_2O_{10}P$ |
| $[PLPE+45Da+H]^+$ | 761.5068 | 761.5081 | -1.7071 | $C_{39}H_{74}N_2O_{10}P$ |
| $[PLPE+45Da+H]^+$ | 761.5069 | 761.5081 | -1.5758 | $C_{39}H_{74}N_2O_{10}P$ |
| $[PLPE+61Da+H]^+$ | 777.5016 | 777.5030 | -1.8006 | $C_{39}H_{74}N_2O_{11}P$ |
| $[PLPE+61Da+H]^+$ | 777.5017 | 777.5030 | -1.6720 | $C_{39}H_{74}N_2O_{11}P$ |
| $[PLPE+61Da+H]^+$ | 777.5015 | 777.5030 | -1.9293 | $C_{39}H_{74}N_2O_{11}P$ |
| $[PLPE+74Da+H]^+$ | 790.4999 | 790.4983 | 2.0240 | $C_{39}H_{73}N_3O_{11}P$ |
| $[PLPE+74Da+H]^+$ | 790.4973 | 790.4983 | -1.2650 | $C_{39}H_{73}N_3O_{11}P$ |
| $[PLPE+74Da+H]^+$ | 790.4973 | 790.4983 | -1.2650 | $C_{39}H_{73}N_3O_{11}P$ |
| $[PLPE+77Da+H]^+$ | 793.4967 | 793.4979 | -1.5123 | $C_{39}H_{74}N_2O_{12}P$ |
| $[PLPE+77Da+H]^+$ | 793.4961 | 793.4979 | -2.2684 | $C_{39}H_{74}N_2O_{12}P$ |
| $[PLPE+77Da+H]^+$ | 793.4959 | 793.4979 | -2.5205 | $C_{39}H_{74}N_2O_{12}P$ |
| $[PLPE+90Da+H]^+$ | 806.4918 | 806.4932 | -1.7359 | $C_{39}H_{73}N_3O_{12}P$ |
| $[PLPE+90Da+H]^+$ | 806.4910 | 806.4932 | -2.7279 | $C_{39}H_{73}N_3O_{12}P$ |
| $[PLPE+90Da+H]^+$ | 806.4912 | 806.4932 | -2.4799 | $C_{39}H_{73}N_3O_{12}P$ |
| $[PAPE+45Da+H]^+$ | 785.5049 | 785.5081 | -4.0738 | $C_{41}H_{74}N_2O_{10}P$ |
| $[PAPE+45Da+H]^+$ | 785.5060 | 785.5081 | -2.6734 | $C_{41}H_{74}N_2O_{10}P$ |
| $[PAPE+45Da+H]^+$ | 785.5060 | 785.5081 | -2.6734 | $C_{41}H_{74}N_2O_{10}P$ |
| $[PAPE+61Da+H]^+$ | 801.5000 | 801.5030 | -3.7430 | $C_{41}H_{74}N_2O_{11}P$ |
| $[PAPE+61Da+H]^+$ | 801.5004 | 801.5030 | -3.2439 | $C_{41}H_{74}N_2O_{11}P$ |
| $[PAPE+61Da+H]^+$ | 801.5018 | 801.5030 | -1.4972 | $C_{41}H_{74}N_2O_{11}P$ |
| $[PAPE+74Da+H]^+$ | 814.4979 | 814.4983 | -0.4911 | $C_{41}H_{73}N_3O_{11}P$ |
| $[PAPE+74Da+H]^+$ | 814.4981 | 814.4983 | -0.2455 | $C_{41}H_{73}N_3O_{11}P$ |
| $[PAPE+74Da+H]^+$ | 814.4975 | 814.4983 | -0.9822 | $C_{41}H_{73}N_3O_{11}P$ |
| $[PAPE+77Da+H]^+$ | 817.4960 | 817.4979 | -2.3242 | $C_{41}H_{74}N_2O_{12}P$ |
| $[PAPE+77Da+H]^+$ | 817.4954 | 817.4979 | -3.0581 | $C_{41}H_{74}N_2O_{12}P$ |
| $[PAPE+77Da+H]^+$ | 817.4957 | 817.4979 | -2.6911 | $C_{41}H_{74}N_2O_{12}P$ |
| $[PAPE+90Da+H]^+$ | 830.4915 | 830.4932 | -2.0470 | $C_{41}H_{73}N_3O_{12}P$ |
| $[PAPE+90Da+H]^+$ | 830.4920 | 830.4932 | -1.4449 | $C_{41}H_{73}N_3O_{12}P$ |
| $[PAPE+90Da+H]^+$ | 830.4911 | 830.4932 | -2.5286 | $C_{41}H_{73}N_3O_{12}P$ |

**Table S5.** Formula, calculated and observed mass, and mass error of $[M+H]^+$ ions observed in the ESI-MS spectra of nitrated and nitroxidized derivatives of POPE, PLPE and PAPE formed due to reaction between $NO_2BF_4$ and each PE. Data was acquired for 20 s and in triplicate in the Q-Exactive Orbitrap mass spectrometer using a concentration of 2 µg $mL^{-1}$. POPE, PE16:0/18:1; PLPE, PE16:0/18:2; PAPE, PE16:0/20:4.

| PE nitration products | Observed Mass (Da) | Calculated Mass (Da) | Error (ppm) | Predicted Formula [M+H]+ |
|---|---|---|---|---|
| $[POPE+45Da+H]^+$ | 763.5246 | 763.5238 | 1.0478 | $C_{39}H_{76}N_2O_{10}P$ |
| $[POPE+45Da+H]^+$ | 763.5245 | 763.5238 | 0.9168 | $C_{39}H_{76}N_2O_{10}P$ |
| $[POPE+45Da+H]^+$ | 763.5249 | 763.5238 | 1.4407 | $C_{39}H_{76}N_2O_{10}P$ |
| $[POPE+61Da+H]^+$ | 779.5193 | 779.5187 | 0.7697 | $C_{39}H_{76}N_2O_{11}P$ |
| $[POPE+61Da+H]^+$ | 779.5193 | 779.5187 | 0.7697 | $C_{39}H_{76}N_2O_{11}P$ |
| $[POPE+61Da+H]^+$ | 779.5197 | 779.5187 | 1.2828 | $C_{39}H_{76}N_2O_{11}P$ |
| $[POPE+74Da+H]^+$ | 792.5106 | 792.5139 | -4.1640 | $C_{39}H_{75}N_3O_{11}P$ |
| $[POPE+74Da+H]^+$ | 792.5113 | 792.5139 | -3.2807 | $C_{39}H_{75}N_3O_{11}P$ |
| $[POPE+74Da+H]^+$ | 792.5118 | 792.5139 | -2.6498 | $C_{39}H_{75}N_3O_{11}P$ |
| $[POPE+77Da+H]^+$ | 795.5137 | 795.5136 | 0.1257 | $C_{39}H_{76}N_2O_{12}P$ |
| $[POPE+77Da+H]^+$ | 795.5137 | 795.5136 | 0.1257 | $C_{39}H_{76}N_2O_{12}P$ |
| $[POPE+77Da+H]^+$ | 795.5142 | 795.5136 | 0.7542 | $C_{39}H_{76}N_2O_{12}P$ |
| $[POPE+90Da+H]^+$ | 808.5094 | 808.5088 | 0.7421 | $C_{39}H_{75}N_3O_{12}P$ |
| $[POPE+90Da+H]^+$ | 808.5096 | 808.5088 | 0.9895 | $C_{39}H_{75}N_3O_{12}P$ |
| $[POPE+90Da+H]^+$ | 808.5100 | 808.5088 | 1.4842 | $C_{39}H_{75}N_3O_{12}P$ |
| $[PLPE+45Da+H]^+$ | 761.5060 | 761.5081 | -2.7577 | $C_{39}H_{74}N_2O_{10}P$ |
| $[PLPE+45Da+H]^+$ | 761.5062 | 761.5081 | -2.4950 | $C_{39}H_{74}N_2O_{10}P$ |
| $[PLPE+45Da+H]^+$ | 761.5062 | 761.5081 | -2.4950 | $C_{39}H_{74}N_2O_{10}P$ |
| $[PLPE+61Da+H]^+$ | 777.5010 | 777.5030 | -2.5723 | $C_{39}H_{74}N_2O_{11}P$ |
| $[PLPE+61Da+H]^+$ | 777.5005 | 777.5030 | -3.2154 | $C_{39}H_{74}N_2O_{11}P$ |
| $[PLPE+61Da+H]^+$ | 777.5009 | 777.5030 | -2.7010 | $C_{39}H_{74}N_2O_{11}P$ |
| $[PLPE+74Da+H]^+$ | 790.5020 | 790.4983 | 4.6806 | $C_{39}H_{73}N_3O_{11}P$ |
| $[PLPE+74Da+H]^+$ | 790.5008 | 790.4983 | 3.1626 | $C_{39}H_{73}N_3O_{11}P$ |
| $[PLPE+74Da+H]^+$ | 790.5013 | 790.4983 | 3.7951 | $C_{39}H_{73}N_3O_{11}P$ |
| $[PLPE+77Da+H]^+$ | 793.4958 | 793.4979 | -2.6465 | $C_{39}H_{74}N_2O_{12}P$ |
| $[PLPE+77Da+H]^+$ | 793.4960 | 793.4979 | -2.3945 | $C_{39}H_{74}N_2O_{12}P$ |
| $[PLPE+77Da+H]^+$ | 793.4961 | 793.4979 | -2.2684 | $C_{39}H_{74}N_2O_{12}P$ |
| $[PLPE+90Da+H]^+$ | 806.4906 | 806.4932 | -3.2238 | $C_{39}H_{73}N_3O_{12}P$ |
| $[PLPE+90Da+H]^+$ | 806.4907 | 806.4932 | -3.0998 | $C_{39}H_{73}N_3O_{12}P$ |
| $[PLPE+90Da+H]^+$ | 806.4905 | 806.4932 | -3.3478 | $C_{39}H_{73}N_3O_{12}P$ |
| $[PAPE+45Da+H]^+$ | 785.5062 | 785.5081 | -2.4188 | $C_{41}H_{74}N_2O_{10}P$ |
| $[PAPE+45Da+H]^+$ | 785.5053 | 785.5081 | -3.5646 | $C_{41}H_{74}N_2O_{10}P$ |
| $[PAPE+45Da+H]^+$ | 785.5057 | 785.5081 | -3.0553 | $C_{41}H_{74}N_2O_{10}P$ |
| $[PAPE+61Da+H]^+$ | 801.5023 | 801.5030 | -0.8734 | $C_{41}H_{74}N_2O_{11}P$ |
| $[PAPE+61Da+H]^+$ | 801.5018 | 801.5030 | -1.4972 | $C_{41}H_{74}N_2O_{11}P$ |
| $[PAPE+61Da+H]^+$ | 801.5019 | 801.5030 | -1.3724 | $C_{41}H_{74}N_2O_{11}P$ |
| $[PAPE+74Da+H]^+$ | 814.4961 | 814.4983 | -2.7010 | $C_{41}H_{73}N_3O_{11}P$ |
| $[PAPE+74Da+H]^+$ | 814.4969 | 814.4983 | -1.7188 | $C_{41}H_{73}N_3O_{11}P$ |
| $[PAPE+74Da+H]^+$ | 814.4965 | 814.4983 | -2.2099 | $C_{41}H_{73}N_3O_{11}P$ |
| $[PAPE+77Da+H]^+$ | 817.4996 | 817.4979 | 2.0795 | $C_{41}H_{74}N_2O_{12}P$ |
| $[PAPE+77Da+H]^+$ | 817.4976 | 817.4979 | -0.3670 | $C_{41}H_{74}N_2O_{12}P$ |
| $[PAPE+77Da+H]^+$ | 817.4973 | 817.4979 | -0.7339 | $C_{41}H_{74}N_2O_{12}P$ |
| $[PAPE+90Da+H]^+$ | 830.4912 | 830.4932 | -2.4082 | $C_{41}H_{73}N_3O_{12}P$ |
| $[PAPE+90Da+H]^+$ | 830.4917 | 830.4932 | -1.8062 | $C_{41}H_{73}N_3O_{12}P$ |
| $[PAPE+90Da+H]^+$ | 830.4913 | 830.4932 | -2.2878 | $C_{41}H_{73}N_3O_{12}P$ |

**Table S6.** Formula, calculated and observed mass, and mass error of $[M+H]^+$ ions observed in the ESI-MS spectra of nitrated and nitroxidized derivatives of POPE, PLPE and PAPE formed due to reaction between $NO_2BF_4$ and each PE. Data was acquired for 20 s and in triplicate in the Q-Exactive Orbitrap mass spectrometer using a concentration of 4 µg $mL^{-1}$. POPE, PE16:0/18:1; PLPE, PE16:0/18:2; PAPE, PE16:0/20:4.

| PE nitration products | Observed Mass (Da) | Calculated Mass (Da) | Error (ppm) | Predicted Formula [M+H]+ |
|---|---|---|---|---|
| $[POPE+45Da+H]^+$ | 763.5222 | 763.5238 | -2.0955 | $C_{39}H_{76}N_2O_{10}P$ |
| $[POPE+45Da+H]^+$ | 763.5220 | 763.5238 | -2.3575 | $C_{39}H_{76}N_2O_{10}P$ |
| $[POPE+45Da+H]^+$ | 763.5222 | 763.5238 | -2.0955 | $C_{39}H_{76}N_2O_{10}P$ |
| $[POPE+61Da+H]^+$ | 779.5167 | 779.5187 | -2.5657 | $C_{39}H_{76}N_2O_{11}P$ |
| $[POPE+61Da+H]^+$ | 779.5165 | 779.5187 | -2.8223 | $C_{39}H_{76}N_2O_{11}P$ |
| $[POPE+61Da+H]^+$ | 779.5170 | 779.5187 | -2.1808 | $C_{39}H_{76}N_2O_{11}P$ |
| $[POPE+74Da+H]^+$ | 792.5105 | 792.5139 | -4.2901 | $C_{39}H_{75}N_3O_{11}P$ |
| $[POPE+74Da+H]^+$ | 792.5106 | 792.5139 | -4.1640 | $C_{39}H_{75}N_3O_{11}P$ |
| $[POPE+74Da+H]^+$ | 792.5105 | 792.5139 | -4.2901 | $C_{39}H_{75}N_3O_{11}P$ |
| $[POPE+77Da+H]^+$ | 795.5113 | 795.5136 | -2.8912 | $C_{39}H_{76}N_2O_{12}P$ |
| $[POPE+77Da+H]^+$ | 795.5115 | 795.5136 | -2.6398 | $C_{39}H_{76}N_2O_{12}P$ |
| $[POPE+77Da+H]^+$ | 795.5113 | 795.5136 | -2.8912 | $C_{39}H_{76}N_2O_{12}P$ |
| $[POPE+90Da+H]^+$ | 808.5069 | 808.5088 | -2.3500 | $C_{39}H_{75}N_3O_{12}P$ |
| $[POPE+90Da+H]^+$ | 808.5069 | 808.5088 | -2.3500 | $C_{39}H_{75}N_3O_{12}P$ |
| $[POPE+90Da+H]^+$ | 808.5070 | 808.5088 | -2.2263 | $C_{39}H_{75}N_3O_{12}P$ |
| $[PLPE+45Da+H]^+$ | 761.5073 | 761.5081 | -1.0505 | $C_{39}H_{74}N_2O_{10}P$ |
| $[PLPE+45Da+H]^+$ | 761.5075 | 761.5081 | -0.7879 | $C_{39}H_{74}N_2O_{10}P$ |
| $[PLPE+45Da+H]^+$ | 761.5074 | 761.5081 | -0.9192 | $C_{39}H_{74}N_2O_{10}P$ |
| $[PLPE+61Da+H]^+$ | 777.5024 | 777.5030 | -0.7717 | $C_{39}H_{74}N_2O_{11}P$ |
| $[PLPE+61Da+H]^+$ | 777.5024 | 777.5030 | -0.7717 | $C_{39}H_{74}N_2O_{11}P$ |
| $[PLPE+61Da+H]^+$ | 777.5023 | 777.5030 | -0.9003 | $C_{39}H_{74}N_2O_{11}P$ |
| $[PLPE+74Da+H]^+$ | 790.4968 | 790.4983 | -1.8975 | $C_{39}H_{73}N_3O_{11}P$ |
| $[PLPE+74Da+H]^+$ | 790.4979 | 790.4983 | -0.5060 | $C_{39}H_{73}N_3O_{11}P$ |
| $[PLPE+74Da+H]^+$ | 790.4967 | 790.4983 | -2.0240 | $C_{39}H_{73}N_3O_{11}P$ |
| $[PLPE+77Da+H]^+$ | 793.4978 | 793.4979 | -0.1260 | $C_{39}H_{74}N_2O_{12}P$ |
| $[PLPE+77Da+H]^+$ | 793.4977 | 793.4979 | -0.2520 | $C_{39}H_{74}N_2O_{12}P$ |
| $[PLPE+77Da+H]^+$ | 793.4978 | 793.4979 | -0.1260 | $C_{39}H_{74}N_2O_{12}P$ |
| $[PLPE+90Da+H]^+$ | 806.4926 | 806.4932 | -0.7440 | $C_{39}H_{73}N_3O_{12}P$ |
| $[PLPE+90Da+H]^+$ | 806.4922 | 806.4932 | -1.2399 | $C_{39}H_{73}N_3O_{12}P$ |
| $[PLPE+90Da+H]^+$ | 806.4923 | 806.4932 | -1.1159 | $C_{39}H_{73}N_3O_{12}P$ |
| $[PAPE+45Da+H]^+$ | 785.5058 | 785.5081 | -2.9280 | $C_{41}H_{74}N_2O_{10}P$ |
| $[PAPE+45Da+H]^+$ | 785.5056 | 785.5081 | -3.1827 | $C_{41}H_{74}N_2O_{10}P$ |
| $[PAPE+45Da+H]^+$ | 785.5051 | 785.5081 | -3.8192 | $C_{41}H_{74}N_2O_{10}P$ |
| $[PAPE+61Da+H]^+$ | 801.5009 | 801.5030 | -2.6201 | $C_{41}H_{74}N_2O_{11}P$ |
| $[PAPE+61Da+H]^+$ | 801.5010 | 801.5030 | -2.4953 | $C_{41}H_{74}N_2O_{11}P$ |
| $[PAPE+61Da+H]^+$ | 801.5011 | 801.5030 | -2.3705 | $C_{41}H_{74}N_2O_{11}P$ |
| $[PAPE+74Da+H]^+$ | 814.4953 | 814.4983 | -3.6832 | $C_{41}H_{73}N_3O_{11}P$ |
| $[PAPE+74Da+H]^+$ | 814.4956 | 814.4983 | -3.3149 | $C_{41}H_{73}N_3O_{11}P$ |
| $[PAPE+74Da+H]^+$ | 814.4960 | 814.4983 | -2.8238 | $C_{41}H_{73}N_3O_{11}P$ |
| $[PAPE+77Da+H]^+$ | 817.4954 | 817.4979 | -3.0581 | $C_{41}H_{74}N_2O_{12}P$ |
| $[PAPE+77Da+H]^+$ | 817.4952 | 817.4979 | -3.3028 | $C_{41}H_{74}N_2O_{12}P$ |
| $[PAPE+77Da+H]^+$ | 817.4953 | 817.4979 | -3.1804 | $C_{41}H_{74}N_2O_{12}P$ |
| $[PAPE+90Da+H]^+$ | 830.4915 | 830.4932 | -2.0470 | $C_{41}H_{73}N_3O_{12}P$ |
| $[PAPE+90Da+H]^+$ | 830.4913 | 830.4932 | -2.2878 | $C_{41}H_{73}N_3O_{12}P$ |
| $[PAPE+90Da+H]^+$ | 830.4911 | 830.4932 | -2.5286 | $C_{41}H_{73}N_3O_{12}P$ |

**Table S7.** Formula, calculated and observed mass and mass error of $[M-H]^-$ ions observed in the ESI-MS spectra of nitrated and nitroxidized derivatives of POPE, PLPE and PAPE formed due to reaction between $NO_2BF_4$ and each PE. Data was acquired for 20 s and in triplicate in the Q-Exactive Orbitrap mass spectrometer using a concentration of 1 µg $mL^{-1}$. POPE, PE16:0/18:1; PLPE, PE16:0/18:2; PAPE, PE16:0/20:4.

| PE nitration products | Observed Mass (Da) | Calculated Mass (Da) | Error (ppm) | Predicted Formula $[M-H]^-$ |
|---|---|---|---|---|
| $[POPE+45Da-H]^-$ | 761.5073 | 761.5081 | -1.0505 | $C_{39}H_{74}N_2O_{10}P$ |
| $[POPE+45Da-H]^-$ | 761.5068 | 761.5081 | -1.7071 | $C_{39}H_{74}N_2O_{10}P$ |
| $[POPE+45Da-H]^-$ | 761.5067 | 761.5081 | -1.8385 | $C_{39}H_{74}N_2O_{10}P$ |
| $[POPE+61Da-H]^-$ | 777.5040 | 777.5030 | 1.2862 | $C_{39}H_{74}N_2O_{11}P$ |
| $[POPE+61Da-H]^-$ | 777.5038 | 777.5030 | 1.0289 | $C_{39}H_{74}N_2O_{11}P$ |
| $[POPE+61Da-H]^-$ | 777.5038 | 777.5030 | 1.0289 | $C_{39}H_{74}N_2O_{11}P$ |
| $[POPE+74Da-H]^-$ | 790.4944 | 790.4983 | -4.9336 | $C_{39}H_{73}N_3O_{11}P$ |
| $[POPE+74Da-H]^-$ | 790.4950 | 790.4983 | -4.1746 | $C_{39}H_{73}N_3O_{11}P$ |
| $[POPE+74Da-H]^-$ | 790.4944 | 790.4983 | -4.9336 | $C_{39}H_{73}N_3O_{11}P$ |
| $[POPE+77Da-H]^-$ | 793.4985 | 793.4979 | 0.7561 | $C_{39}H_{74}N_2O_{12}P$ |
| $[POPE+77Da-H]^-$ | 793.4990 | 793.4979 | 1.3863 | $C_{39}H_{74}N_2O_{12}P$ |
| $[POPE+77Da-H]^-$ | 793.4989 | 793.4979 | 1.2602 | $C_{39}H_{74}N_2O_{12}P$ |
| $[POPE+90Da-H]^-$ | 806.4944 | 806.4932 | 1.4879 | $C_{39}H_{73}N_3O_{12}P$ |
| $[POPE+90Da-H]^-$ | 806.4945 | 806.4932 | 1.6119 | $C_{39}H_{73}N_3O_{12}P$ |
| $[POPE+90Da-H]^-$ | 806.4947 | 806.4932 | 1.8599 | $C_{39}H_{73}N_3O_{12}P$ |
| $[PLPE+45Da-H]^-$ | 759.4925 | 759.4925 | 0.0000 | $C_{39}H_{72}N_2O_{10}P$ |
| $[PLPE+45Da-H]^-$ | 759.4926 | 759.4925 | 0.1317 | $C_{39}H_{72}N_2O_{10}P$ |
| $[PLPE+45Da-H]^-$ | 759.4927 | 759.4925 | 0.2633 | $C_{39}H_{72}N_2O_{10}P$ |
| $[PLPE+61Da-H]^-$ | 775.4875 | 775.4874 | 0.1290 | $C_{39}H_{72}N_2O_{11}P$ |
| $[PLPE+61Da-H]^-$ | 775.4876 | 775.4874 | 0.2579 | $C_{39}H_{72}N_2O_{11}P$ |
| $[PLPE+61Da-H]^-$ | 775.4877 | 775.4874 | 0.3869 | $C_{39}H_{72}N_2O_{11}P$ |
| $[PLPE+74Da-H]^-$ | -- | 788.4826 | -- | $C_{39}H_{71}N_3O_{11}P$ |
| $[PLPE+74Da-H]^-$ | -- | 788.4826 | -- | $C_{39}H_{71}N_3O_{11}P$ |
| $[PLPE+74Da-H]^-$ | -- | 788.4826 | -- | $C_{39}H_{71}N_3O_{11}P$ |
| $[PLPE+77Da-H]^-$ | 791.4828 | 791.4823 | 0.6317 | $C_{39}H_{72}N_2O_{12}P$ |
| $[PLPE+77Da-H]^-$ | 791.4828 | 791.4823 | 0.6317 | $C_{39}H_{72}N_2O_{12}P$ |
| $[PLPE+77Da-H]^-$ | 791.4829 | 791.4823 | 0.7581 | $C_{39}H_{72}N_2O_{12}P$ |
| $[PLPE+90Da-H]^-$ | 804.4777 | 804.4775 | 0.2486 | $C_{39}H_{71}N_3O_{12}P$ |
| $[PLPE+90Da-H]^-$ | 804.4779 | 804.4775 | 0.4972 | $C_{39}H_{71}N_3O_{12}P$ |
| $[PLPE+90Da-H]^-$ | 804.4781 | 804.4775 | 0.7458 | $C_{39}H_{71}N_3O_{12}P$ |
| $[PAPE+45Da-H]^-$ | 783.4924 | 783.4925 | -0.1276 | $C_{41}H_{72}N_2O_{10}P$ |
| $[PAPE+45Da-H]^-$ | 783.4920 | 783.4925 | -0.6382 | $C_{41}H_{72}N_2O_{10}P$ |
| $[PAPE+45Da-H]^-$ | 783.4902 | 783.4925 | -2.9356 | $C_{41}H_{72}N_2O_{10}P$ |
| $[PAPE+61Da-H]^-$ | 799.4893 | 799.4874 | 2.3765 | $C_{41}H_{72}N_2O_{11}P$ |
| $[PAPE+61Da-H]^-$ | 799.4897 | 799.4874 | 2.8768 | $C_{41}H_{72}N_2O_{11}P$ |
| $[PAPE+61Da-H]^-$ | 799.4898 | 799.4874 | 3.0019 | $C_{41}H_{72}N_2O_{11}P$ |
| $[PAPE+74Da-H]^-$ | 812.4833 | 812.4826 | 0.8616 | $C_{41}H_{71}N_3O_{11}P$ |
| $[PAPE+74Da-H]^-$ | 812.4833 | 812.4826 | 0.8616 | $C_{41}H_{71}N_3O_{11}P$ |
| $[PAPE+74Da-H]^-$ | 812.4832 | 812.4826 | 0.7385 | $C_{41}H_{71}N_3O_{11}P$ |
| $[PAPE+77Da-H]^-$ | 815.4834 | 815.4823 | 1.3489 | $C_{41}H_{72}N_2O_{12}P$ |
| $[PAPE+77Da-H]^-$ | 815.4841 | 815.4823 | 2.2073 | $C_{41}H_{72}N_2O_{12}P$ |
| $[PAPE+77Da-H]^-$ | 815.4836 | 815.4823 | 1.5941 | $C_{41}H_{72}N_2O_{12}P$ |
| $[PAPE+90Da-H]^-$ | 828.4772 | 828.4775 | -0.3621 | $C_{41}H_{71}N_3O_{12}P$ |
| $[PAPE+90Da-H]^-$ | 828.4760 | 828.4775 | -1.8106 | $C_{41}H_{71}N_3O_{12}P$ |
| $[PAPE+90Da-H]^-$ | 828.4772 | 828.4775 | -0.3621 | $C_{41}H_{71}N_3O_{12}P$ |

**Table S8.** Formula, calculated and observed mass and mass error of $[M-H]^-$ ions observed in the ESI-MS spectra of nitrated and nitroxidized derivatives of POPE, PLPE and PAPE formed due to reaction between $NO_2BF_4$ and each PE. Data was acquired for 20 s and in triplicate in the Q-Exactive Orbitrap mass spectrometer using a concentration of 2 µg $mL^{-1}$. POPE, PE16:0/18:1; PLPE, PE16:0/18:2; PAPE, PE16:0/20:4.

| PE nitration products | Observed Mass (Da) | Calculated Mass (Da) | Error (ppm) | Predicted Formula [M-H]- |
|---|---|---|---|---|
| [POPE+45Da-H]$^-$ | 761.5085 | 761.5081 | 0.5253 | $C_{39}H_{74}N_2O_{10}P$ |
| [POPE+45Da-H]$^-$ | 761.5083 | 761.5081 | 0.2626 | $C_{39}H_{74}N_2O_{10}P$ |
| [POPE+45Da-H]$^-$ | 761.5083 | 761.5081 | 0.2626 | $C_{39}H_{74}N_2O_{10}P$ |
| [POPE+61Da-H]$^-$ | 777.5032 | 777.5030 | 0.2572 | $C_{39}H_{74}N_2O_{11}P$ |
| [POPE+61Da-H]$^-$ | 777.5031 | 777.5030 | 0.1286 | $C_{39}H_{74}N_2O_{11}P$ |
| [POPE+61Da-H]$^-$ | 777.5030 | 777.5030 | 0.0000 | $C_{39}H_{74}N_2O_{11}P$ |
| [POPE+74Da-H]$^-$ | 790.4944 | 790.4983 | -4.9336 | $C_{39}H_{73}N_3O_{11}P$ |
| [POPE+74Da-H]$^-$ | 790.4950 | 790.4983 | -4.1746 | $C_{39}H_{73}N_3O_{11}P$ |
| [POPE+74Da-H]$^-$ | 790.4944 | 790.4983 | -4.9336 | $C_{39}H_{73}N_3O_{11}P$ |
| [POPE+77Da-H]$^-$ | 793.4984 | 793.4979 | 0.6301 | $C_{39}H_{74}N_2O_{12}P$ |
| [POPE+77Da-H]$^-$ | 793.4976 | 793.4979 | -0.3781 | $C_{39}H_{74}N_2O_{12}P$ |
| [POPE+77Da-H]$^-$ | 793.4978 | 793.4979 | -0.1260 | $C_{39}H_{74}N_2O_{12}P$ |
| [POPE+90Da-H]$^-$ | 806.4940 | 806.4932 | 0.9919 | $C_{39}H_{73}N_3O_{12}P$ |
| [POPE+90Da-H]$^-$ | 806.4939 | 806.4932 | 0.8680 | $C_{39}H_{73}N_3O_{12}P$ |
| [POPE+90Da-H]$^-$ | 806.4939 | 806.4932 | 0.8680 | $C_{39}H_{73}N_3O_{12}P$ |
| [PLPE+45Da-H]$^-$ | 759.4933 | 759.4925 | 1.0533 | $C_{39}H_{72}N_2O_{10}P$ |
| [PLPE+45Da-H]$^-$ | 759.4932 | 759.4925 | 0.9217 | $C_{39}H_{72}N_2O_{10}P$ |
| [PLPE+45Da-H]$^-$ | 759.4933 | 759.4925 | 1.0533 | $C_{39}H_{72}N_2O_{10}P$ |
| [PLPE+61Da-H]$^-$ | 775.4883 | 775.4874 | 1.1606 | $C_{39}H_{72}N_2O_{11}P$ |
| [PLPE+61Da-H]$^-$ | 775.4881 | 775.4874 | 0.9027 | $C_{39}H_{72}N_2O_{11}P$ |
| [PLPE+61Da-H]$^-$ | 775.4884 | 775.4874 | 1.2895 | $C_{39}H_{72}N_2O_{11}P$ |
| [PLPE+74Da-H]$^-$ | -- | 788.4826 | -- | $C_{39}H_{71}N_3O_{11}P$ |
| [PLPE+74Da-H]$^-$ | -- | 788.4826 | -- | $C_{39}H_{71}N_3O_{11}P$ |
| [PLPE+74Da-H]$^-$ | -- | 788.4826 | -- | $C_{39}H_{71}N_3O_{11}P$ |
| [PLPE+77Da-H]$^-$ | 791.4820 | 791.4823 | -0.3790 | $C_{39}H_{72}N_2O_{12}P$ |
| [PLPE+77Da-H]$^-$ | 791.4820 | 791.4823 | -0.3790 | $C_{39}H_{72}N_2O_{12}P$ |
| [PLPE+77Da-H]$^-$ | 791.4817 | 791.4823 | -0.7581 | $C_{39}H_{72}N_2O_{12}P$ |
| [PLPE+90Da-H]$^-$ | 804.4783 | 804.4775 | 0.9944 | $C_{39}H_{71}N_3O_{12}P$ |
| [PLPE+90Da-H]$^-$ | 804.4786 | 804.4775 | 1.3673 | $C_{39}H_{71}N_3O_{12}P$ |
| [PLPE+90Da-H]$^-$ | 804.4787 | 804.4775 | 1.4917 | $C_{39}H_{71}N_3O_{12}P$ |
| [PAPE+45Da-H]$^-$ | 783.4932 | 783.4925 | 0.8934 | $C_{41}H_{72}N_2O_{10}P$ |
| [PAPE+45Da-H]$^-$ | 783.4929 | 783.4925 | 0.5105 | $C_{41}H_{72}N_2O_{10}P$ |
| [PAPE+45Da-H]$^-$ | 783.4931 | 783.4925 | 0.7658 | $C_{41}H_{72}N_2O_{10}P$ |
| [PAPE+61Da-H]$^-$ | 799.4879 | 799.4874 | 0.6254 | $C_{41}H_{72}N_2O_{11}P$ |
| [PAPE+61Da-H]$^-$ | 799.4871 | 799.4874 | -0.3752 | $C_{41}H_{72}N_2O_{11}P$ |
| [PAPE+61Da-H]$^-$ | 799.4868 | 799.4874 | -0.7505 | $C_{41}H_{72}N_2O_{11}P$ |
| [PAPE+74Da-H]$^-$ | 812.4831 | 812.4826 | 0.6154 | $C_{41}H_{71}N_3O_{11}P$ |
| [PAPE+74Da-H]$^-$ | 812.4838 | 812.4826 | 1.4770 | $C_{41}H_{71}N_3O_{11}P$ |
| [PAPE+74Da-H]$^-$ | 812.4833 | 812.4826 | 0.8616 | $C_{41}H_{71}N_3O_{11}P$ |
| [PAPE+77Da-H]$^-$ | 815.4823 | 815.4823 | 0.0000 | $C_{41}H_{72}N_2O_{12}P$ |
| [PAPE+77Da-H]$^-$ | 815.4825 | 815.4823 | 0.2453 | $C_{41}H_{72}N_2O_{12}P$ |
| [PAPE+77Da-H]$^-$ | 815.4821 | 815.4823 | -0.2453 | $C_{41}H_{72}N_2O_{12}P$ |
| [PAPE+90Da-H]$^-$ | 828.4768 | 828.4775 | -0.8449 | $C_{41}H_{71}N_3O_{12}P$ |
| [PAPE+90Da-H]$^-$ | 828.4764 | 828.4775 | -1.3277 | $C_{41}H_{71}N_3O_{12}P$ |
| [PAPE+90Da-H]$^-$ | 828.4764 | 828.4775 | -1.3277 | $C_{41}H_{71}N_3O_{12}P$ |

**Table S9.** Formula, calculated and observed mass and mass error of $[M-H]^-$ ions observed in the ESI-MS spectra of nitrated and nitroxidized derivatives of POPE, PLPE and PAPE formed due to reaction between $NO_2BF_4$ and each PE. Data was acquired for 20 s and in triplicate in the Q-Exactive Orbitrap mass spectrometer using a concentration of 4 µg $mL^{-1}$. POPE, PE16:0/18:1; PLPE, PE16:0/18:2; PAPE, PE16:0/20:4.

| PE nitration products | Observed Mass (Da) | Calculated Mass (Da) | Error (ppm) | Predicted Formula [M-H]- |
|---|---|---|---|---|
| [POPE+45Da-H]$^-$ | 761.5090 | 761.5081 | 1.1819 | $C_{39}H_{74}N_2O_{10}P$ |
| [POPE+45Da-H]$^-$ | 761.5088 | 761.5081 | 0.9192 | $C_{39}H_{74}N_2O_{10}P$ |
| [POPE+45Da-H]$^-$ | 761.5093 | 761.5081 | 1.5758 | $C_{39}H_{74}N_2O_{10}P$ |
| [POPE+61Da-H]$^-$ | 777.5036 | 777.5030 | 0.7717 | $C_{39}H_{74}N_2O_{11}P$ |
| [POPE+61Da-H]$^-$ | 777.5034 | 777.5030 | 0.5145 | $C_{39}H_{74}N_2O_{11}P$ |
| [POPE+61Da-H]$^-$ | 777.5036 | 777.5030 | 0.7717 | $C_{39}H_{74}N_2O_{11}P$ |
| [POPE+74Da-H]$^-$ | 790.4952 | 790.4983 | -3.9216 | $C_{39}H_{73}N_3O_{11}P$ |
| [POPE+74Da-H]$^-$ | 790.4952 | 790.4983 | -3.9216 | $C_{39}H_{73}N_3O_{11}P$ |
| [POPE+74Da-H]$^-$ | 790.4952 | 790.4983 | -3.9216 | $C_{39}H_{73}N_3O_{11}P$ |
| [POPE+77Da-H]$^-$ | 793.4982 | 793.4979 | 0.3781 | $C_{39}H_{74}N_2O_{12}P$ |
| [POPE+77Da-H]$^-$ | 793.4984 | 793.4979 | 0.6301 | $C_{39}H_{74}N_2O_{12}P$ |
| [POPE+77Da-H]$^-$ | 793.4986 | 793.4979 | 0.8822 | $C_{39}H_{74}N_2O_{12}P$ |
| [POPE+90Da-H]$^-$ | 806.4943 | 806.4932 | 1.3639 | $C_{39}H_{73}N_3O_{12}P$ |
| [POPE+90Da-H]$^-$ | 806.4941 | 806.4932 | 1.1159 | $C_{39}H_{73}N_3O_{12}P$ |
| [POPE+90Da-H]$^-$ | 806.4942 | 806.4932 | 1.2399 | $C_{39}H_{73}N_3O_{12}P$ |
| [PLPE+45Da-H]$^-$ | 759.4904 | 759.4925 | -2.7650 | $C_{39}H_{72}N_2O_{10}P$ |
| [PLPE+45Da-H]$^-$ | 759.4906 | 759.4925 | -2.5017 | $C_{39}H_{72}N_2O_{10}P$ |
| [PLPE+45Da-H]$^-$ | 759.4907 | 759.4925 | -2.3700 | $C_{39}H_{72}N_2O_{10}P$ |
| [PLPE+61Da-H]$^-$ | 775.4863 | 775.4874 | -1.4185 | $C_{39}H_{72}N_2O_{11}P$ |
| [PLPE+61Da-H]$^-$ | 775.4862 | 775.4874 | -1.5474 | $C_{39}H_{72}N_2O_{11}P$ |
| [PLPE+61Da-H]$^-$ | 775.4864 | 775.4874 | -1.2895 | $C_{39}H_{72}N_2O_{11}P$ |
| [PLPE+74Da-H]$^-$ | 788.4858 | 788.4826 | 4.0584 | $C_{39}H_{71}N_3O_{11}P$ |
| [PLPE+74Da-H]$^-$ | 788.4858 | 788.4826 | 4.0584 | $C_{39}H_{71}N_3O_{11}P$ |
| [PLPE+74Da-H]$^-$ | 788.4843 | 788.4826 | 2.1560 | $C_{39}H_{71}N_3O_{11}P$ |
| [PLPE+77Da-H]$^-$ | 791.4807 | 791.4823 | -2.0215 | $C_{39}H_{72}N_2O_{12}P$ |
| [PLPE+77Da-H]$^-$ | 791.4809 | 791.4823 | -1.7688 | $C_{39}H_{72}N_2O_{12}P$ |
| [PLPE+77Da-H]$^-$ | 791.4806 | 791.4823 | -2.1479 | $C_{39}H_{72}N_2O_{12}P$ |
| [PLPE+90Da-H]$^-$ | 804.4757 | 804.4775 | -2.2375 | $C_{39}H_{71}N_3O_{12}P$ |
| [PLPE+90Da-H]$^-$ | 804.4755 | 804.4775 | -2.4861 | $C_{39}H_{71}N_3O_{12}P$ |
| [PLPE+90Da-H]$^-$ | 804.4756 | 804.4775 | -2.3618 | $C_{39}H_{71}N_3O_{12}P$ |
| [PAPE+45Da-H]$^-$ | 783.4924 | 783.4925 | -0.1276 | $C_{41}H_{72}N_2O_{10}P$ |
| [PAPE+45Da-H]$^-$ | 783.4924 | 783.4925 | -0.1276 | $C_{41}H_{72}N_2O_{10}P$ |
| [PAPE+45Da-H]$^-$ | 783.4926 | 783.4925 | 0.1276 | $C_{41}H_{72}N_2O_{10}P$ |
| [PAPE+61Da-H]$^-$ | 799.4872 | 799.4874 | -0.2502 | $C_{41}H_{72}N_2O_{11}P$ |
| [PAPE+61Da-H]$^-$ | 799.4878 | 799.4874 | 0.5003 | $C_{41}H_{72}N_2O_{11}P$ |
| [PAPE+61Da-H]$^-$ | 799.4875 | 799.4874 | 0.1251 | $C_{41}H_{72}N_2O_{11}P$ |
| [PAPE+74Da-H]$^-$ | 812.4828 | 812.4826 | 0.2462 | $C_{41}H_{71}N_3O_{11}P$ |
| [PAPE+74Da-H]$^-$ | 812.4822 | 812.4826 | -0.4923 | $C_{41}H_{71}N_3O_{11}P$ |
| [PAPE+74Da-H]$^-$ | 812.4828 | 812.4826 | 0.2462 | $C_{41}H_{71}N_3O_{11}P$ |
| [PAPE+77Da-H]$^-$ | 815.4820 | 815.4823 | -0.3679 | $C_{41}H_{72}N_2O_{12}P$ |
| [PAPE+77Da-H]$^-$ | 815.4818 | 815.4823 | -0.6131 | $C_{41}H_{72}N_2O_{12}P$ |
| [PAPE+77Da-H]$^-$ | 815.4822 | 815.4823 | -0.1226 | $C_{41}H_{72}N_2O_{12}P$ |
| [PAPE+90Da-H]$^-$ | 828.4792 | 828.4775 | 2.0520 | $C_{41}H_{71}N_3O_{12}P$ |
| [PAPE+90Da-H]$^-$ | 828.4781 | 828.4775 | 0.7242 | $C_{41}H_{71}N_3O_{12}P$ |
| [PAPE+90Da-H]$^-$ | 828.4790 | 828.4775 | 1.8106 | $C_{41}H_{71}N_3O_{12}P$ |

**Table S10.** Neutral losses and product ions intensities observed in the HCD-MS/MS spectra of $[M+H]^+$ ions of nitrated and nitroxidized derivatives of POPC (PC16:0/18:1), PLPC (PC16:0/18:2), PAPC (PC16:0/20:4), POPE (PE16:0/18:1), PLPE (PE16:0/18:2) and PAPE (PE16:0/20:4). Data were acquired in triplicate in Q-Exactive Orbitrap mass spectrometer using three different concentrations (1 µg $mL^{-1}$, 2 µg $mL^{-1}$ and 4 µg $mL^{-1}$) and NCE (20, 25 and 30).

**https://www.mdpi.com/1420-3049/25/9/2120/s1**.

**Table S11.**Neutral losses and product ions intensity observed in HCD-MS/MS spectra of $[M+OAc]^-$ ions of nitrated and nitroxidized derivatives of POPC (PC16:0/18:1), PLPC (PC16:0/18:2), PAPC (PC16:0/20:4) and $[M–H]^-$ ions of nitrated and nitroxidized derivatives of POPE (PE16:0/18:1), PLPE (PE16:0/18:2) and PAPE (PE16:0/20:4). Data were acquired in triplicate in Q-Exactive Orbitrap mass spectrometer using three different concentrations (1 µg $mL^{-1}$, 2 µg $mL^{-1}$ and 4 µg $mL^{-1}$) and NCE (20, 25 and 30

**https://www.mdpi.com/1420-3049/25/9/2120/s1.**

**Table S12:** Formula, calculated and observed mass, and mass error of $[M+H]^+$ ions observed in the HILIC-LC-MS spectra of SW13/cl.2 cell lipid extracts (from control cells) treated with 1 µL (1 ng), 2 µL (2 ng), 4 µL (4 ng) and 8 µL (8 ng) of nitrated POPC (1 µg $mL^{-1}$) . Data was acquired for three biological replicates in two different days.

| $[NO_2$-POPC+H$]^+$ | | | | | |
|---|---|---|---|---|---|
| **PC nitration products** | **Samples** | **Observed Mass (Da)** | **Calculated Mass (Da)** | **Error (ppm)** | **Predicted Formula $[M+H]^+$** |
| 1 ng of nitrated POPC | TE_1 | 805.5683 | 805. 5707 | -2.979 | $C_{42}H_{82}N_2O_{10}P$ |
| | TE_2 | 805.5717 | 805. 5707 | 1.241 | $C_{42}H_{82}N_2O_{10}P$ |
| | TE_3 | 805.5709 | 805. 5707 | 0.248 | $C_{42}H_{82}N_2O_{10}P$ |
| | TE_1´ | 805.5715 | 805. 5707 | 0.993 | $C_{42}H_{82}N_2O_{10}P$ |
| | TE_2´ | 805.5703 | 805. 5707 | -0.497 | $C_{42}H_{82}N_2O_{10}P$ |
| | TE_3´ | 805.5739 | 805. 5707 | 3.972 | $C_{42}H_{82}N_2O_{10}P$ |
| 2 ng of nitrated POPC | TE_1 | 805.5738 | 805. 5707 | 3.848 | $C_{42}H_{82}N_2O_{10}P$ |
| | TE_2 | 805.5734 | 805. 5707 | 3.352 | $C_{42}H_{82}N_2O_{10}P$ |
| | TE_3 | 805.5679 | 805. 5707 | -3.476 | $C_{42}H_{82}N_2O_{10}P$ |
| | TE_1´ | 805.5713 | 805. 5707 | 0.745 | $C_{42}H_{82}N_2O_{10}P$ |
| | TE_2´ | 805.5714 | 805. 5707 | 0.869 | $C_{42}H_{82}N_2O_{10}P$ |
| | TE_3´ | 805.5739 | 805. 5707 | 3.972 | $C_{42}H_{82}N_2O_{10}P$ |
| 4 ng of nitrated POPC | TE_1 | 805.5716 | 805. 5707 | 1.117 | $C_{42}H_{82}N_2O_{10}P$ |
| | TE_2 | 805.5693 | 805. 5707 | -1.738 | $C_{42}H_{82}N_2O_{10}P$ |
| | TE_3 | 805.5709 | 805. 5707 | 0.248 | $C_{42}H_{82}N_2O_{10}P$ |
| | TE_1´ | 805.5685 | 805. 5707 | -2.731 | $C_{42}H_{82}N_2O_{10}P$ |
| | TE_2´ | 805.5716 | 805. 5707 | 1.117 | $C_{42}H_{82}N_2O_{10}P$ |
| | TE_3´ | 805.5708 | 805. 5707 | 0.124 | $C_{42}H_{82}N_2O_{10}P$ |
| 8 ng of nitrated POPC | TE_1 | 805.5705 | 805. 5707 | -0.248 | $C_{42}H_{82}N_2O_{10}P$ |
| | TE_2 | 805.5707 | 805. 5707 | 0.000 | $C_{42}H_{82}N_2O_{10}P$ |
| | TE_3 | 805.5698 | 805. 5707 | -1.117 | $C_{42}H_{82}N_2O_{10}P$ |
| | TE_1´ | 805.5708 | 805. 5707 | 0.124 | $C_{42}H_{82}N_2O_{10}P$ |
| | TE_2´ | 805.5702 | 805. 5707 | -0.621 | $C_{42}H_{82}N_2O_{10}P$ |
| | TE_3´ | 805.5704 | 805. 5707 | -0.372 | $C_{42}H_{82}N_2O_{10}P$ |

**Table S13:** Formula, calculated and observed mass, and mass error of $[M+H]^+$ ions observed in the HILIC-LC-MS spectra of lipid extracts from SW13/cl.2 cells treated with nitrated POPC (10 µmol $L^{-1}$) in culture.

| **SW13/cl.2 cells treated with nitrated POPC in culture** | | | | | |
|---|---|---|---|---|---|
| **PC nitration products** | **Samples** | **Observed Mass (Da)** | **Calculated Mass (Da)** | **Error (ppm)** | **Predicted Formula $[M+H]^+$** |
| $[NO_2$-POPC+H$]^+$ | SW13/cl.2_1 | 805.5703 | 805. 5707 | -0.497 | $C_{42}H_{82}N_2O_{10}P$ |
| | SW13/cl.2_2 | 805.5713 | 805. 5707 | 0.745 | $C_{42}H_{82}N_2O_{10}P$ |
| | SW13/cl.2_3 | 805.5722 | 805. 5707 | 1.862 | $C_{42}H_{82}N_2O_{10}P$ |
| | SW13/cl.2_1' | 805.5696 | 805. 5707 | -1.365 | $C_{42}H_{82}N_2O_{10}P$ |
| | SW13/cl.2_2' | 805.5697 | 805. 5707 | -1.241 | $C_{42}H_{82}N_2O_{10}P$ |
| | SW13/cl.2_3' | 805.5706 | 805. 5707 | -0.124 | $C_{42}H_{82}N_2O_{10}P$ |

**Table S14:** Peak areas of the extracted ion chromatograms (XIC) of $NO_2$-POPC species identified in SW13/cl.2 cell lipid extracts (from control cells) treated with 1 ng of nitrated POPC obtained using MzMine software. Data was acquired for three biological replicates in two different days.

| Non-Normalized peak area | | | | | | | | |
|---|---|---|---|---|---|---|---|---|
| ***m/z*** | **Retention time (RT)** | Identity | **TE_1** | **TE_2** | **TE_3** | **TE_1'** | **TE_2'** | **TE_3'** |
| 678.51 | 10 | **PC_Internal Standard** | 4.35E+08 | 7.46E+08 | 4.27E+08 | 4.41E+08 | 4.89E+08 | 5.45E+08 |
| 805.57 | 9 | **[$NO_2$-POPC+H]$^+$** | 1.55E+07 | 1.94E+07 | 1.97E+07 | 1.68E+07 | 1.64E+07 | 1.37E+07 |

| Normalized peak area | | | | | | |
|---|---|---|---|---|---|---|
| Identity | **TE_1** | **TE_2** | **TE_3** | **TE_1'** | **TE_2'** | **TE_3'** |
| **[$NO_2$-POPC+H]$^+$** | 3.55E-02 | 2.60E-02 | 4.61E-02 | 3.81E-02 | 3.35E-02 | 2.52E-02 |

| Normalized peak area of $NO_2$-POPC - 1 ng | | | | | | |
|---|---|---|---|---|---|---|
| Identity | **TE_1** | **TE_2** | **TE_3** | **TE_1'** | **TE_2'** | **TE_3'** |
| **[$NO_2$-POPC+H]$^+$** | 7.10E-01 | 5.21E-01 | 9.21E-01 | 7.62E-01 | 6.70E-01 | 5.04E-01 |

**Table S15:** Peak areas of the extracted ion chromatograms (XIC) of $NO_2$-POPC species identified in SW13/cl.2 cell lipid extracts (from control cells) treated treated with 2 ng of nitrated POPC obtained using MzMine software. Data was acquired for three biological replicates in two different days.

| Non-Normalized peak area | | | | | | | | |
|---|---|---|---|---|---|---|---|---|
| ***m/z*** | **Retention time (RT)** | Identity | **TE_1** | **TE_2** | **TE_3** | **TE_1'** | **TE_2'** | **TE_3'** |
| 678.51 | 10 | **PC_Internal Standard** | 6.37E+08 | 6.41E+08 | 6.48E+08 | 6.85E+08 | 7.33E+08 | 6.92E+08 |
| 805.57 | 8 | **[$NO_2$-POPC+H]$^+$** | 2.29E+07 | 2.75E+07 | 2.49E+07 | 3.68E+07 | 3.26E+07 | 3.62E+07 |

| Normalized peak area | | | | | | |
|---|---|---|---|---|---|---|
| Identity | **TE_1** | **TE_2** | **TE_3** | **TE_1'** | **TE_2'** | **TE_3'** |
| **[$NO_2$-POPC+H]$^+$** | 3.59E-02 | 4.30E-02 | 3.83E-02 | 5.38E-02 | 4.44E-02 | 5.23E-02 |

| Normalized peak area of $NO_2$-POPC - 2 ng | | | | | | |
|---|---|---|---|---|---|---|
| Identity | **TE_1** | **TE_2** | **TE_3** | **TE_1'** | **TE_2'** | **TE_3'** |
| **[$NO_2$-POPC+H]$^+$** | 7.18E-01 | 8.59E-01 | 7.67E-01 | 1.08E+00 | 8.88E-01 | 1.05E+00 |

**Table S16:** Peak areas of the extracted ion chromatograms (XIC) of $NO_2$-POPC species identified in SW13/cl.2 cell lipid extracts (from control cells) treated with 4 ng of nitrated POPC obtained using MzMine software. Data was acquired for three biological replicates in two different days.

| Non-Normalized peak area | | | | | | | | |
|---|---|---|---|---|---|---|---|---|
| ***m/z*** | **Retention time (RT)** | Identity | **TE_1** | **TE_2** | **TE_3** | **TE_1'** | **TE_2'** | **TE_3'** |
| 678.51 | 10 | **PC_Internal Standard** | 5.64E+08 | 5.87E+08 | 5.80E+08 | 6.67E+08 | 6.24E+08 | 3.09E+08 |
| 805.57 | 9 | **[$NO_2$-POPC+H]$^+$** | 2.41E+07 | 3.64E+07 | 2.84E+07 | 4.92E+07 | 3.64E+07 | 2.00E+07 |

| Normalized peak area | | | | | | |
|---|---|---|---|---|---|---|
| Identity | **TE_1** | **TE_2** | **TE_3** | **TE_1'** | **TE_2'** | **TE_3'** |
| **[$NO_2$-POPC+H]$^+$** | 4.27E-02 | 6.21E-02 | 4.89E-02 | 7.37E-02 | 5.83E-02 | 6.48E-02 |

| Normalized peak area of $NO_2$-POPC - 4 ng | | | | | | |
|---|---|---|---|---|---|---|
| Identity | **TE_1** | **TE_2** | **TE_3** | **TE_1'** | **TE_2'** | **TE_3'** |
| **[$NO_2$-POPC+H]$^+$** | 8.53E-01 | 1.24E+00 | 9.78E-01 | 1.47E+00 | 1.17E+00 | 1.30E+00 |

**Table S17:** Peak areas of the extracted ion chromatograms (XIC) of $NO_2$-POPC species identified in SW13/cl.2 cell lipid extracts (from control cells) treated with 8 ng of nitrated POPC obtained using MzMine software. Data was acquired for three biological replicates in two different days.

| Non-Normalized peak area | | | | | | | | |
|---|---|---|---|---|---|---|---|---|
| ***m/z*** | **Retention time (RT)** | Identity | **TE_1** | **TE_2** | **TE_3** | **TE_1'** | **TE_2'** | **TE_3'** |
| 678.51 | 10 | **PC_Internal Standard** | 6.28E+08 | 6.27E+08 | 6.39E+08 | 6.28E+08 | 7.76E+08 | 7.60E+08 |
| 805.57 | 9 | **$[NO_2$-POPC+H$]^+$** | 4.33E+07 | 4.61E+07 | 4.39E+07 | 4.43E+07 | 6.82E+07 | 6.69E+07 |

| Normalized peak area | | | | | | |
|---|---|---|---|---|---|---|
| Identity | **TE_1** | **TE_2** | **TE_3** | **TE_1'** | **TE_2'** | **TE_3'** |
| **$[NO_2$-POPC+H$]^+$** | 6.90E-02 | 7.35E-02 | 6.86E-02 | 7.06E-02 | 8.79E-02 | 8.81E-02 |

| Normalized peak area of $NO_2$-POPC - 8 ng | | | | | | |
|---|---|---|---|---|---|---|
| Identity | **TE_1** | **TE_2** | **TE_3** | **TE_1'** | **TE_2'** | **TE_3'** |
| **$[NO_2$-POPC+H$]^+$** | 1.38E+00 | 1.47E+00 | 1.37E+00 | 1.41E+00 | 1.76E+00 | 1.76E+00 |

**Table S18**: Peak areas of the extracted ion chromatograms (XIC) of $NO_2$-POPC species identified in lipid extracts from SW13/cl.2 cells treated with nitrated POPC (10 µmol $L^{-1}$) in culture obtained using MzMine software. Data was acquired for three biological replicates in two different days.

| Non-Normalized peak area | | | | | | | | |
|---|---|---|---|---|---|---|---|---|
| ***m/z*** | **Retention time (RT)** | Identity | **SW13/cl.2_1** | **SW13/cl.2_2** | **SW13/cl.2_3** | **SW13/cl.2_1'** | **SW13/cl.2_2'** | **SW13/cl.2_3'** |
| 678.51 | 10 | **PC_Internal Standard** | 4.61E+08 | 5.61E+08 | 5.63E+08 | 4.66E+08 | 5.49E+08 | 5.54E+08 |
| 805.57 | 9 | **$[NO_2$-POPC+H$]^+$** | 3.09E+07 | 2.73E+07 | 2.82E+07 | 2.46E+07 | 2.36E+07 | 3.15E+07 |

| Normalized peak area | | | | | | |
|---|---|---|---|---|---|---|
| Identity | **SW13/cl.2_1** | **SW13/cl.2_2** | **SW13/cl.2_3** | **SW13/cl.2_1'** | **SW13/cl.2_2'** | **SW13/cl.2_3'** |
| **$[NO_2$-POPC+H$]^+$** | 6.69E-02 | 4.86E-02 | 5.01E-02 | 5.29E-02 | 4.29E-02 | 5.68E-02 |

| Normalized peak area of $NO_2$-POPC - 5 µg of lipid extract | | | | | | |
|---|---|---|---|---|---|---|
| Identity | **SW13/cl.2_1** | **SW13/cl.2_2** | **SW13/cl.2_3** | **SW13/cl.2_1'** | **SW13/cl.2_2'** | **SW13/cl.2_3'** |
| **$[NO_2$-POPC+H$]^+$** | 1.34E+00 | 9.73E-01 | 1.00E+00 | 1.06E+00 | 8.59E-01 | 1.14E+00 |